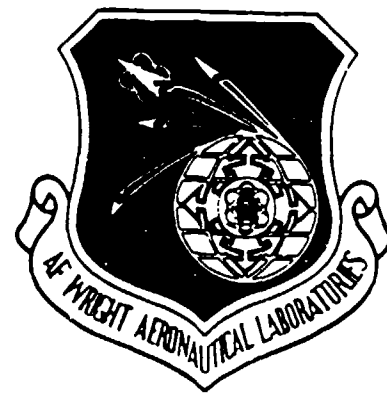AFWAL-TR-85-2025

HIGH ENERGY DENSITY RECHARGEABLE BATTERY PHASE II
(LITHIUM-METAL SULFIDE DEVELOPMENT)

Geoffrey Barlow
Gould Defense Systems Inc.
Gould Research Center
40 Gould Center
Rolling Meadows, Illinois 60008

AD-A213 755

May 1985

Final Report for Period March 1982 - February 1984

Approved for public release; distribution unlimited

AERO PROPULSION LABORATORY
AIR FORCE WRIGHT AERONAUTICAL LABORATORIES
AIR FORCE SYSTEMS COMMAND
WRIGHT-PATTERSON AIR FORCE BASE, OHIO 45433

89 10 23 006
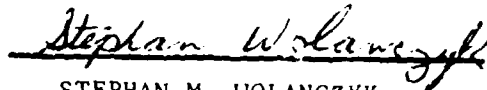
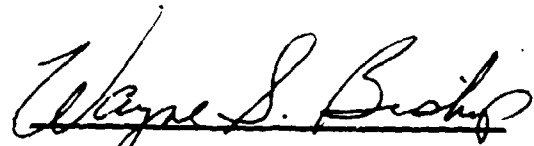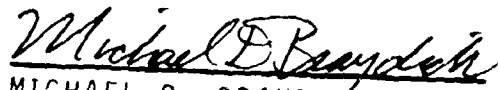STEPHAN M. WOLANCZYK
Project Engineer

WAYNE S. BISHOP
Tech Area Manager
Batteries and Fuel Cells

FOR THE COMMANDER

MICHAEL D. BRAYDICH, Maj, USAF
Deputy Director
Aerospace Power Division
Aero Propulsion & Power Laboratory

REPORT DOCUMENTATION PAGE

1a. REPORT SECURITY CLASSIFICATION	1b. RESTRICTIVE MARKINGS
UNCLASSIFIED	

2a. SECURITY CLASSIFICATION AUTHORITY	3. DISTRIBUTION/AVAILABILITY OF REPORT
2b. DECLASSIFICATION/DOWNGRADING SCHEDULE N/A	Approved for Public Release Distribution Unlimited

4. PERFORMING ORGANIZATION REPORT NUMBER(S)	5. MONITORING ORGANIZATION REPORT NUMBER(S)
	AFWAL-TR-85-2025

6a. NAME OF PERFORMING ORGANIZATION	6b. OFFICE SYMBOL (If applicable)	7a. NAME OF MONITORING ORGANIZATION
Gould Defense Systems Inc. Gould Research Center		Air Force Wright Aeronautical Laboratories Aero Propulsion Laboratory

6c. ADDRESS (City, State and ZIP Code)	7b. ADDRESS (City, State and ZIP Code)
40 Gould Center Rolling Meadows, Illinois 60008	Wright-Patterson AFB Ohio 45433

8a. NAME OF FUNDING/SPONSORING ORGANIZATION	8b. OFFICE SYMBOL (If applicable)	9. PROCUREMENT INSTRUMENT IDENTIFICATION NUMBER
Aero Propulsion Laboratory	AFWAL/POOC-1	F33615-82-C-2223

8c. ADDRESS (City, State and ZIP Code)	10. SOURCE OF FUNDING NOS.			
Air Force Wright Aeronautical Laboratories Wright-Patterson AFB, OH 45433	PROGRAM ELEMENT NO.	PROJECT NO.	TASK NO.	WORK UNIT NO.

11. TITLE (Include Security Classification) UNCLASSIFIED *See Cover*	62203F	3145	22	88

12. PERSONAL AUTHOR(S)
G. Barlow

13a. TYPE OF REPORT	13b. TIME COVERED	14. DATE OF REPORT (Yr., Mo., Day)	15. PAGE COUNT
Final	FROM March 82 TO Feb 84	May 1985	133

16. SUPPLEMENTARY NOTATION

17. COSATI CODES			18. SUBJECT TERMS (Continue on reverse if necessary and identify by block number)
FIELD	GROUP	SUB. GR.	Electrochemical Systems
10	01		High Energy Density Rechargeable *Lithium Iron Sulfide*
09	03		Electric Vehicles

19. ABSTRACT (Continue on reverse if necessary and identify by block number)

Lithium-Aluminum-Silicon

This investigation of high energy density rechargeable batteries attempts to advance the development of high temperature electrochemical systems and assess their suitability for military satellite missions in geosynchronous and mid-altitude orbits. A 5-plate, monopolar, lithium alloy, iron monosulfide cell used in EV's was first considered. These cells performed far below the goal of 100 Wh/kg and were therefore modified to a 7-plate, 100 Ah, Li-Al-Si alloy negative electrode, iron monosulfide positive electrode, magnesium powder separator, and ternary lithium halide electrolyte. After optimization of level I cells, two approaches were employed for subsequent cell designs. One was a stable iron disulfide positive electrode developed for incorporation into a monopolar cell. The other was the development of a bipolar cell design. Results of a Li-FeS test showed a 100 Wh/kg, one-hour discharge cell is not possible. However, cycle life was increased to 1500, and performance did not degrade after the freeze-thaw routine. The Li-Al-Si alloy

20. DISTRIBUTION/AVAILABILITY OF ABSTRACT	21. ABSTRACT SECURITY CLASSIFICATION
UNCLASSIFIED/UNLIMITED ☒ SAME AS RPT. ☐ DTIC USERS ☐	UNCLASSIFIED

22a. NAME OF RESPONSIBLE INDIVIDUAL	22b. TELEPHONE NUMBER (Include Area Code)	22c. OFFICE SYMBOL
Stephan Wolanczyk	(513) 255-6235	AFWAL/POOC-1

DD FORM 1473, 83 APR EDITION OF 1 JAN 73 IS OBSOLETE.

18 (continued)
Satellite Missions
Lithium
Iron Sulfides
Bipolar Cells

19 (continued)
negative electrode is less prone to capacity loss with cycling when operated at high current densities than a Li-Al electrode. Above 350°C the iron disulfide electrode showed rapid upper-plateau capacity decline rate. Cell shorting occurs quickly in this type of cell due to the separator's inability to withstand the expansion forces generated by the positive electrode during discharge. Overall performance achieved was inadequate for a main power source in geosynchronous and mid-altitude orbiting military satellites.

Accession For	
NTIS GRA&I	☑
DTIC TAB	☐
Unannounced	☐
Justification	
By	
Distribution/	
Availability Codes	
Dist	Avail and/or Special
A-1	

Summary

The objective of Phase II of the Air Force Program on High Energy Density Rechargeable Batteries is to advance the development of high temperature electrochemical systems and assess their suitability for the mission requirements in military satellites at mid-altitude and geosynchronous orbits. This report covers a 24 month effort (Mar 82-Feb 84) by Gould Defense System Inc. to develop and characterize the lithium-metal sulfide electro-chemical system for these satellite applications.

The starting point for this cell development effort was a 5-plate monopolar lithium alloy-iron monosulfide cell which Gould had developed under DOE funding for application in electric vehicles. However, since the satellite mission requirements are very different from an electric vehicle duty cycle, in that much higher rates of discharge are required, the first step was to characterize the EV cell under simulated satellite operating regimes in order to establish a performance baseline. This characterization showed the performance of the EV cell to be highly sensitive to discharge rate and to be far below the first design iteration (Level I) goal of 110 Wh/kg at 1 hour discharge rate. Consequently, major design modifications to the cell hardware and changes to the electrode and separator formulations were made to improve the high rate performance significantly before a large group of cells (40 total) were built for detailed characterization under simulated satellite operating regimes. This Level I cell was a 7-plate 100Ah, low (height to width) aspect ratio monopolar design comprising a Li-Al-Si alloy negative electrode, iron monosulfide positive electrode, a magnesium oxide powder separator and a ternary lithium halide electrolyte.

Since the cell performance goals for the satellite application are very ambitious, and it was unlikely that a first iteration design would attain the desired performance, two further design iterations were planned during the program. Consequently, in addition to the engineering cell design work a

significant parallel effort was conducted into the more fundamental electrochemical aspects of component development. This effort concentrated on the formulation and characterization of electrode and separator compositions which would lead to improvements in high discharge rate performance and life of the cell.

After completing an optimization of the electrodes and separator compositions for the Level I cells, two different approaches were pursued for the subsequent cell design iterations. One was the development of a stable iron disulfide positive electrode for incorporation into a monopolar cell. The other was the development of a bipolar cell design concept. Initially this would comprise a Li alloy - FeS electrode couple, but ultimately it was anticipated that the iron monosulfide electrode would be replaced by an iron disulfide electrode.

From the extensive cell testing that was performed during the contract period, a number of significant results were obtained. The results from Level I cell group tests indicate that it is unlikely a specific energy greater than 100Wh/kg is possible at a one hour discharge rate for a monopolar iron monosulfide cell. This is primarily due to the excessive cell hardware weight required in the monopolar cell design. However, a significant improvement in cell life was obtained over previous cell builds in that a number of cells cycled for between 1000 and 1500 cycles before failure. The freeze-thaw capability of the lithium-metal sulfide system also was clearly demonstrated by subjecting cells to ~ 30 freeze-thaw routines and there being no greater degradation in performance than in cells which had not been subjected to freeze-thaw routines. In addition, charging experiments showed that the lithium-metal sulfide cell can be rapidly recharged with minimal loss in capacity provided the upper voltage cut-off limit is adjusted to compensate for the increased ohmic losses.

The more fundamental electrochemical investigations demonstrated that a lithium-aluminum silicon alloy negative electrode is much less prone to

capacity loss with cycling when operated at high current densities than a lithium-aluminum electrode. Work on the iron disulfide electrode showed the upper plateau capacity decline rate to be temperature dependent, in that the decline increased rapidly with increasing temperature above 350°C. Consequently, a lower melting point electrolyte is desireable than the ternary lithium halide salt used in the iron monosulfide cell. However, the major failure mode of the small (5Ah) iron disulfide cells built during the program was the inability of the separator to withstand the expansion forces generated by the positive electrode during discharge, this quickly leads to shorting of the cell. A number of separator systems were evaluated in the disulfide cells in order to improve life, but to date none showed the desireable stability for an extremely long life cell.

In our search for a lower melting point electrolyte, it was found that all electrolytes containing any significant quantity of potassium ions markedly degraded the high rate performance of both iron monosulfide and disulfide cells. This is probably due to the relatively stable intermediate potassium containing phases that are formed during discharge that are difficult to recharge. Preliminary work on a bipolar cell design did show that such a design is feasible since early prototype cells were cycled for up to 100 cycles before cell imbalance became excessive.

In conclusion, although steady progress was made in the development of the lithium-metal sulfide system during the period of this contract, the best performance achieved was well below that deemed necessary (ie 165Wh/kg at 1 hr discharge rate) for the main power source in geosynchronous and mid-altitude orbiting military satellites.

TABLE OF CONTENTS

TABLE OF CONTENTS CONTINUED

LIST OF ILLUSTRATIONS

LIST OF ILLUSTRATIONS (CONCLUDED)

LIST OF TABLES

Introduction

The objective of Phase II of the Air Force High Energy Density Rechargeable Battery Program is to further the development of high temperature batteries and evaluate their performance for potential application as the main power source in military satellites in the 1990's and beyond. This report covers the work performed by Gould Research Center during the period Mar 82-Feb 84 in the development and evaluation of a lithium alloy-metal sulfide, molten salt electrolyte, rechargeable cells under simulated geosynchronous and mid-altitude mission profiles.

The high temperature lithium alloy-metal sulfide electrochemical system has been under development since the early 1970's, primarily as a power source for electric vehicle (EV) propulsion. Gould has been involved in this technology development since the mid 1970's when it became a participant in the DOE funded programs to develop an advanced EV battery.

During this period the lithium-metal sulfide (Li-MS) technology has evolved from a small laboratory bicell (ie central positive electrode surrounded by two half thickness negative electrodes) into a ~ 200 Ah multiplate monopolar engineering cell that could be readily incorporated into a full size prototype EV battery. In addition to the many engineering design changes that have been made during this evolution, a significant number of material changes also have been necessary. All the changes have been made in an effort to improve performance, life and reduce cost. Unfortunately, a reduction in material costs is not necessarily synonomous with improvements in performance and life, therefore often one or more of these parameters have been compromised. This is not the case in the order of priorities for a satellite cell since performance and life are of the utmost importance and low cost is desirable but not essential.

At the commencement of this program minimal performance and life data pertinent to satellite mission requirements were available for the Li-MS

system since all previous testing had been specifically directed towards the EV application. However, in comparing the two applications there is some similarity. The time available to charge a satellite battery depends upon the orbit but typically would range between 22.5 and 5 hours, for the geosynchronous and mid-altitude orbits respectively. The charge time for an EV battery would typically be in the order of 8 hours, therefore the charging of the Li-MS battery was not perceived as a major problem. On the other hand, the discharge rates required for the satellite application are much higher than those typically considered for the EV application (ie < 1 hour compared to > 3 hours for EV's). The initial objective, therefore, was to characterize the performance of the EV cell at these higher discharge rates before embarking on major modifications to the cell hardware and electrode and separator formulations. Hence, a performance baseline would be established on which progress could be measured throughout the program.

Early into the program the Air Force indicated that their primary interest was in the mid-altitude application, hence major emphasis was placed on developing a cell that would have high performance at discharge rates in the range 1-3C and could be fully recharged at ~ C/5 rate with a life of at least 1000 cycles. The "state-of-the-art" performance of an EV cell at the beginning of the contract and the program goals for the three sequential design iterations are shown in Figure 1.

The following sections of this report will discuss in detail the development and characterization of a group of forty cells towards the Level I goals and the development of two alternative approaches; an iron disulfide positive electrode and a bipolar cell stack design which would lead to higher performance cell designs than the Level I monosulfide monopolar cell.
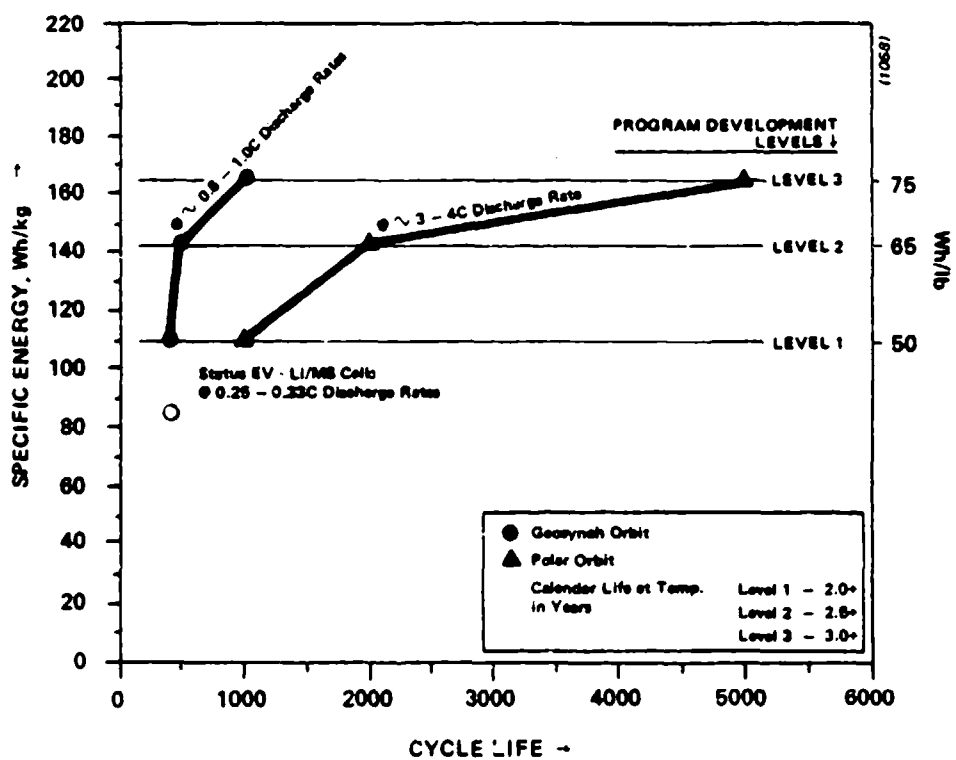
Figure 1. Summary of Goals for Air Force High Energy Density Battery for
Satellites.

Cell Design

The Level I cell design was evolved from a 200 Ah EV monopolar cell which had been developed earlier under a DOE contract. This Level I cell is a 100Ah, 7 plate (3 positive and 4 negative electrode) design with a low (height:width) aspect ratio (see Figure 2). The electrochemical components of the cell comprises a lithium-aluminum/lithium-silicon alloy mixture negative electrode, an iron monosulfide (FeS) positive electrode, a ternary lithium halide salt electrolyte and a magnesium oxide powder separator. The pressed powder electrodes have a relatively high surface area and therefore are capable of good utilization at high rates of operation. The salt electrolyte has a high ionic conductivity when molten at the cell operating temperature of $\sim 455^{\circ}C$. The pressed electrode active material plaques are held either side of a sheet metal current collector by two photoetched particle retainer baskets, (Figure 3 shows the negative electrode assembly, the positive electrode is similar).

The cell is assembled by alternating (negative and positive) electrode packages interleaved with powder separator plaques (Figure 4), these isolate the electrodes electronically from each other. The cell package is isolated from the sides and base of the metal cell can by strips of separator material. The outer face of the end negative electrodes are in contact with the cell can, hence the cell operates with the cell container at the negative electrode potential. The electrodes are connected in parallel by a bus bar/distributor plate/terminal assembly. The positive terminal being electrically isolated from the cell container by a ceramic feedthrough compression seal (Figure 5).

Cell Development

In evolving the Level I cell for high rate performance and long life, from a 5 plate (2 positive, 3 negative electrodes) 200 Ah, high aspect ratio
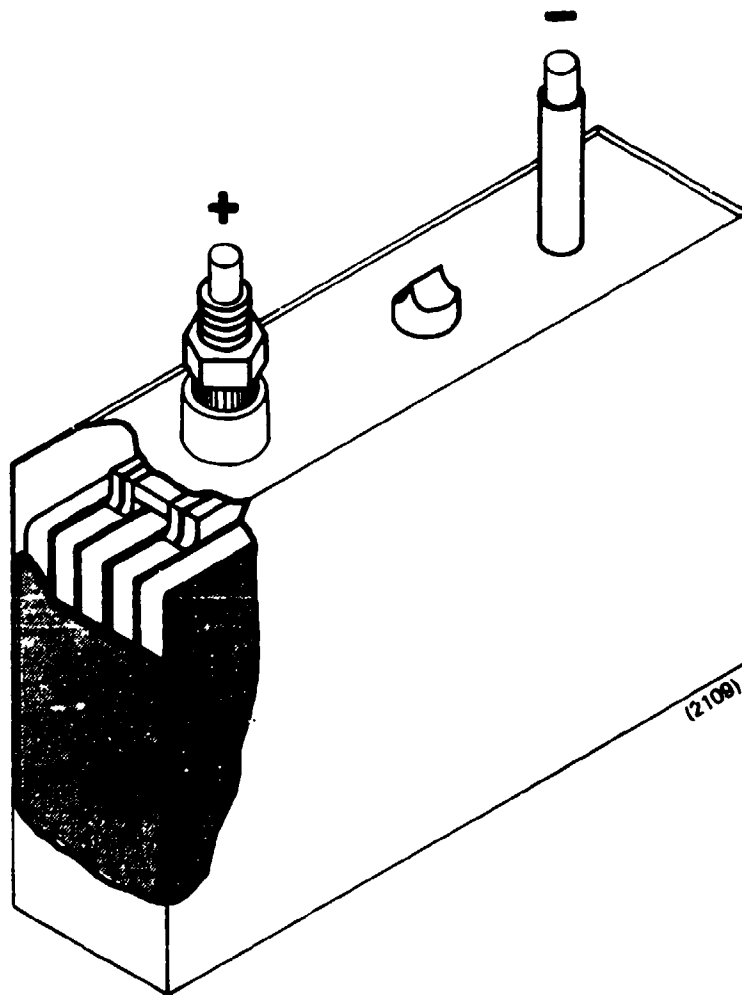
Figure 2. Cutaway of a 100 Ah Li-alloy/Metal Sulfide Level I cell

LITHIUM-METAL SULFIDE NEGATIVE ELECTRODE PACKAGE

PHOTO-ETCHED BASKET

CURRENT COLLECTOR

NEGATIVE ACTIVE MATERIAL
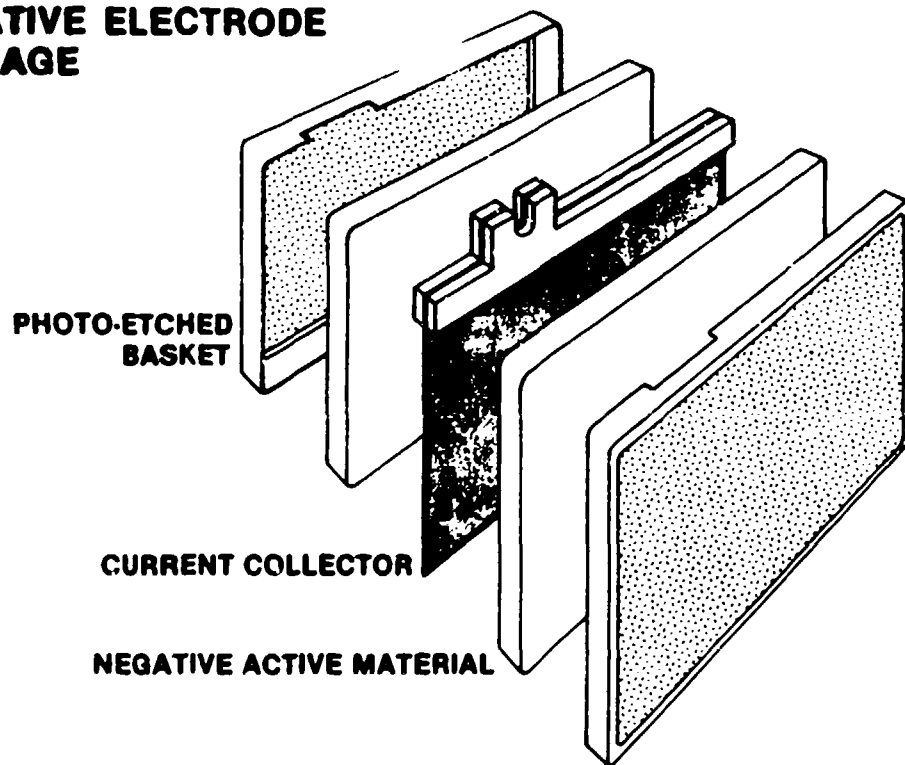
121071

Figure 3. Exploded View of the Negative Electrode Assembly

-6-

LITHIUM·METAL SULFIDE
CELL PACKAGE
(5 PLATE DESIGN)

POSITIVE ELECTRODES

NEGATIVE ELECTRODES

SEPARATORS
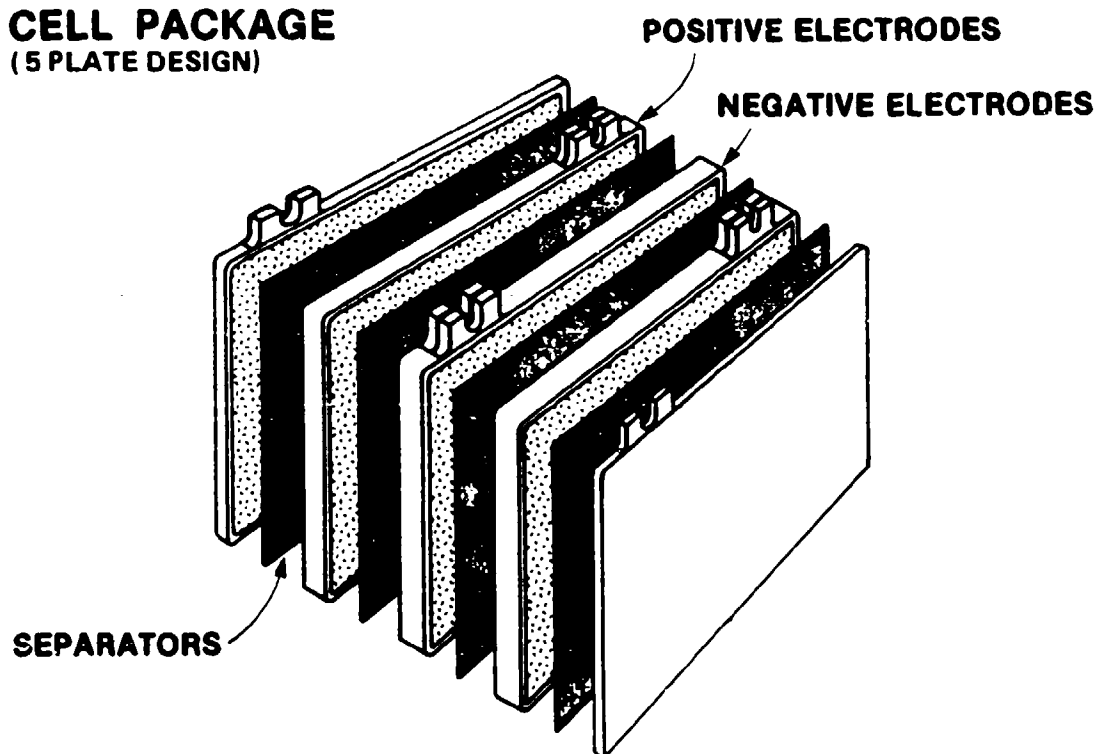
121081

Figure 4. Exploded view of Cell Package Assembly

-7-

COPPER CORE

NICKEL

STAINLESS STEEL

PACKED BORON
NITRIDE POWDER BED

BERYLLIA BUSHINGS

CELL COVER

NICKEL
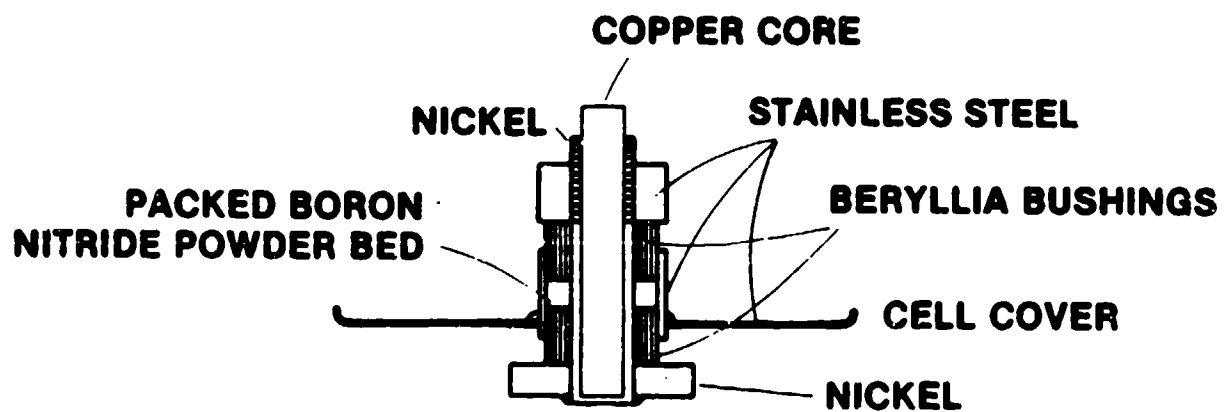
(2112)

Figure 5. Cross-Section of Positive Terminal Feedthrough Seal

EV cell two major approaches were pursued. One was to improve the engineering design of the cell, particularly in the area of current collection, and the other was to optimize the electrode active material and separator formulations for high current density operation and life. However, before making significant changes to the existing EV cell design its performance was characterized at discharge rates representative of the satellite mission requirements. This performance data is summarized in Figure 6 which shows the specific energy and sustained power delivered at various rates of discharge. The specific energy is highly rate sensitive since it declines from ~ 90 Wh/kg at a C/4 discharge to ~ 25 Wh/kg at a 3C discharge. Obviously design modifications were necessary if the program goals were to be met.

Simplistically there are two ways in which the specific energy of a cell can be improved, one is to pack more energy into it by utilizing more energetic active materials, and the other is to minimize the weight of the cell hardware. However, when high power is also a requisite, a more sophisticated design approach is necessary since specific energy is often compromised in order to increase power. As an initial step in the design process, a simplified terminal effect analysis was preformed to give direction to the necessary design changes.

Terminal Effect Analysis

The ohmic resistance in the electrodes of a monopolar cell results in a non-uniform distribution of the faradaic current density along the length of the electrodes which contributes to cell polarization; Kasper, (Reference 1) called this the "terminal effect".

This effect was quantified, following the simplified technique of Tobias and Wijsman (Reference 2), as it relates to the Level I cell design. Using this technique, the extent of the terminal effect is expressed analytically in terms of a single dimensionless parameter, ϕ, which is essentially a ratio of the electronic resistances of the electrodes in their

-9-
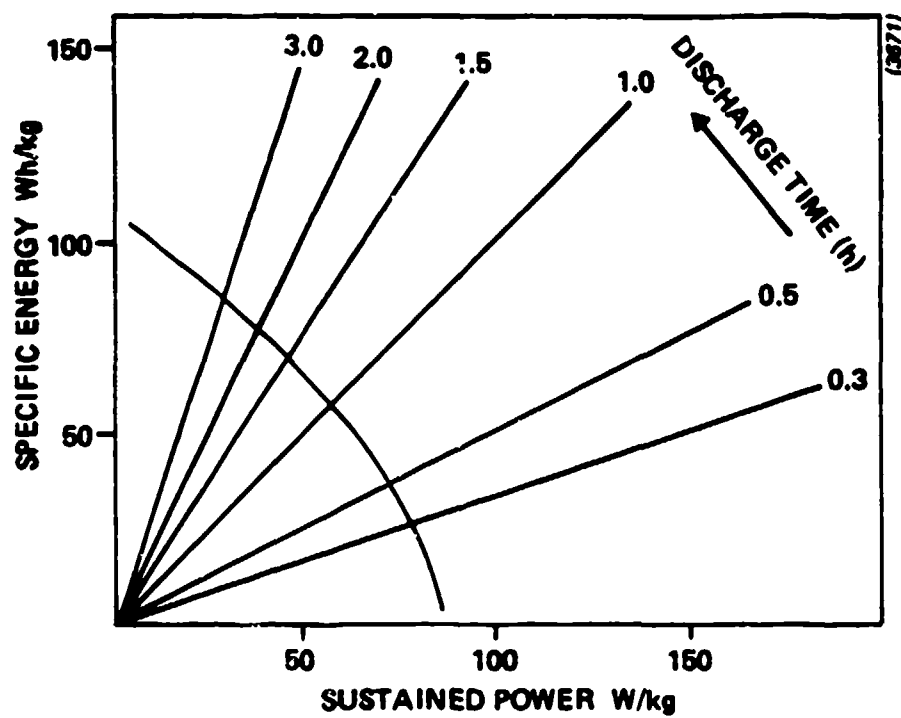
Figure 6. Specific Energy-Rate Behavior for 200 Ah, High Aspect Ratio EV Cell

vertical dimension to the faradaic (polarization) and ionic resistances between electrodes. The larger the value of ϕ (ie relatively large electrode resistances), the greater are the non-uniformities of the inter-electrode current distribution and the cell polarization. When ϕ is zero (ie absence of terminal effect) there will be no losses in the electrodes, hence the inter-electrode current density will be uniform.

In designing a high specific energy battery a compromise exists with regard to the terminal effect. In order to minimize the terminal effect the electrode current collectors should be as thick as possible for maximum conductivity down the length of the electrode, however, weight and volume considerations dictate the opposite (ie thin collectors). In practice, the optimum design is achieved via an interactive process of terminal effect analysis and experimental performance valuation, since the impact of terminal effect on specific energy is impossible to calculate a priori.

The terminal effect analysis was performed for particular combinations of cell aspect ratio (height:width), current collector thickness and current collector material, these being the design factors which can be readily varied in a practical cell; Table 1 and Figure 7 summarize the results.

TABLE 1

SUMMARY OF TERMINAL EFFECT ANALYSIS

Nomenclature

L = Electrode length (cm)
ρ = Electrode resistance (Ω-cm)
t = Electrode thickness (cm)
b = Cell polarization parameter (Ω-cm^2)
x = Distance down electrode from terminal (cm)

Equations: $\phi = 2L \sqrt{\dfrac{\rho}{tb}}$

Terminals

same end

$$\frac{i(x)}{i_{av}} = \frac{\phi \cosh \phi}{\sinh \phi} (1-x/L)$$

opposite ends

$$\frac{i(x)}{i_{av}} = \frac{\phi}{2\sinh\phi} \left[\cosh \frac{(\phi x)}{L} + \cosh \left\{ \frac{\phi(1-x)}{L} \right\} \right]$$

Height:Width Aspect Ratio	Current Material	Collector Thickness (mils)	ϕ	Position of Terminals			
				Same End		Opposite End	
				$\frac{i_{max}}{i_{av}}$	$\frac{i_{min}}{i_{av}}$	$\frac{i_{max}}{i_{av}}$	$\frac{i_{min}}{i_{av}}$
				%	%	%	%
High (1.37)	Nickel	8	1.58	174	67	120	90
Low (0.73)	Nickel	8	1.13	137	82	110	95
Low	Nickel	16	0.80	120	90	105	97

PERCENT

180 — i_{max}/i_{ave} ● Terminals at same end

160 —   ○ Terminals at opposite ends

140

120

100

80

60 — i_{min}/i_{ave}

ASPECT RATIO	HIGH	LOW	LOW	LOW
Collector Material	Ni	Ni	Ni	Mo
Thickness (Mil)	8	8	16	8
α	1.58	1.13	0.80	0.81
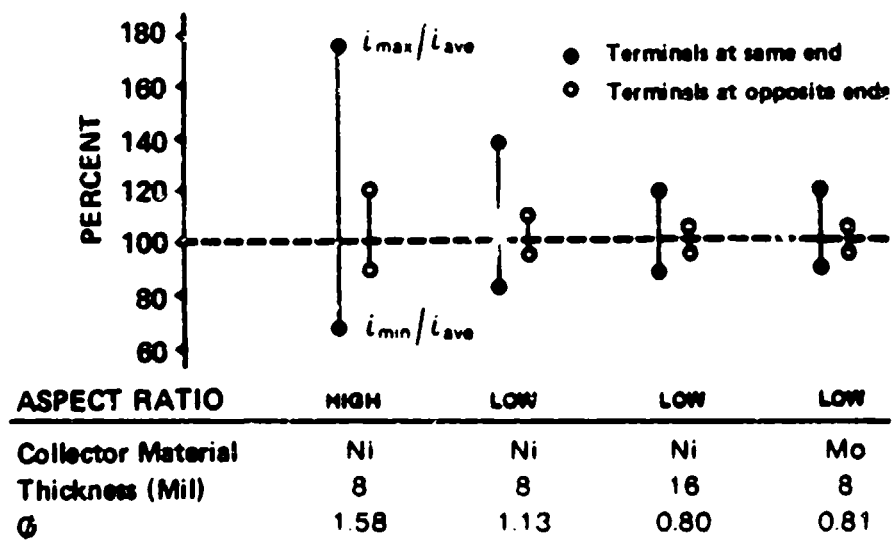
13672Ib

Figure 7. Summary of Results from Terminal Effect Analysis

-13-

The primary interest in this analysis was the magnitude of the current density variation, expressed as a percentage of the average current density for the maximum and minimum. These data apply only at the start of discharge for the cell, which most likely represents the worst case for current density variation; as discharge proceeds, regions of high initial current density will develop increased faradaic resistance faster (ie faradaic resistance increases with depth of discharge), which results in a current density leveling effect. Two cases are analyzed for each combination of design factors, negative and positive terminals at the same end of the electrodes and at opposite ends. Placing the terminals at opposite ends (eg positive at top, negative at bottom) tends to cancel out the current density skew owing to the terminal effect; the faradaic current density is a maximum at the two ends and a minimum at the mid-distance. When both terminals are located at the same end, the maximum faradaic current density occurs at the terminal end and the minimum at the opposite end.

The most important design factor in the terminal effect analysis is the aspect ratio; the current density variation is reduced from a difference of 174%-67% to 137%-82% by changing the (height:width) aspect ratio from 1.37 to 0.73. Incremental improvements are achieved thereafter by increasing the current collector thickness and improving its conductivity (eg molybdenum versus nickel).

In order to verify the predictions of the terminal effect analysis and quantify the magnitude of the improvements a series of experimental cells were built incorporating a number of design changes.

Cell Aspect Ratio

The previous analysis predicted that a more uniform current density distribution would be obtained by decreasing the aspect ratio of the electrodes (ie aspect ratios < 1). This was verified experimentally by constructing cells in which the aspect ratio was reduced from a 1.37 ratio

(used for the EV cells) to 0.73 while still maintaining a constant electrode area. The performance of both high and low aspect ratio, 5 plate 200 Ah cells are compared in Figure 8. The low aspect ratio cell has superior performance at discharges greater than the C rate. The slightly inferior performance of the low aspect ratio cell at the lower discharge rates (ie. < C/1.5) is attributable to the increase in the cell hardware weight (ie heavier bus bar) which were not optimized for this particular cell. It was concluded from these tests that a low aspect ratio electrode design should be incorporated in the Level I cell.

Electrode Thickness

The thickness of the electrodes in an electrochemical cell can have a major impact on the cell performance, particularly with respect to active material utilization and polarization with rate of operation. It is well known that thin electrodes (ie <0.050 in) exhibit superior performance to thick electrodes (ie > 0.100 in) at high rates of discharge. However, in most cells designs the thickness of the electrodes are usually defined by compromising between performance and cost (ie thin electrodes are generally associated with higher manufacturing costs). Consequently the EV cell had tended to a low cost design with relatively thick electrodes.

A performance comparison between an EV cell and a cell which had thinner electrodes, both cells having the same negative:positive capacity ratio and capacity, was made in order to verify that a thinner electrode design would give superior performance at the higher discharge rates dictated by the satellite application.

In complying with the above criteria it was necessary to increase the number of plates in the thin electrode cell. In addition, a practical limitation in pressing unsupported electrode active material plaques dictated that the electrodes could not be less than 0.050 in. Thus, a 7 plate (3 positive and 4 negative electrodes) cell with 0.105 in. negative and 0.050 in.
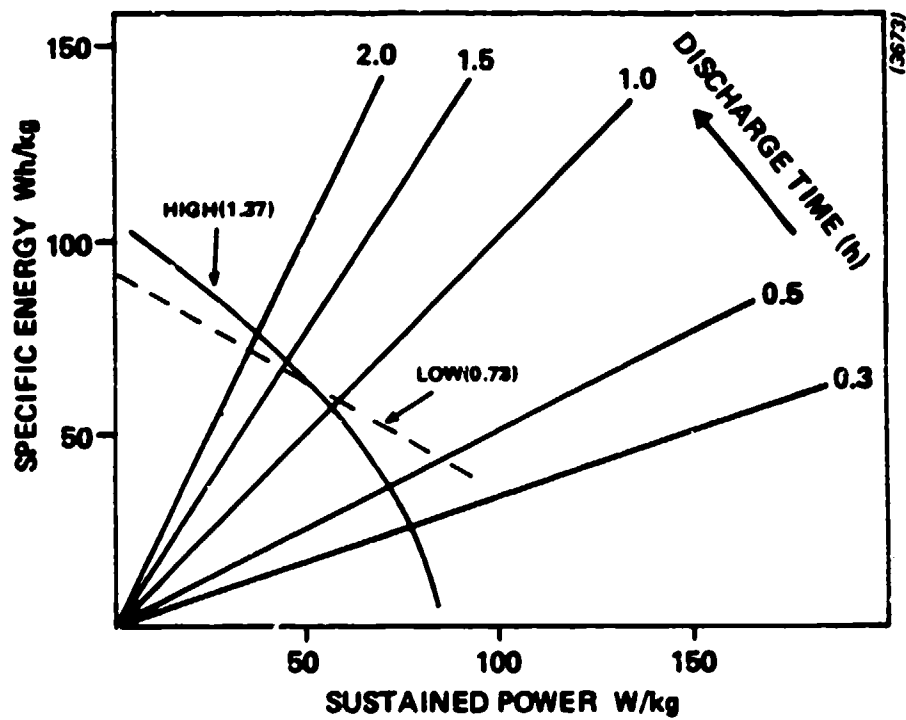
Figure 8. The Effect of Cell Aspect Ratio on Performance

positive plaques was compared to a 5 plate (2 positive and 3 negative electrodes) EV cell with 0.145 in. negative and 0.070 in. positive plaques. The performance of these two cells is shown in Figure 9. The 7 plate, thin electrode cell has superior specific energy to the 5 plate cell at all discharge rates greater than C/1.5. This improved performance is due to the lower average and more uniform current density on the electrodes for a given discharge rate. The lower specific energy of the 7 plate cell at discharge rates < C/1.5 is attributed to the increase in cell hardware weight (ie extra current collectors and particle retainer baskets) which had not been optimized for this cell. It was concluded that thinner electrodes would be beneficial in the Level I cell.

Current Collector Thickness

The primary current collector in the lithium-metal sulfide cell electrodes is a solid-metal sheet centrally placed between two active material plaques, this provides the main current path to the electrodes. The thickness of the collector and the conductivity of the material from which it is made directly influence the collector's current carrying capability. Therefore, it is essential that this component is adequately sized to carry the high currents required by the satellite application without high ohmic losses which decrease the cell voltage.

In order to determine the appropriate thickness of collector two identical cells, except for their current collectors 8 mils and 16 mils thick respectively, were characterized over a range of discharge rates from C/4 to 3C. The results of this characterization are summarized in Figure 10. The Nickel 200 alloy, 8 mil thick collector exhibits comparable performance to the 16 mil thick collector up to a 2C discharge rate beyond which the thicker, lower resistance collector is advantageous. However, since we proposed to use thinner electrodes in the Level I cell design (see previous section on Electrode Thickness) an 8 mil thick nickel collector was deemed adequate for the Level I cell.
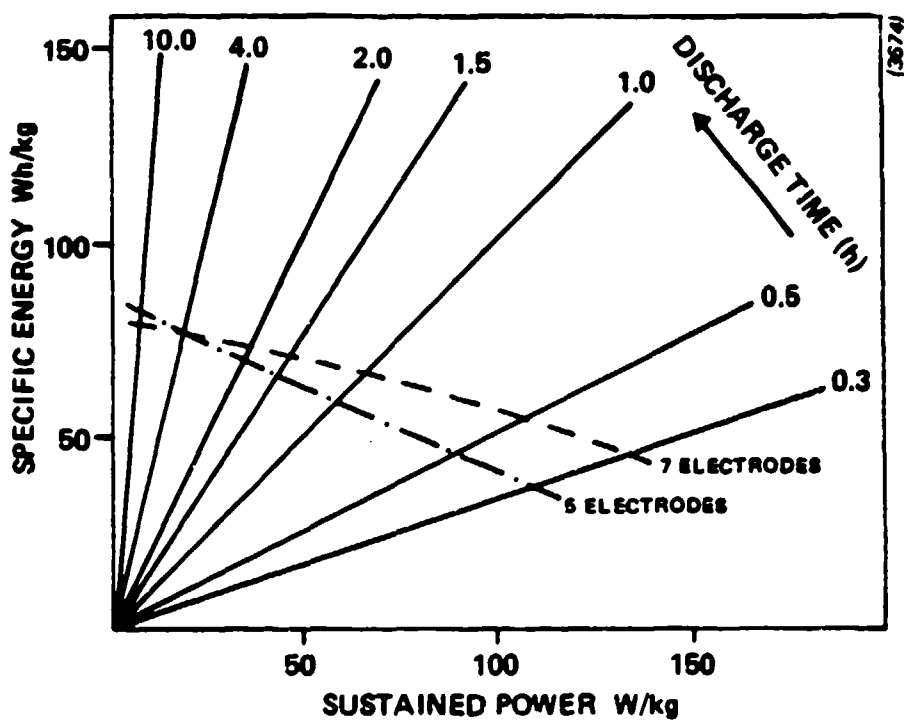
Figure 9. The Effect of the Number of Electrodes and Thickness on Cell Performance

SPECIFIC ENERGY Wh/kg

150

100

50

10.0   4.0   2.0   1.5   1.0

DISCHARGE TIME (h)

0.5

0.3

8 mil

16 mil

(3675)

50   100   150

SUSTAINED POWER W/kg
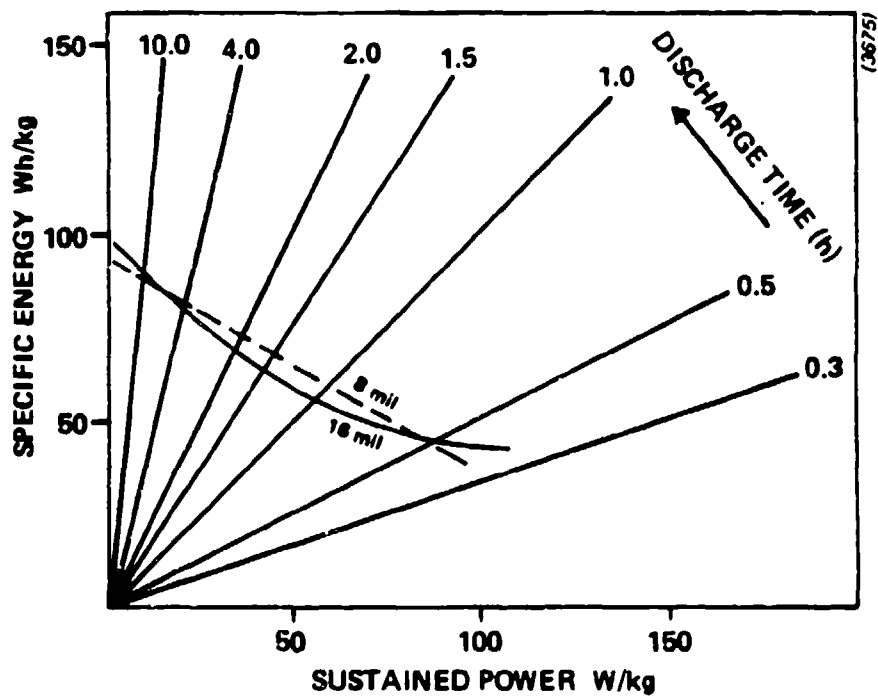
Figure 10. The Effect of Current Collector Thickness on Cell Performance

Terminal Position

The last engineering parameter investigated prior to finalizing the Level I cell design was the position of the positive and negative terminals on the cell. Typically, most monopolar cells and batteries have the terminals located on top of the cell/battery with the current tap attached to the top edge of the respective polarity electrode via a distribution plate/bus bar assembly. The reason for placing the terminals in this location is primarily to minimize electrolyte leakage through the terminal to case seals, particularly in flooded electrolyte cell designs. However, this is not the best location for the terminals to obtain the most uniform current density distribution on the electrodes. A more uniform distribution can be accomplished by positioning the current taps on the positive and negative electrodes on opposite sides and diagonally opposing each other. Since the Gould lithium-metal sulfide cell is a starved electrolyte design it is possible to construct a cell with diagonally opposed terminals.

Cells with conventional same-side and diagonally-opposed terminals were built and characterized for performance at various discharge rates. The performance data from these cells are compared in Figure 11. There is no significant advantage to be gained in terms of specific energy for the diagonally opposed terminal cells except at discharge rates greater than 2C. This is primarily due to the substantial increase in the cell hardware weight which results from the design changes necessary to incorporate the diagonally opposed terminals. Since discharges greater than the 2C rate are anticipated rather infrequently in the satellite application, it was decided that the diagonally opposed terminal concept not be included in the Level I cell design.

The performance improvements to the "state-of-the-art" EV cell so far discussed, have all related to engineering parameter changes. However, it is also possible to improve the cell performance by modifying the chemical and electrochemical parameters of the electrodes, separator and electrolyte. The
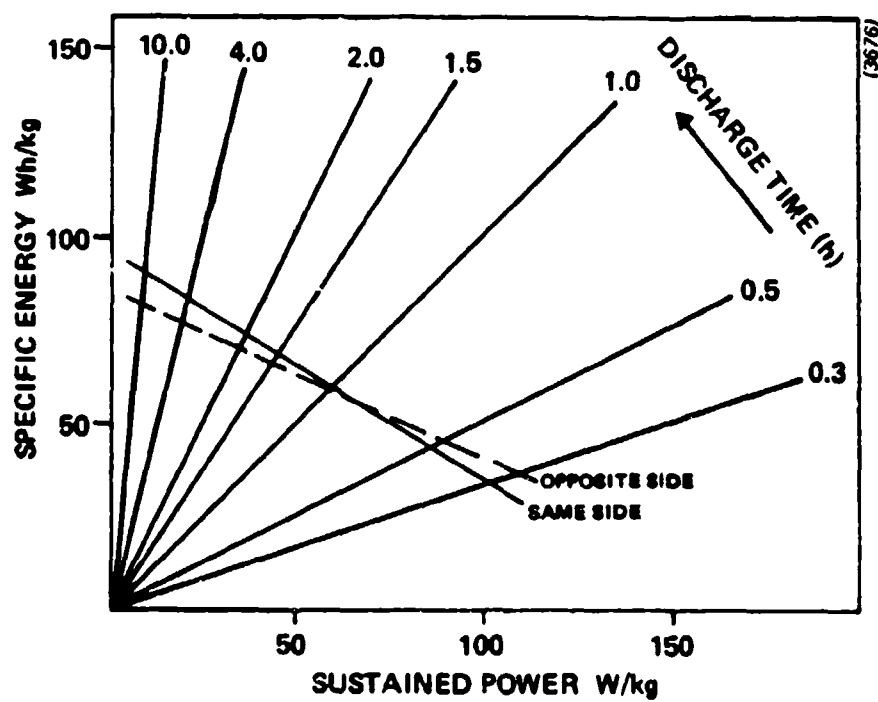
Figure 11. The Effect of Terminal Location on Cell Performance

following section discusses the performance improvements that were achieved by optimizing these parameters.

Component Development

Modification of the electrode and separator formulations lead to some improvement in the cell specific energy but more particularly to the stable operation of the components at the high discharge rates demanded by the satellite application. This was achieved primarily by reducing and redistributing electrolyte within the components.

Prior to this development program a gravimetric and volumetric analysis on a typical "state-of-the-art" EV cell had shown that the active materials and separator accounted for only 30% of the total cell weight (see Table 2), the balance being the electrolyte (30 w/o) and the cell hardware (40 w/o). Obviously a significant reduction in these latter two components would greatly improve the cell specific energy. Also, it was postulated that a reduction in the quantity of electrolyte would improve the physical stability of the electrodes and separator so that the cell life would be prolonged, since penetration of the separator by positive active material had been identified previously as the main cause of cell failure. However, an adequate quantity of electrolyte needs to be present in the components to provide good ionic conductivity during cell operation.

Table 2. Summary of Gravimetric and Volumetric Breakdown for Li-Alloy/Metal Sulfide EV Cell.

	% Cell Weight	% Cell Volume
Li:Al Alloy	11.6	20.0
FeS	10.5	7.0
Electrolyte	29.0	29.5
Separator (MgO)	6.4	5.0
Hardware	40.5	7.5
Miscellaneous	2.0	0
	100.0	100.0

Electrolyte Optimization

The study to optimize the electrolyte content in electrodes and separator was carried out in small (~5Ah) pellet cells containing a reference electrode, (Figure 12). Such a cell permits both positive and negative electrode potentials and the cell voltage to be monitored continuously during cycling, hence the onset of polarization can be readily observed. The quantity of electrolyte and its distribution within the electrodes and separator were found to have a significant influence on the performance and life of cells. In general a high electrolyte content (ie flooded condition) cell showed the best high rate performance but the cell life was severely limited. The converse was observed in low electrolyte (ie starved) cells. Hence a delicate compromise had to be established in order to maximize both life and performance.

The electrode and separator formulations chosen as the baseline for the electrolyte optimization study are shown in Table 3. These formulations contained the minimum amount of electrolyte deemed necessary to easily fabricate good handleable plaques. However, calculations indicated that both the positive electrode and the separator were likely to exude electrolyte at the cell operating temperature. Hence additional electrode and separator compositions were formulated (Table 3) in which the amount of electrolyte was reduced to a level such that there would be no exudation. These new compositions also required that the plaque manufacturing procedures be modified in order to obtain handleable components.

Performance characterization tests on these cells showed that decreasing the amount of electrolyte in the positive electrode and separator from the baseline compositions was beneficial to increasing life (ie the capacity less per cycle was reduced) and that active material utilization at high rates of discharge (ie current densities in the order of 400 mA /cm^2 ≡ 3C rate) was not markedly reduced. However, if the electrolyte was reduced also in the negative electrode then there was a substantial decline in performance at the higher rate of discharge, see Figure 13. A further observation during

5.7 cm

POSITIVE CURRENT COLLECTOR

POSITIVE ACTIVE MASS

SEPARATOR

ACTIVE AREA = 26 cm^2

HOUSING

NEGATIVE ACTIVE MASS

NEGATIVE CURRENT COLLECTOR
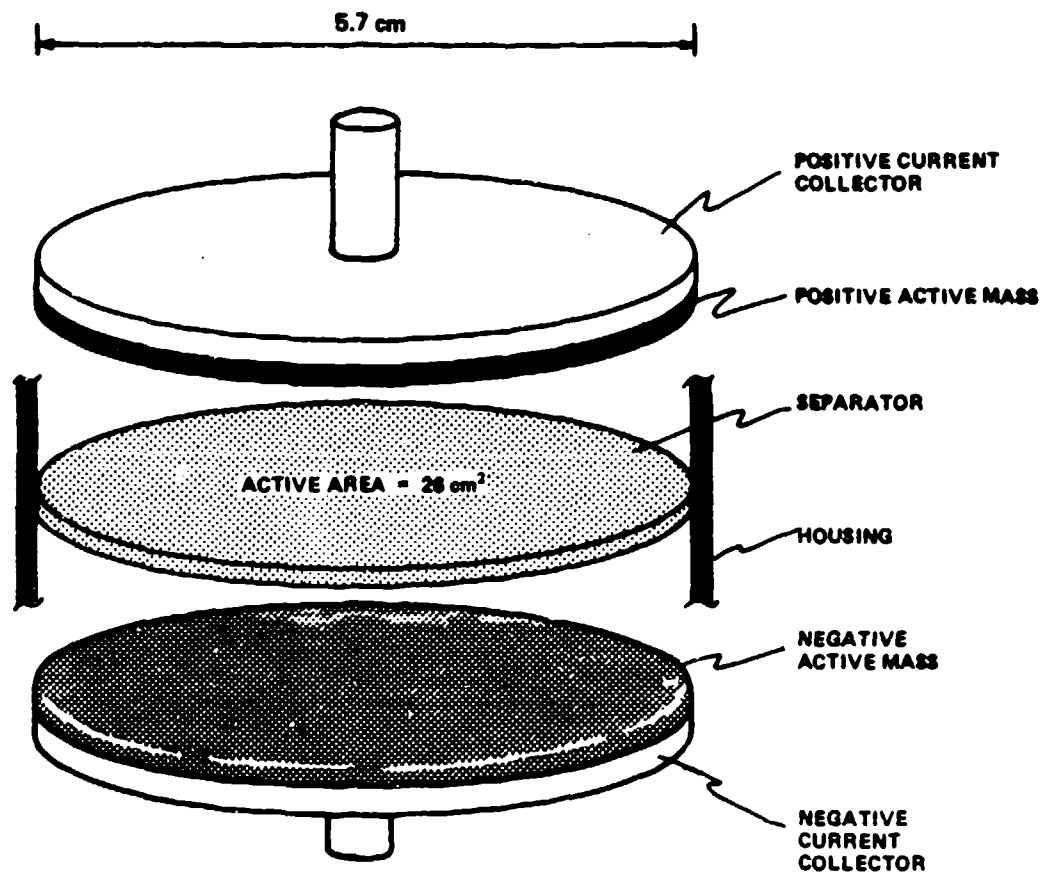
(3288)

Figure 12.   Expanded View of Pellet Cell

-24-

Table 3. Electrode and Separator Formulations for Baseline and Low
         Electrolyte Cells

	Baseline Cell w/o	Low Electrolyte w/o
Positive Electrode		
Formulation	M13	M15
FeS	63.3	74.0
Fe	4.0	5.0
Mo	2.7	3.0
Electrolyte	30.0	18.0
Separator		
Formulation	E17	E9
Mgo	28.0	35.0
Electrolyte	72.0	65.0
Negative Electrode		
Formulation	L27	L27
LiAl	65.0	65.0
Electrolyte	35.0	35.0
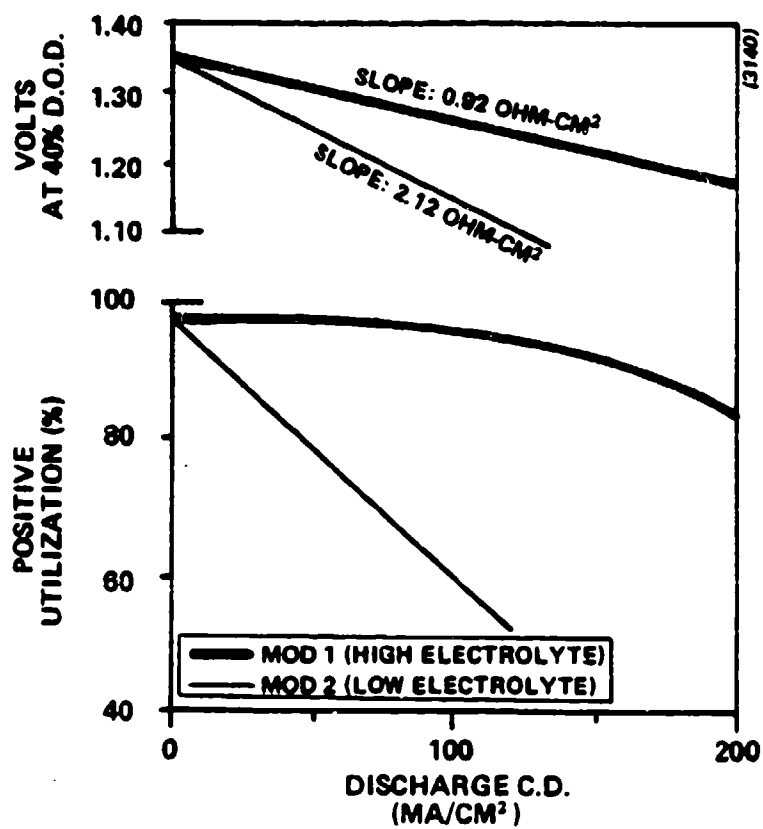
Figure 13. Effect of Electrolyte Content on Cell Performance

these cell tests was the redistribution of electrolyte from the negative electrode to positive electrode, particularly when the cells were subjected to repeated high rate discharges.

Negative Electrode

The initial electrolyte optimization work was carried out in cells containing lithium-aluminum alloy negative electrodes. However, the r rence electrode measurements indicated that after cycling the cells ac high discharge rates there was a transition from positive to negative electrode limited behavior even though the cells were constructed with excess negative capacity (ie 1.3:1 negative:positive capacity ratio), see Figure 14. This transition was attributed to sintering of the lithium depleted α-Al, at the face of the electrode adjacent to the separator, towards the end of discharge. This results in a loss of surface area and electrochemical activity of the active material.

In order to overcome the problem, a lithium-silicon alloy addition was made to the electrode such that the two binary lithium alloys were in the ratio 4:1, Li-Al:Li-Si by weight. In this electrode a third of the available lithium is associated with the silicon alloy. Cells with this modified negative electrode composition exhibited a significant improvement in their capacity retention after being cycled at high rates. (See Figure 15) The improvement was attributed to the greater reactivity of the lithium-silicon which is preferentially discharged until the Li_2Si phase is formed, at which point the two alloys discharge simultaneously. Also, since the lithium-silicon particles are distributed throughout the electrode matrix they are believed to retard the agglomeration of the lithium-aluminum. Two additional advantages to using the mixed binary alloy negative electrodes are the improved cell specific energy at the higher discharge rates and the attainment of maximum performance earlier during formation than had been observed with Li-Al negative electrode cells. The only disadvantage of the Li-Al:Li-Si
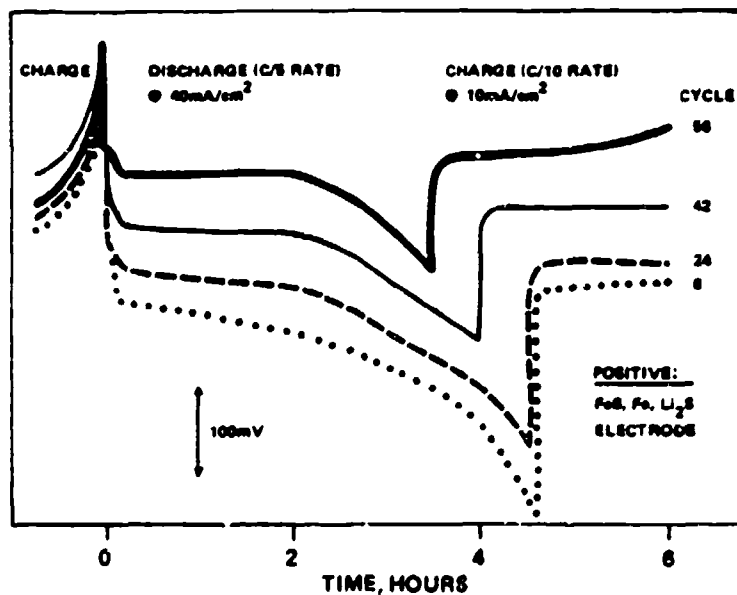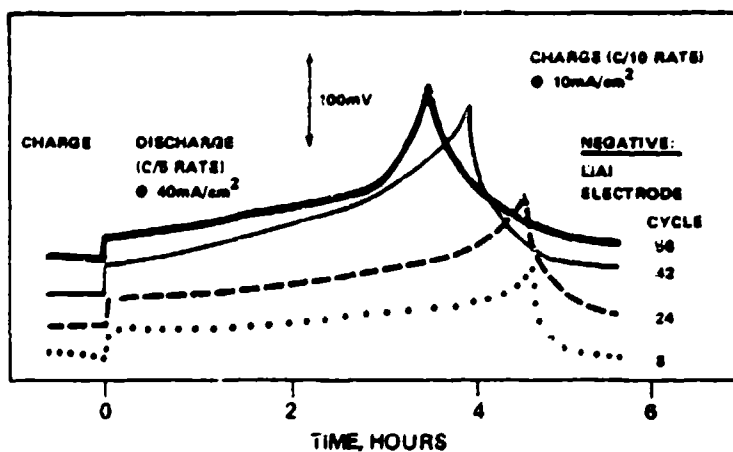
Figure 14. Effect of Cycling on Polarization of Negative Li-Al and Positive FeS Electrodes

Figure 15. Effect of Cycling on Polarization of Negative Li-Al-Si and Positive FeS Electrodes

negative electrode cells was the reduction in coulombic efficiency from ~ 99%
to ~ 97.5%. The failure mode observed in cells when the electrolyte content
was high is exudation of positive active material into the separator, this
leads to shorting of the cell and capacity decline. A reduction in
electrolyte content of the positive electrode to ~ 28 volume % increased the
time to failure, but at the expense of increased polarization resistance.

The behavior of this latter type cell, low electrolyte content in the
positive electrode and high in the negative, is typified by cell L2815A in
Figure 16(a), which shows the polarization resistance and extrapolated cell
voltage with depth of discharge for current densities in the range 20-
270mA/cm^2. The polarization resistance of this cell increases rapidly with
depth of discharge, which was not seen in cells with high electrolyte content
in the positive electrode. The other cell L33N1A, in Figure 16(b), is one in
which the total quantitly of electrolyte within the cell was approximately the
same as in cell L2815A, but had been redistributed so that the positive
electrode contained a higher amount of electrolyte. A small addition of
magnesium oxide powder was also made to the positive electrode in an effort to
stabilize the electrode matrix. The polarization resistance of this cell,
L33N1A, was markedly reduced at the higher depths of discharge, this being
primarily due to a significant decrease in the positive electrode
resistance. In addition the active material utilization was higher and the
decline in utilization with increasing current density was lower than for cell
L2815A. The polarization resistance was calculated from the cell voltage and
electrode potentials at different depths of discharge from the constant
current discharge data at various rates. Pulsed d.c. measurements showed the
IR contribution to remain fairly constant at ~ 0.64 ohm-cm^{-2} for all cells at
all depths of discharge; this is primarily due to the separator resistance.
The IR resistance is included in the polarization resistances values plotted
in Figure 16. The performance of cells L33N1A and L2815A is summarized in
Table 4 for early (<25) cycles and later in the life of the cells (ie. >35
cycles). The polarization resistance data at ~ 50% DOD shows that while the
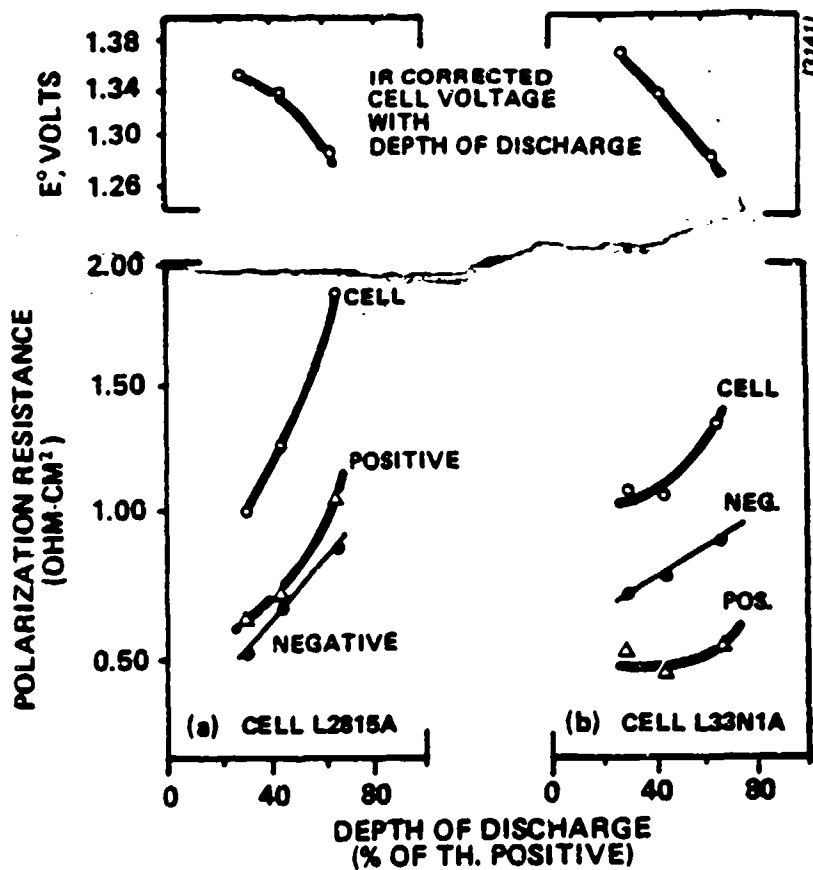
Figure 16. Effect of Electrolyte Redistribution in Li-Al-Si/FeS Cell on Polarization Resistance

Table 4. Comparison of Cell Performance to Show the Effect of Electrolyte Redistribution with Cycling

	L2815A M15		L33N1A N1	
1. Cell Details				
Cell Identification	L2815A		L33N1A	
Positive Formulation	M15		N1	
FeS: Electrolyte Ratio	4.11:1		2.19:1	
Negative Formulation	L28		L33	
Negative Electrolyte Content w/o	35		25	
Theoretical Capacity (positive) Ah	6.9		6.2	
Cycles	< 25	> 30	< 25	> 30
2. Utilization (U=Uo + aj) to 1.0V				
Uo (%)	92.2	86.3	96.7	83.9
Slope a, ($ - cm^2$/A)	-172.3	-87.1	-149.0	-71.1
3. Polarization Resistance at 50% DOD (IR of separator 0.64 ohm-cm^2 included in cell resistance)				
a) Cell (V=Vo + bj)				
Vo (volts)	1.335	1.339	1.328	1.319
b (ohm-cm^2)	-1.246	-1.208	-1.034	-1.075
b) Positive Electrode ($E^+ = Eo^+ + b^+ j$)				
b^+ (ohm-cm^2)	-0.652	-0.235	-0.340	-0.363
c) Negative Electrode ($E^- = E_0^- + b^- j$)				
b^- (ohm-cm^{-2})	0.595	0.973	0.720	0.712

Note: j = current density A/cm^2
$V = E^+ - E^-$
$b = b^+ - b^-$

total cell resistance is essentially unchanged for the two cells as they are cycled, a redistribution in the contribution each electrode makes to the polarization resistance has taken place in cell L2815A, whereas in cell L33N1A the component resistances have remained relatively unchanged.

The more basic electrochemical data generated during this component development work proved invaluable in designing the Level I cell, since we were able to show that a blended Li-Al:Li-Si alloy negative electrode gave superior performance to a LiAl electrode, particularly at high rates of discharges. Also, good high rate discharge performance could be maintained and life extended by reducing the amount of electrolyte in the cell and redistributing it within the individual components. The electrode and separator formulations selected for the Level I cell are given in Table A1 of the Appendix.

Cell Test Program

This section discusses the test program designed to evaluate cells under simulated conditions to those in orbiting satellites and a brief description of the dedicated computer controlled test facility that was constructed to perform the cell testing.

Test Regimes

The proposed application for the high-temperature, high-energy-density batteries is for the main power source in both mid-altitude and geosynchronous orbiting satellites.

A satellite in a mid-altitude orbit, circles the Earth every six hours and is eclipsed by the Earth from the Sun for 0.75 hour, during each orbit. During the eclipse period, the battery would be required to supply the entire electrical requirements of the satellite. The remaining 5.25 hours would be available for recharging the battery by the photovoltaic collectors aboard the satellite (Figure 17). For a satellite in a geosynchronous orbit the operating conditions are somewhat more complicated in that every six months a

-33-
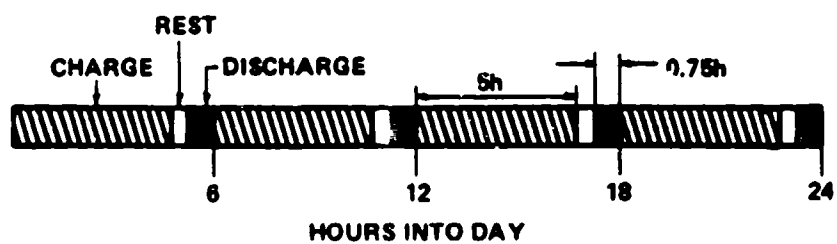
(3469)

Figure 17. Battery Duty Cycle on Mid-Altitude Orbit

45 day eclipse season occurs and the duration of the eclipse is a sinusoidal function of the number of days into the eclipse season. A geosynchronous satellite orbits every 24 hours and the eclipse period varies between a minimum of 0.2 hours and a maximum of 1.2 hours during the 45 day eclipse season. Therefore, during the eclipse season the time available for recharging the battery would vary between 23.8 and 22.8 hours (Figure 18).

Although the test program was initially designed to simulate operating conditions under both types of orbit, major emphasis was placed on the mid-altitude test regimes since these are more arduous than the geosynchronous and it was indicated by the Air Force that the batteries, once proven, would be first flight-tested in a mid-altitude orbit.

Mid-Altitude Tests

The mid-altitude regime tests on the Level I cells were performed in six separate sub-groups with each sub-group containing five cells. The test regimes for the sub-groups are shown in Table 5. The first three sub-groups were designed to examine the effect of depth of discharge on cycle life by cycling the cells to 40, 60 and 80% depth of discharge during the permitted 0.75 hour discharge time. The fourth sub-group test was designed to determine the high-rate performance degradation with cycling. This was accomplished by first characterizing the cells for energy and power at discharge rates between C/1.5 and 3C to 100% depth of discharge followed by cycling the cells to 60% DOD on the mid-altitude regime (0.75 hr discharge : 5.25 hr charge) for approximately 150 cycles before recharacterizing the cells for energy and power. This routine was repeated until the cells failed. The fifth sub-group test was designed to determine the ability of the cells to withstand thermal shock by repeatedly subjecting them to a freeze-thaw routine. The cells were cycled on a mid-altitude regime to 70% DOD for 12 cycles and then were cooled-down from the operating temperature of ~ 450°C to room temperature. After being at ambient temperature for 72 hours the cells were reheated and cycled for a further 12 cells before the cells were cooled once again. This freeze-

ANNUAL SCHEDULE
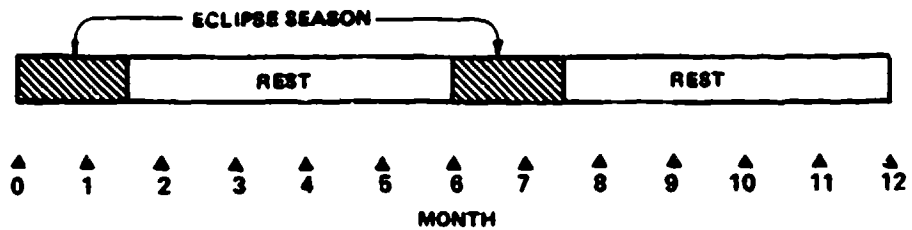
CYCLE ROUTINE (ECLIPSE SEASON)
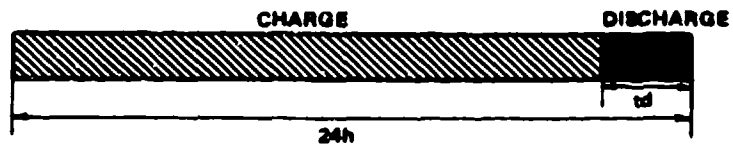
DISCHARGE TIME
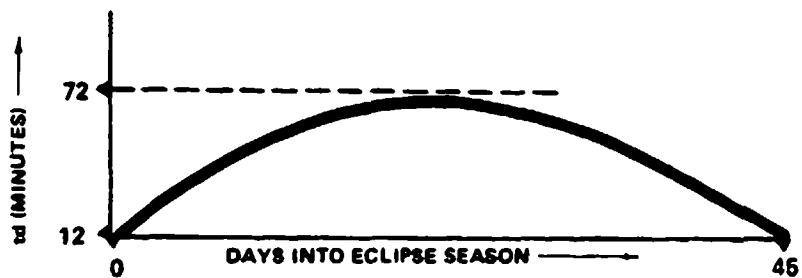
(3016)

Figure 18.   Battery Duty Cycle on Geosynchronous Orbit

Table 5. Test Plan for Level I Cells

Test Regime			Test Bay No.	Test priority	Number of cells to be tested	Max. Capacity Discharged Ah*	Discharge Current A	Charge Current A
GEOSYNCHRONOUS								
Cycle Time	Discharge Time	%DOD						
24 h	1.2 h	60	5	1	5	57	47.5	3.1
24 h	1.2 h	80	6	2	5	76	63.3	4.0
8 h	Sinusoidal 1.2 h max. 0.2 h min.	80 16.7	2	8	5	76	63.3	12.2
MID-ALTITUDE 6 h	0.75 h	40	3	3	5	32	42.7	6.9
6 h	0.75 h	80	4	4	5	48	64.0	10.1
6 h	0.75 h	80	7	5	5	64	85.3	13.3
Freeze Thaw 6 h	0.75 h	70	8	6	5	56	74.7	11.7
6 h	0.75 h + High Rate Characterization during life (energy vs power)	60	1	7	3	48	64.0	10.1
Peak Power			9	9	2	76	-----	13.3
Shock and Vibration 6 h 0.75 60				10		48	64.0	10.1
					TOTAL 40			

Nominal cell capacity at: i) 1.2 h discharge to 100% DOD is 95 Ah.
ii) 0.75 h discharge to 100% DOD is 80 Ah.

-37-

thaw routine was repeated until the cells failed. The final group of cells were to be subjected to a number of special tests which included peak power, shock and vibration etc., all of which are essential for characterizing the capabilities and limitations of the battery system.

Geosynchronous Tests

The geosynchronous regime tests were performed in three sub-groups with each sub-group containing five cells. The test regimes for these sub-groups are shown in Table 5. The first two sub-groups tests were designed to examine the effect of depth of discharge on cycle life by cycling the cells to 60 and 80% depth of discharge during the permitted 1.2 hours discharge time. The third sub-group test simulated the sinusoidally varying depth of discharge the cells would be subjected to during a 45 day eclipse season. The cells were constant current discharged at the C/1.5 rate for times varying between 0.2 and 1.2 hours in accordance with the formula:

$$t_D = 12 + \text{Absolute Value} \left[60 \sin \frac{(\underline{N}) \pi}{45} \right]$$

where t_D is the discharge time in minutes

N is the number of days into the eclipse period between 1 and 45

Cell Test Facility

In order to perform the above test program an extensive computer controlled test facility was designed and built during the first year of the program. This facility comprises nine test bays, eight of which can accommodate 6 cells and the remaining bay 10 cells, for a total of 58 individual cell test positions. Each of the 6-cell bay cycler units has a separate charge and discharge circuit (Figures 19 and 20), in order that cells can be switched independently from one mode to the other. The 10-cell bay cycler has only one circuit which can be switched between the charge or discharge mode. This bay was designed for forming cells and performing

CHARGE
POWER
SUPPLY

CELL
CIRCUIT
DETAIL

CELL BYPASS

SHUNT

RTD

CELL
TEMP

CELL
VOLTAGE
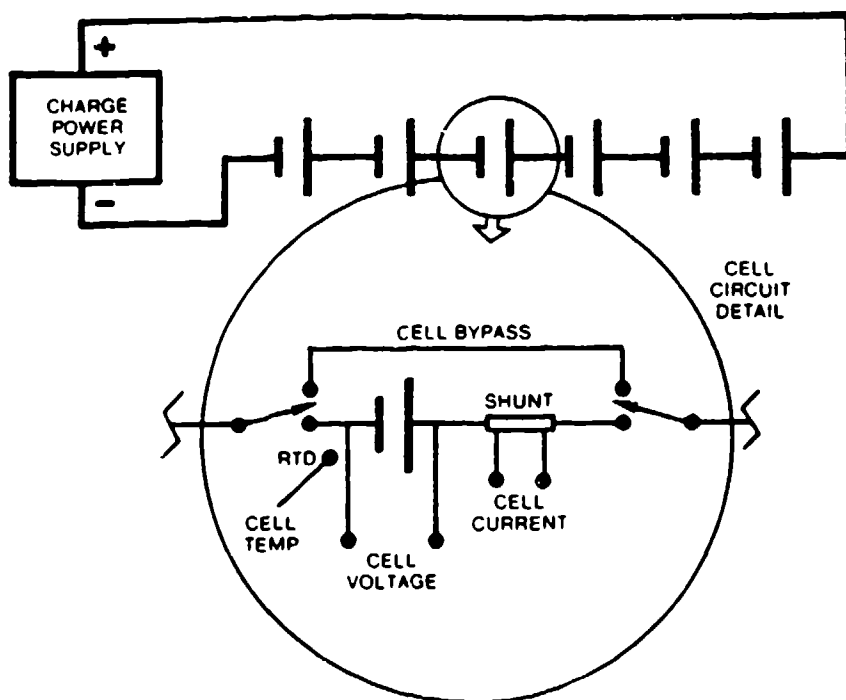
CELL
CURRENT

(3678)

Figure 19. Schematic Drawing of Charge Circuit for Test Bay

-39-
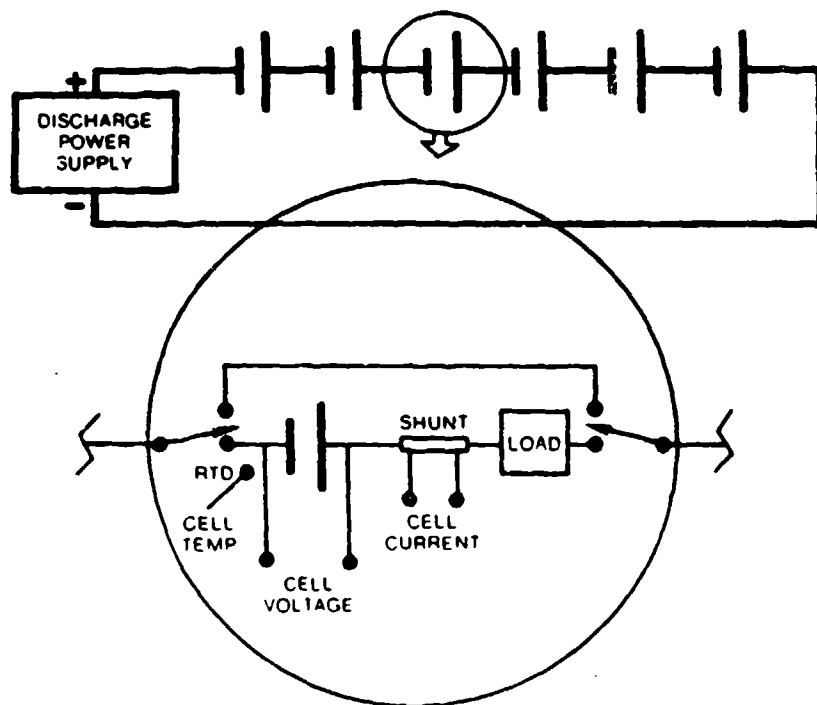
(3679)

Figure 20.   Schematic Drawing of Discharge Circuit for Test Bay

special characterization tests. Cycling of the cells and data acquisition is performed automatically and round-the-clock by a dedicated computer controlled system. The heart of the system is an HP1000 computer and associated peripherals to which the bay cycler units are connected via an HP3497 control and data acquisition unit (Figure 21). The system allows access to real time raw data for all cells and after data manipulation, summary information on each cycle can be obtained in tabular or graphic form.

The cell parameters of current, voltage and temperature are monitored continuously with respect to time since they are used to control the charge and discharge. From these measurements and other cell parameters (eg weight and volume), which are entered into the cell file prior to the start of testing, the cell performance characteristics are automatically calculated.

The mode of operation for the Level I cell tests was a constant current charge and discharge. Initially the end of charge on a cell was signified by a rapid rise in the cell voltage to a cut-off of 1.65 volts. With cycling, however, as the cell leakage current increases; the end of charge is determined by a time limit (ie. 22.8 hours for the geosynchronous tests and 5.25 hours for the mid-altitude tests) prior to reaching the set voltage cut-off. On discharge, a time limit signalled the end of discharge until the cell could no longer maintain an average discharge voltage of 0.75 of the rated voltage under load; when this occurred a cell was deemed failed.
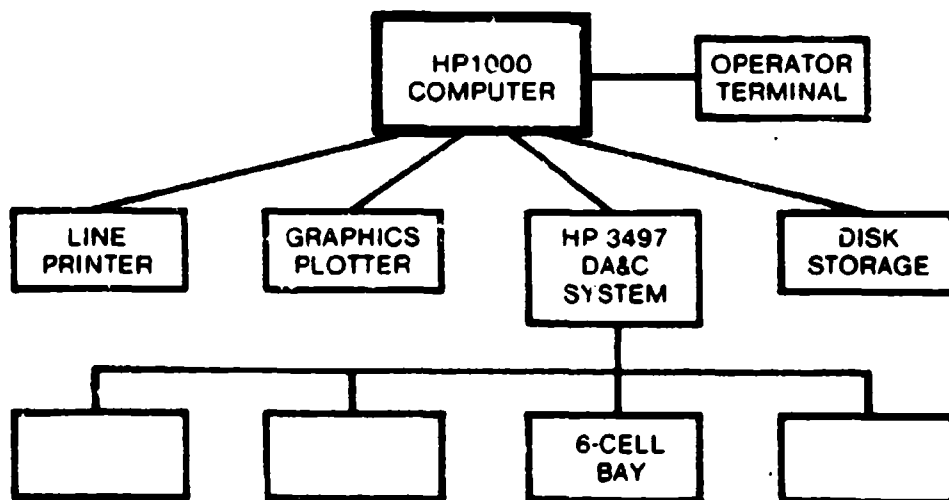
(3684)

Each 6-Cell Test Bay, Controlled and Monitored by the Main Computer
Via a Data Acquisition and Control System, is Configured to Provide
One Regime of the Test Plan

Figure 21.   Block Diagram of the Cell Test Facility

Test Procedure

Before placing the cells on test under the mid-altitude and geosynchronous regimes outlined in the test plan, it was necessary to form and qualify the cells by a standard characterization test. Cells that failed to meet the qualification criteria were rejected and not used in the mid-altitude and geosynchronous test programs. The cells were formed and characterized according to the cycling schedule shown in Table 6.

The qualification criteria for cell acceptance was that all the major performance parameters (ie. capacity, coulombic efficiency etc.) should be within two standard deviations of the mean value of the particular parameter for the group of 40 cells. It was believed from past experience that such qualification criteria were sufficiently stringent to eliminate any weak cell from further testing.

In order to determine the appropriate charge and discharge currents for the Level I cell tests under the mid-altitude and geosynchronous regimes, the cells had first to be characterized for their 100% depth of discharge capacity at discharges of 0.75 and 1.2 hours respectively. Once these capacities were determined it was possible to calculate the discharge currents based on the depth of discharge to which the cells were to be operated and the time of the discharge. The charge currents were calculated on the assumptions that the cells would have an average leakage current of 500 mA and they would be fully charged after 5.0 and 22 hours on the mid-altitude and geosynchronous regimes respectively. These assumptions allowed for variations in capacity and coulombic efficiency of the newly formed and characterized cells. This would permit also an acceptable decline in cell performance with cycling before the cells were deemed failed due to their inability to be fully charged within the maximum permitted time. An example of the discharge and charge current calculation is given in Table 7.

Once forty cells were qualified for testing, the cells were randomly

-43-

Table 6. Cell Formation and Acceptance Tests for Level I Cells

Test	Remarks & Acceptance Criteria
1. Vacuum leak check assembled cell.	Discard cells with major leaks, rework any small welding defects.
2. Measure cold resistance.	If resistance is less than 100 ohms, discard cell.
3. Formation cycles.	

	Charge		Discharge							
Cycle #	Current (amps)	Cutoff (volts)	Current (amps)	Cutoff (volts)		With cycling there should be an increase in the utilization and stabilization in the Ah efficiency and leakage current.				
1-3	7.5	1.65	7.5	0.9						
4	15.0	1.65	15.0	0.9						

4. Characterization Cycles

	Charge		Discharge				Cycle #	Ah Eff. %	Utilization %	Leakage Current (mA)	Cell Voltage (volts)
Cycle #	Current (amps)	Cutoff (volts)	Current (amps)	Cutoff (volts)	Rate (hours)						
5-7	15.0	1.65	30.0	0.9	3		7	> 95	≥ 80	< 500	≥1.20
8-9	15.0	1.65	60.0	0.75	1.5		9	> 94	≥ 75	< 500	≥1.10
10-11	15.0	1.65	90.0	0.65	1.0		11	> 94	> 70	< 500	≥1.04
12	15.0	1.65	30.0	0.9	3		12	≥ 95	> 80	< 500	≥1.20

5. Cell Self-Discharge Open circuit cell at top of charge on Cycle #11, stand for 72 hours and recharge to 1.65 volt cutoff.	Compare cell self-discharge rates statistically, reject cells which fall outside 95% confidence limit.
6. Cell Impedance Determine cell impedance by current interrupt technique at 50% DOD on Cycle #12.	Compare cell impedance values statistically.

Table 7. Example of Discharge and Charge Current Calculation

o **Cells to be cycled on mid-altitude regime to 80% DOD**

- Cell capacity for 0.75 hour discharge to 100% DOD is 80Ah.
- Discharge time to 80% DOD is 0.75 hours.
  Hence discharge current = (80 x 0.8) ÷ 0.75 = 85.3Ah
- Maximum charge time is 5.25 hours
- Assume a) cells will be fully charged in 5 hours
         b) cell leakage current is 0.50A
         c) cell capacity to be recharged is 80 x 0.8 = 64Ah
  Overcharge required due to cell leakage current is 5·x 0.5 ≈ 2.5 Ah
  Total charge = 64 + 2.5 = 66.5Ah

Therefore charge current = 66.5 ÷ 5 = 13.3Ah

Coulombic Efficiency = $\dfrac{Ah_{out}}{Ah_{in}} = \dfrac{64}{66.5} = 96.2\%$
(assuming 0.5A leakage current)

Maximum leakage current (A) = $\dfrac{Ah_{in} - Ah_{out}}{\text{time of cycle (h)}} = \dfrac{(13.3 \times 5.25) - 64}{6}$
(permissible before cell fails to fully recharge)
$= 0.97A$

assigned into the various mid-altitude and geosynchronous sub-groups in order that the cycling tests results would not be unduly affected by the four separate batches of cells (ie the cells were built in batches of ten due to equipment limitations). After the cells were assigned to a particular group they were placed in the allotted test bay and cycled continuously under the appropriate charge/discharge regimes until they failed. All the test data was stored on hard disk for regular periodic review in order to ensure testing was proceeding according to plan and analysis on completion of the tests.

Level I Cell Test Results

Documented in this section is the data that was generated during the Level I cell test program and discussion of the major findings which resulted from analysis of the data.

Qualification Tests

The results of the qualification tests performed on the group of cells built for the Level I test program are given in Tables 8-12. The performance of the cells at discharge currents of 60, 90 and 30 amps including the statistical data generated to identify weak cells within the group are given in Tables 8-10 respectively. Four cells (A34, A46, A47 and A49) consistently fell below the acceptance criteria and therefore were rejected from the main test group. A number of other cells fell outside the acceptance criteria on one of the characterization cycles, but this was because they performed better than average, so it was decided not to reject these cells since experience has shown that Li-alloy/FeS cells do not attain their maximum stable performance until they have completed at least twenty cycles. There was a high probability, therefore, that a number of other cells in the group would improve in performance with cycling. The self-discharge results are given in Table 11. The calculated leakage currents for all the cells, except A34 which had given poor performance during the characterization tests, were below 800 mA with the majority in the 300-500 mA range. Hence, only cell A34 was rejected on the basis of its high self-discharge current.

These qualification tests proved acceptable for determining the performance of the cells and eliminating the weakest cells, but they gave no indication whatsoever about cell life. In future, it would be better if the cells were allowed to stabilize in performance (ie at least 20 cycles) before the qualification tests were performed.

Table 8. Level I Cell Performance on 60 AMP Discharge

CYCLE   9

CELL	AMPHRS	% AEFF	% UTIL	AVVOLT	WHR/KG	W/KG	LEAK CURRENT
A5	98.6	97.0	83.6	1.131	61.4	37.4	.362
A6	99.2	97.2	84.2	1.119	61.4	37.0	.339
A7	95.2	96.9	81.1	1.154	61.2	38.5	.378
A8	98.5	96.8	83.6	1.130	61.8	37.7	.392
A9	97.9	96.7	83.3	1.129	61.0	37.2	.405
A10	99.7	97.6	84.5	1.130	62.3	37.5	.295
A11	99.1	96.6	83.5	1.140	62.6	37.7	.407
A12	102.2	96.4	86.1	1.169	66.5	38.9	.428
A13	99.9	95.3	84.6	1.167	64.0	38.7	.571
A14	97.8	95.9	82.7	1.158	63.4	38.7	.493
A15	96.8	97.2	83.0	1.165	62.8	38.7	.342
A16	101.7	96.4	84.6	1.163	65.7	38.7	.430
A17	100.9	95.6	84.5	1.158	64.3	38.1	.533
A18	100.7	97.0	85.0	1.146	64.1	37.0	.366
A19	101.8	96.8	85.8	1.144	64.6	36.8	.381
A20	102.2	96.9	85.6	1.140	64.4	37.6	.370
A21	101.6	97.0	85.1	1.136	63.0	37.7	.358
A22	102.5	97.1	84.5	1.133	64.0	37.4	.349
A23	102.5	97.0	85.0	1.128	64.0	37.4	.363
A24	100.4	96.6	83.0	1.142	63.4	37.9	.416
A25	102.6	95.9	85.4	1.139	64.5	37.7	.498
A26	103.0	96.3	84.9	1.147	65.0	38.0	.453
A27	102.4	96.4	84.1	1.148	64.7	37.8	.436
A28	100.5	96.8	83.1	1.133	62.8	37.5	.476
A29	101.7	96.7	83.7	1.134	63.5	37.4	.398
A30	100.6	96.7	82.7	1.142	63.2	37.7	.406
A31	95.2	96.5	80.0	1.143	60.0	37.8	.427
A32	93.2	96.4	77.5	1.149	59.1	38.1	.439
A33	97.2	93.7	81.3	1.150	61.9	38.2	.767
A34	96.2	88.3	80.3	1.148	61.0	38.0	1.442
A35	98.9	96.1	82.6	1.146	62.6	37.8	.470
A36	101.2	96.6	84.0	1.133	63.2	37.3	.410
A37	99.3	96.6	82.2	1.142	62.4	37.7	.412
A38	100.1	96.3	83.5	1.138	62.8	37.5	.447
A39	96.9	96.4	80.9	1.136	60.5	37.3	.433
A40	97.1	96.5	80.9	1.136	60.6	37.4	.425
A41	100.4	96.4	83.5	1.153	63.3	37.8	.432
A42	100.2	96.6	83.5	1.131	62.3	37.6	.413
A43	99.6	97.0	82.0	1.158	63.5	38.0	.361
A44	99.7	96.9	83.4	1.144	62.9	37.6	.370
A45	95.4	97.3	80.0	1.140	59.8	37.4	.324
A46	86.7	96.9	73.4	1.095	52.7	35.7	.371
A47	86.0	97.4	72.7	1.079	51.7	35.0	.313
A48	93.5	97.3	78.4	1.134	58.2	36.3	.327
A49	86.3	97.9	71.9	1.093	52.0	35.2	.251
MEAN:	98.5	96.4	82.4	1.139	62.0	37.6	.433
STD DEV:	4.1	1.4	3.2	.018	3.2	.8	.174
UPR LIM:	106.7	99.2	88.9	1.175	68.4	39.2	.781
LWR LIM:	90.3	93.6	75.9	1.104	55.7	35.9	.085

CELLS OUTSIDE THE 95% CONFIDENCE LIMITS

A34	0.0	88.3	0.0	0.000	0.0	0.0	1.442
A46	86.7	0.0	73.4	1.095	52.7	35.7	0.000
A47	86.0	0.0	72.7	1.079	51.7	35.0	0.000
A49	86.3	0.0	71.9	1.093	52.0	35.2	0.000

Table 9. Level I Cell Performance on 90 AMP Discharge

CYCLE 11

CELL	AMPHRS	X AEFF	X UTIL	AVVOLT	WHR/KG	W/KG	LEAK CURRENT
A5	97.1	98.0	82.4	1.073	57.4	53.1	.255
A6	98.8	99.4	83.9	1.062	58.0	52.8	.074
A7	95.4	97.7	81.3	1.097	58.3	54.9	.296
A8	95.5	96.0	81.1	1.064	56.4	53.2	.520
A9	96.8	94.0	82.4	1.069	57.2	53.0	.809
A10	98.6	97.6	83.5	1.063	57.9	52.8	.306
A11	96.5	95.9	81.4	1.083	57.9	53.7	.546
A12	100.0	97.0	84.2	1.106	61.5	56.8	.391
A13	99.7	95.0	84.4	1.097	60.0	56.2	.547
A14	94.9	96.5	80.2	1.074	58.1	56.5	.458
A15	93.1	97.5	79.0	1.101	57.1	56.6	.324
A16	100.2	96.5	83.3	1.074	60.9	56.3	.451
A17	99.7	95.7	83.5	1.008	59.7	55.3	.555
A18	101.1	97.3	85.3	1.082	60.7	52.2	.350
A19	100.0	97.0	85.0	1.085	60.6	52.1	.391
A20	101.2	97.0	84.7	1.077	60.2	53.3	.385
A21	99.9	97.0	83.7	1.076	59.5	53.6	.388
A22	151.7	97.2	83.0	1.068	59.9	52.9	.367
A23	101.4	97.3	84.2	1.066	59.9	53.0	.350
A24	98.4	96.0	81.3	1.076	58.5	53.4	.413
A25	101.3	95.9	84.3	1.079	60.4	53.7	.535
A26	101.7	96.2	83.8	1.082	60.5	53.7	.492
A27	101.9	96.3	83.7	1.084	60.7	53.5	.470
A28	98.5	96.3	81.4	1.069	58.1	53.0	.400
A29	102.0	96.7	84.0	1.069	60.0	52.9	.426
A30	98.7	97.1	81.2	1.076	58.5	53.2	.375
A31	88.9	97.1	74.7	1.091	53.5	54.0	.373
A32	90.5	97.3	75.3	1.089	54.4	53.9	.347
A33	92.4	94.1	77.3	1.093	55.9	54.5	.764
A34	92.1	88.6	76.9	1.095	55.8	54.3	1.485
A35	93.6	96.0	78.2	1.089	56.4	53.9	.416
A36	99.1	97.3	82.2	1.071	58.5	52.3	.384
A37	95.2	97.0	78.9	1.085	56.9	53.6	.380
A38	99.0	96.7	82.6	1.075	58.0	52.6	.427
A39	92.7	97.3	77.3	1.082	55.1	52.7	.342
A40	96.1	97.0	80.1	1.080	57.1	52.7	.385
A41	96.1	96.0	79.9	1.094	57.6	53.1	.417
A42	98.7	97.1	82.2	1.073	58.2	52.0	.372
A43	97.2	97.3	80.1	1.092	58.5	54.3	.340
A44	98.9	97.5	82.0	1.076	58.7	53.7	.318
A45	91.1	97.9	76.3	1.082	54.2	53.9	.275
A46	83.1	96.5	70.4	1.023	47.2	52.4	.449
A47	84.1	97.2	71.1	1.018	47.7	51.9	.365
A48	90.7	97.6	76.1	1.066	53.1	53.6	.313
A49	81.1	98.4	67.6	1.028	45.9	51.9	.203
MEAN:	96.3	96.7	80.6	1.077	57.4	53.6	.429
STD DEV:	5.1	1.5	4.1	.018	3.5	1.3	.203
UPR LIM:	106.5	99.8	88.8	1.114	64.4	56.1	.835
LWR LIM:	86.2	93.6	72.5	1.041	50.4	51.1	.024

CELLS OUTSIDE THE 95% CONFIDENCE LIMITS

CELL	AMPHRS	X AEFF	X UTIL	AVVOLT	WHR/KG	W/KG	LEAK CURRENT
A12	0.0	0.0	0.0	0.000	0.0	56.8	0.000
A13	0.0	0.0	0.0	0.000	0.0	56.2	0.000
A14	0.0	0.0	0.0	0.000	0.0	56.5	0.000
A15	0.0	0.0	0.0	0.000	0.0	56.6	0.000
A16	0.0	0.0	0.0	0.000	0.0	56.3	0.000
A34	0.0	88.6	0.0	0.000	0.0	0.0	1.485
A46	83.1	0.0	70.4	1.023	47.2	0.0	0.000
A47	84.1	0.0	71.1	1.018	47.7	0.0	0.000
A49	81.1	0.0	67.6	1.028	45.9	0.0	0.000

Table 10. Level I Cell Performance on 30 AMP Discharge

CYCLE	12						
CELL	AMPHRS	% AEFF	% UTIL	AVVOLT	WHR/KG	W/KG	LEAK CURRENT
A5	99.1	98.8	84.1	1.233	67.3	20.3	.121
A6	99.3	99.1	84.3	1.231	67.6	20.4	.894
A7	98.2	98.2	83.7	1.247	68.2	20.8	.184
A8	98.9	98.8	84.8	1.230	68.0	20.6	.200
A9	98.1	99.3	83.5	1.235	66.9	20.4	.073
A10	99.4	100.9	84.2	1.234	67.7	20.5	-.086
A11	100.0	99.1	84.3	1.239	68.6	20.5	.088
A12	102.6	98.4	86.4	1.255	71.6	20.9	.158
A13	100.3	97.6	84.9	1.255	70.0	20.9	.244
A14	99.4	98.9	84.6	1.243	69.1	20.8	.100
A15	98.8	100.3	84.7	1.245	68.5	20.7	-.031
A16	102.1	98.2	84.9	1.249	70.8	20.8	.178
A17	101.6	98.8	85.1	1.247	69.7	20.5	.203
A18	101.2	99.0	85.4	1.248	70.1	20.1	.103
A19	101.6	98.5	85.6	1.248	70.2	20.1	.151
A20	101.1	98.9	84.6	1.240	69.2	20.6	.100
A21	100.2	99.3	83.9	1.237	68.6	20.6	.066
A22	101.9	99.9	83.9	1.232	69.2	20.5	.015
A23	101.2	99.9	84.0	1.224	68.6	20.4	.009
A24	99.0	100.5	82.4	1.237	68.2	20.5	-.049
A25	101.5	98.1	84.4	1.245	69.8	20.7	.195
A26	102.9	98.1	84.0	1.241	70.2	20.6	.190
A27	102.0	99.1	84.4	1.245	70.4	20.5	.095
A28	101.4	99.5	83.9	1.235	69.1	20.4	.052
A29	102.4	99.0	84.3	1.239	69.0	20.5	.097
A30	101.2	100.3	83.2	1.232	68.6	20.4	-.026
A31	100.3	99.5	84.3	1.232	68.2	20.4	.030
A32	100.4	99.7	83.5	1.235	68.4	20.5	.028
A33	99.2	95.2	83.0	1.234	67.8	20.5	.489
A34	97.5	88.9	81.4	1.233	66.5	21.2	1.166
A35	101.7	99.7	84.9	1.236	69.4	20.4	.034
A36	103.1	99.7	85.5	1.236	70.2	20.4	.029
A37	102.5	100.6	85.0	1.234	69.6	20.4	-.050
A38	103.0	99.5	86.0	1.236	70.3	20.4	.053
A39	100.5	100.4	83.9	1.230	67.9	20.3	-.039
A40	102.7	100.6	85.6	1.231	69.6	20.3	-.061
A41	102.7	100.1	85.4	1.239	69.7	20.4	-.000
A42	103.7	100.6	86.4	1.230	70.1	20.5	-.050
A43	102.0	99.9	84.1	1.230	69.5	20.8	.007
A44	101.7	100.2	85.1	1.234	69.2	20.0	-.021
A45	100.7	101.0	84.4	1.227	67.9	20.7	-.101
A46	94.1	96.3	79.7	1.210	63.2	20.7	.382
A47	94.5	97.4	79.9	1.202	63.3	20.5	.261
A48	95.3	96.4	80.0	1.224	64.1	20.6	.340
A49	93.6	99.2	78.0	1.205	62.1	20.4	.079
MEAN:	100.4	98.9	84.0	1.236	68.5	20.5	.114
STD DEV:	2.4	2.0	1.7	.011	2.0	.2	.204
UPR LIM:	105.2	102.8	87.5	1.257	72.5	21.0	.522
LWR LIM:	95.5	95.0	80.5	1.214	64.5	20.1	-.294

CELLS OUTSIDE THE 95% CONFIDENCE LIMITS

A18	0.0	0.0	0.0	0.000	0.0	20.1	0.000
A19	0.0	0.0	0.0	0.000	0.0	20.1	0.000
A34	0.0	88.9	0.0	0.000	0.0	21.2	1.166
A46	94.1	0.0	79.7	1.210	63.2	0.0	0.000
A47	94.5	0.0	79.9	1.202	63.3	0.0	0.000
A48	95.3	0.0	80.0	0.000	64.1	0.0	0.000
A49	93.6	0.0	78.0	1.205	62.1	0.0	0.000

Table 11. Self-Discharge Data on Level I Cells

CELL	CYC	START DATE & TIME	END DATE & TIME	HOURS	AMP-HR	AVG-AMPS
A5	11	1983: 57: 8: 6:10	1983: 60:12:10:41	76.075	29.41	.3866
A6	11	1983: 57: 8:12:26	1983: 60:12: 0:33	75.935	28.92	.3809
A7	11	1983: 57: 8: 8:57	1983: 60:12:21:29	76.342	32.15	.4211
A8	11	1983: 57:15: 8:43	1983: 60:12:24:43	69.267	32.99	.4761
A9	11	1983: 57: 8: 6:10	1983: 60:12: 4:10	75.969	27.08	.3659
A10	11	1983: 78: 8:19:11	1983: 82:15:50:13	103.651	36.32	.3504
A11	11	1983: 57: 8: 7:13	1983: 60:12: 7:28	76.004	28.49	.3740
A12	11	1983: 63: 3:46:98	1983: 66:16:54:22	85.124	33.35	.3918
A13	11	1983: 63: 3:57:28	1983: 66:17:30:23	85.603	44.24	.5163
A14	11	1983: 63: 3: 5:53	1983: 66:16:57:30	85.860	34.13	.3975
A15	11	1983: 63: 2:43:13	1983: 66:16:25: 0	85.696	26.04	.3039
A16	11	1983: 63: 3:52:15	1983: 66:17:22:13	85.499	40.25	.4708
A17	11	1983: 63: 3:55:23	1983: 66:17:22:13	85.447	40.26	.4712
A18	11	1983: 57:15:46:53	1983: 60:12: 1: 1	68.235	27.22	.3989
A19	11	1983: 57:15:49: 0	1983: 60:12: 9:36	68.343	29.33	.4292
A20	11	1983: 71: 4:55:15	1983: 74:11: 0:10	78.082	33.19	.4251
A21	11	1983: 71: 4:47:42	1983: 74:10:53:41	78.100	31.66	.4054
A22	11	1983: 71: 4:53: 6	1983: 74:10:40:17	77.920	30.33	.3892
A23	11	1983: 71: 4:53: 6	1983: 74:10:47:13	77.902	30.01	.3852
A24	11	1983: 78: 8:34:49	1983: 82:16: 0:21	103.426	36.02	.3860
A25	11	1983: 71: 5: 3:51	1983: 74:11:39:10	78.589	42.05	.5432
A26	11	1983: 71: 5: 0:37	1983: 74:11:29:37	78.483	40.56	.5168
A27	11	1983: 71: 5:12:23	1983: 74:11:10:89	77.976	33.99	.4359
A28	11	1983: 78: 8:40: 2	1983: 82:16:32:19	103.871	44.79	.4312
A29	11	1983: 71: 5: 2:44	1983: 74:11:14:14	78.192	34.85	.4457
A30	11	1983: 71: 4:36:98	1983: 74:10:51:36	78.244	29.17	.3720
A31	11	1983: 78: 7: 3: 9	1983: 82:16: 2:89	104.909	37.34	.3557
A32	11	1983: 78: 7:15:89	1983: 82:15:51:49	104.603	34.74	.3321
A33	11	1983: 71: 4:11:47	1983: 74:13.13:19	81.026	64.64	.7978
A34	11	1983: 71: 4:06:15	1983: 74:10:85: 3	85.980	123.96	1.4417
A35	11	1983: 71: 4: 2: 2	1983: 74:10:54:51	78.880	29.83	.3782
A36	11	1983: 71: 4:24:31	1983: 74:10:40:20	78.230	29.74	.3802
A37	11	1983: 78: 8: 6:26	1983: 82:15:40: 6	103.661	31.55	.3044
A38	11	1983: 71: 4:37:46	1983: 74:11: 2:22	78.410	33.22	.4237
A39	11	1983: 71: 3:40: 5	1983: 74:10:26:44	78.644	24.35	.3096
A40	11	1983: 71: 4:14: 2	1983: 74:10:22:25	78.148	23.29	.298:
A41	11	1983: 71: 4:12:57	1983: 74:10:29:50	78.284	25.10	.3217
A42	11	1983: 71: 4:21:34	1983: 74:10:28:53	78.122	25.15	.3219
A43	11	1983: 86: 7:26:22	1983: 89:13.30: 3	78.061	23.32	.2987
A44	11	1983: 86: 7:41:58	1983: 89:13.34:18	77.872	24.43	.3137
A45	11	1983: 86: 7: :3	1983: 89:13: : 70	78.635	16.96	.2159

-51-

Table 12. Impedance Data on Level I Cells

CELL	VOLTAGE	CURRENT AMPS	dV(mV) t=0	mOHM t=0	dV(mV) t=1 sec	mOHM t=1 sec	dV(mV) t=15	mOHM t=15
A5	1.2331	29.96	44.8	1.54	53.6	1.86	73.4	2.45
A6	1.2286	30.02	48.6	1.62	56.4	1.88	76.7	2.55
A7	1.2511	30.00	43.5	1.45	50.4	1.68	62.0	2.07
A8	1.2469	30.04	48.5	1.62	56.8	1.89	70.2	2.34
A9	1.2466	29.74	47.6	1.60	53.8	1.81	70.2	2.34
A10	1.2493	30.10	46.3	1.53	52.6	1.74	66.7	2.21
A11	1.2511	29.88	45.3	1.52	51.9	1.74	66.5	2.23
A12	1.2553	30.00	42.5	1.41	50.9	1.69	62.4	2.07
A13	1.2566	30.00	42.5	1.42	50.1	1.67	60.5	2.02
A14	1.2514	30.00	42.8	1.43	49.2	1.64	64.4	2.15
A15	1.2504	29.96	43.3	1.45	50.4	1.68	65.2	2.18
A16	1.2542	29.99	45.7	1.53	52.8	1.76	64.1	2.14
A17	1.2401	29.99	45.3	1.51	52.4	1.75	64.9	2.17
A18	1.2548	29.84	44.8	1.54	52.0	1.79	62.8	2.16
A19	1.2570	29.88	44.8	1.52	51.8	1.76	61.2	2.11
A20	1.2487	30.04	47.2	1.57	53.9	1.79	67.1	2.23
A21	1.2483	30.10	47.0	1.56	54.1	1.80	66.0	2.22
A22	1.2396	30.14	46.2	1.53	53.7	1.78	70.0	2.32
A23	1.2385	31.12	49.6	1.65	55.7	1.85	70.9	2.35
A24	1.2571	30.10	43.2	1.43	49.3	1.63	60.7	2.01
A25	1.2516	30.00	46.6	1.55	52.2	1.74	64.5	2.14
A26	1.2581	30.20	42.6	1.41	48.6	1.61	60.8	2.01
A27	1.2542	29.82	48.0	1.61	52.7	1.77	66.4	2.24
A28	1.2542	30.16	46.8	1.55	52.0	1.72	63.6	2.11
A29	1.2447	29.86	46.8	1.57	53.6	1.80	60.2	2.20
A30	1.2522	29.92	42.8	1.43	49.2	1.64	63.1	2.11
A31	1.2504	30.20	44.6	1.48	50.3	1.67	60.1	1.99
A32	1.2604	30.10	44.9	1.49	50.0	1.66	58.2	1.93
A33	1.2561	29.96	45.1	1.51	49.9	1.67	59.9	2.00
A35	1.2595	29.76	40.9	1.38	46.9	1.58	57.6	1.94
A36	1.2563	30.16	45.0	1.49	50.0	1.66	61.4	2.03
A37	1.2622	30.10	43.9	1.46	49.2	1.63	58.3	1.94
A38	1.2500	30.12	46.4	1.54	51.8	1.72	63.6	2.11
A39	1.2591	29.80	45.2	1.52	49.5	1.66	59.2	1.99
A40	1.2628	29.84	44.4	1.49	49.1	1.64	57.4	1.92
A41	1.2632	29.98	41.6	1.39	46.0	1.54	55.1	1.84
A42	1.2577	30.18	45.2	1.50	48.8	1.62	58.7	1.95
A43	1.2564	30.66	43.3	1.41	48.7	1.59	58.8	1.92
A44	1.2540	30.70	43.7	1.42	48.8	1.59	61.2	1.99
A45	1.2545	30.64	45.4	1.49	51.0	1.66	63.0	2.06

Life Tests

The major portion of the Level I test program was directed towards determining cell life under simulated mid-altitude and geosynchronous satellite operating conditions.

Mid-Altitude Tests

i) Depth of Discharge

Groups of 5 cells were cycled to 40, 60 and 80% DOD (based on a cell capacity of 80 Ah) in 0.75 hours and recharged in a maximum of 5.25 hours. Cells that reached top of charge in less than 5.25 hours were allowed to rest before the next discharge (see Figure 17). Since the total cycle time was 6 hours the cells accumulated exactly 4 cycles /day. This cycling routine was performed continuously until the cells failed.

The cycle life data from these tests are plotted in Figures 22 to 30. The plots are of coulombic (Ah) efficiency, leakage current and average discharge voltage versus number of cycles for each depth of discharge. Some plots, for the sake of clarity, show only the worst and best cells within the group. In general, the overall shape of the curves for each set of cell data are very similar irrespective of whether a cell is short or long-lived. A plateau region is followed by a fairly sharp deviation in either a positive or negative direction. The length of the plateau region essentially determines the life of the cell.

On comparing the data for cells discharged to the three different depths of discharge, the coulombic efficiency early in the life of a cell is dependent upon the depth of discharge. The greater the depth of discharge the higher the coulombic efficiency, although for all cells it is $\geq$ 94%. The leakage current for all cells lies between 150-400 mA early in the life of the cells and remains within this range until the onset of failure when it increases dramatically.
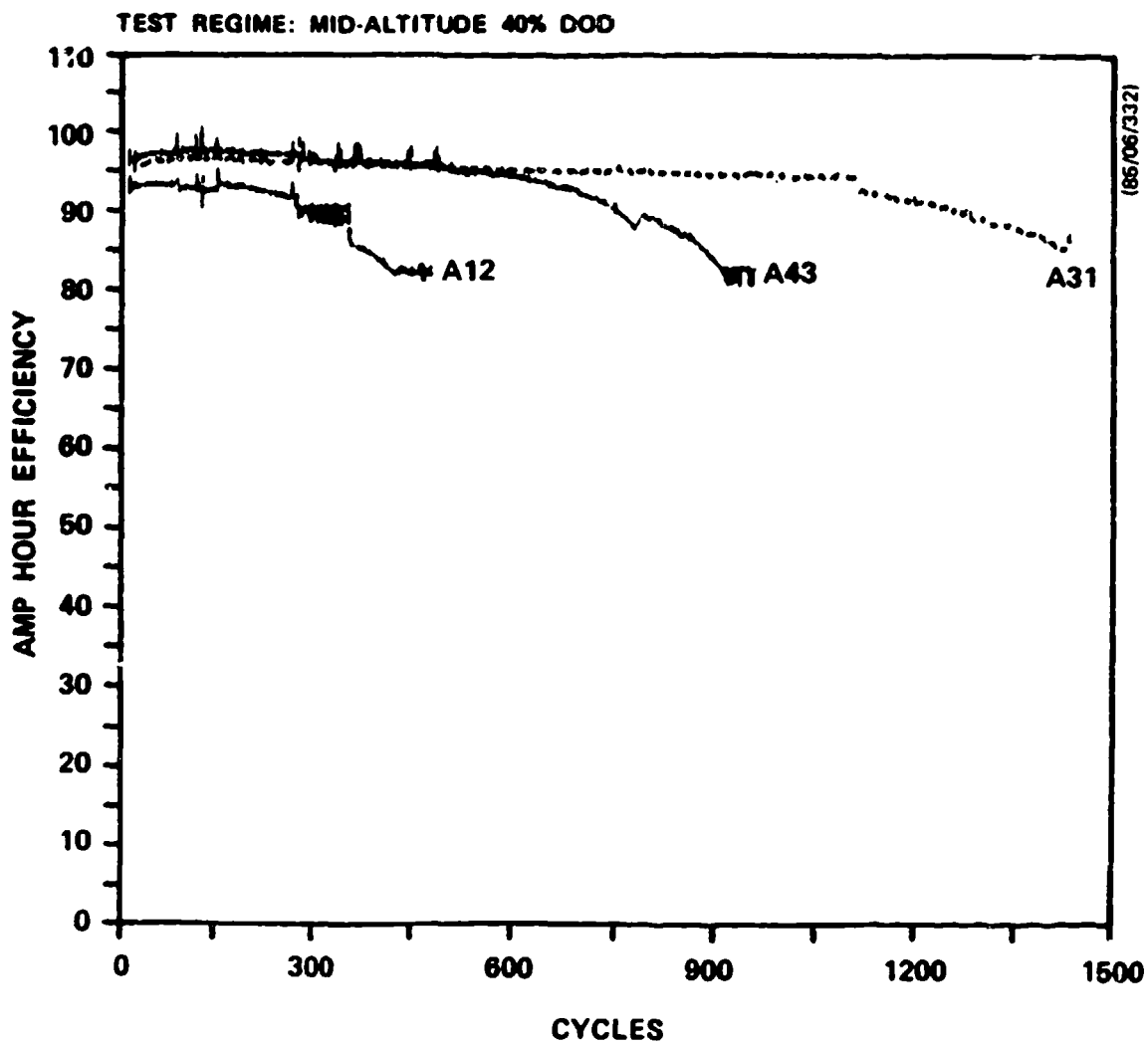
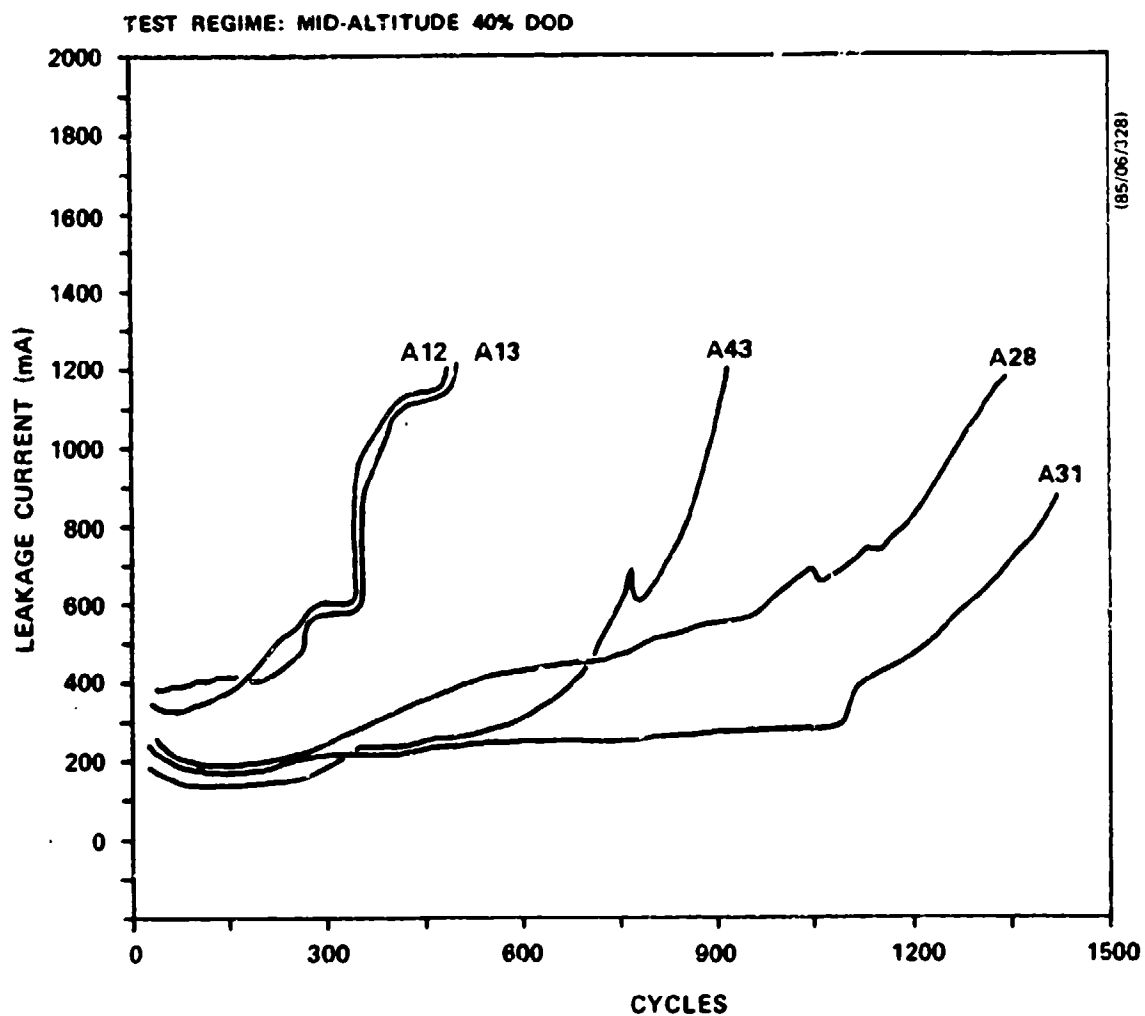Figure 22. Coulombic Efficiency with Cycling for 40% DOD Test on Mid-Altitude Regime

TEST REGIME: MID-ALTITUDE 40% DOD

(85/06/128)

LEAKAGE CURRENT (mA)

2000
1800
1600
1400
1200
1000
800
600
400
200
0

A12 A13   A43   A28

A31

0   300   600   900   1200   1500

CYCLES

Figure 23.   Leakage Current with Cycling for 40% DOD Test on Mid-Altitude
Regime

-55-
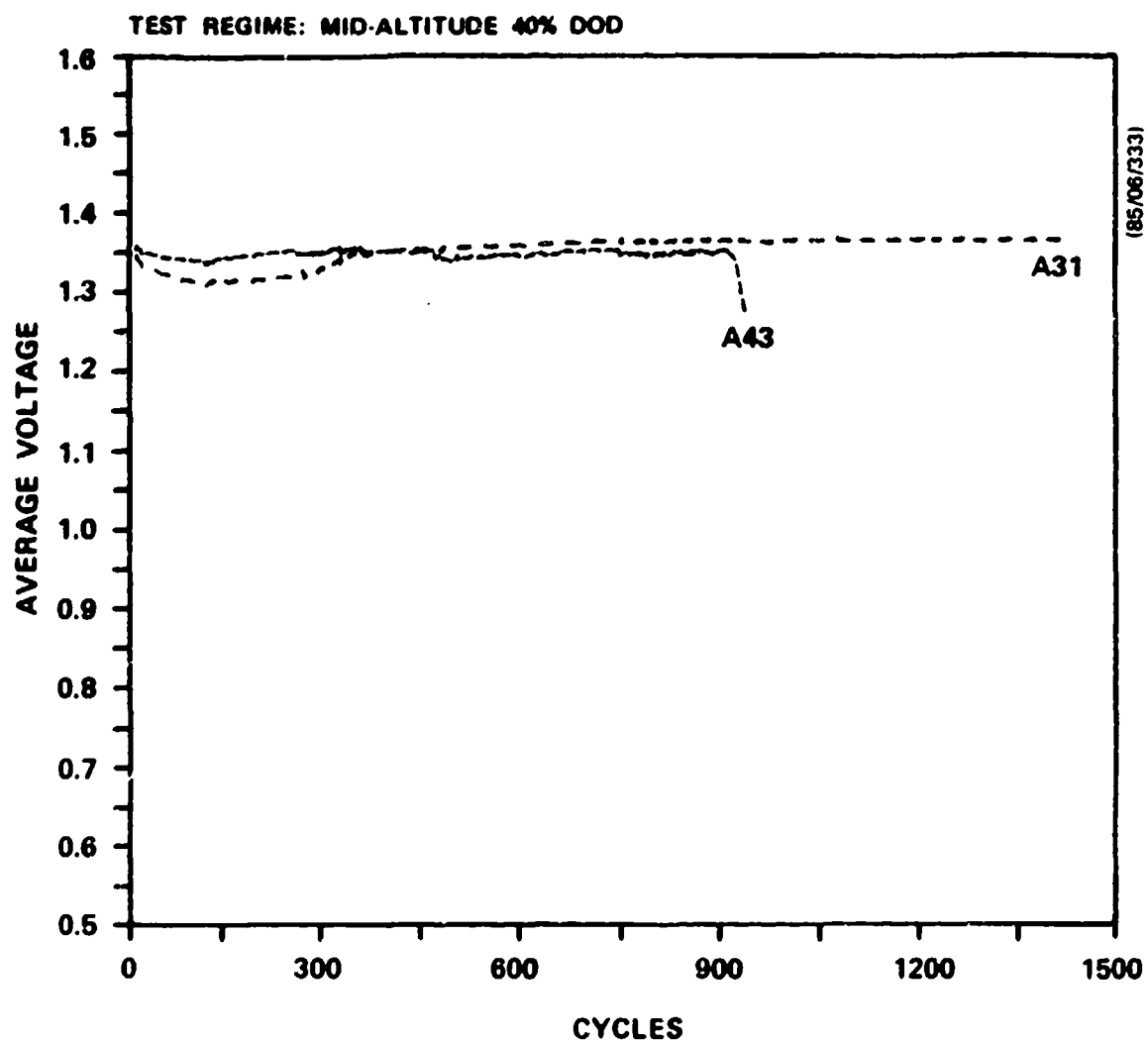
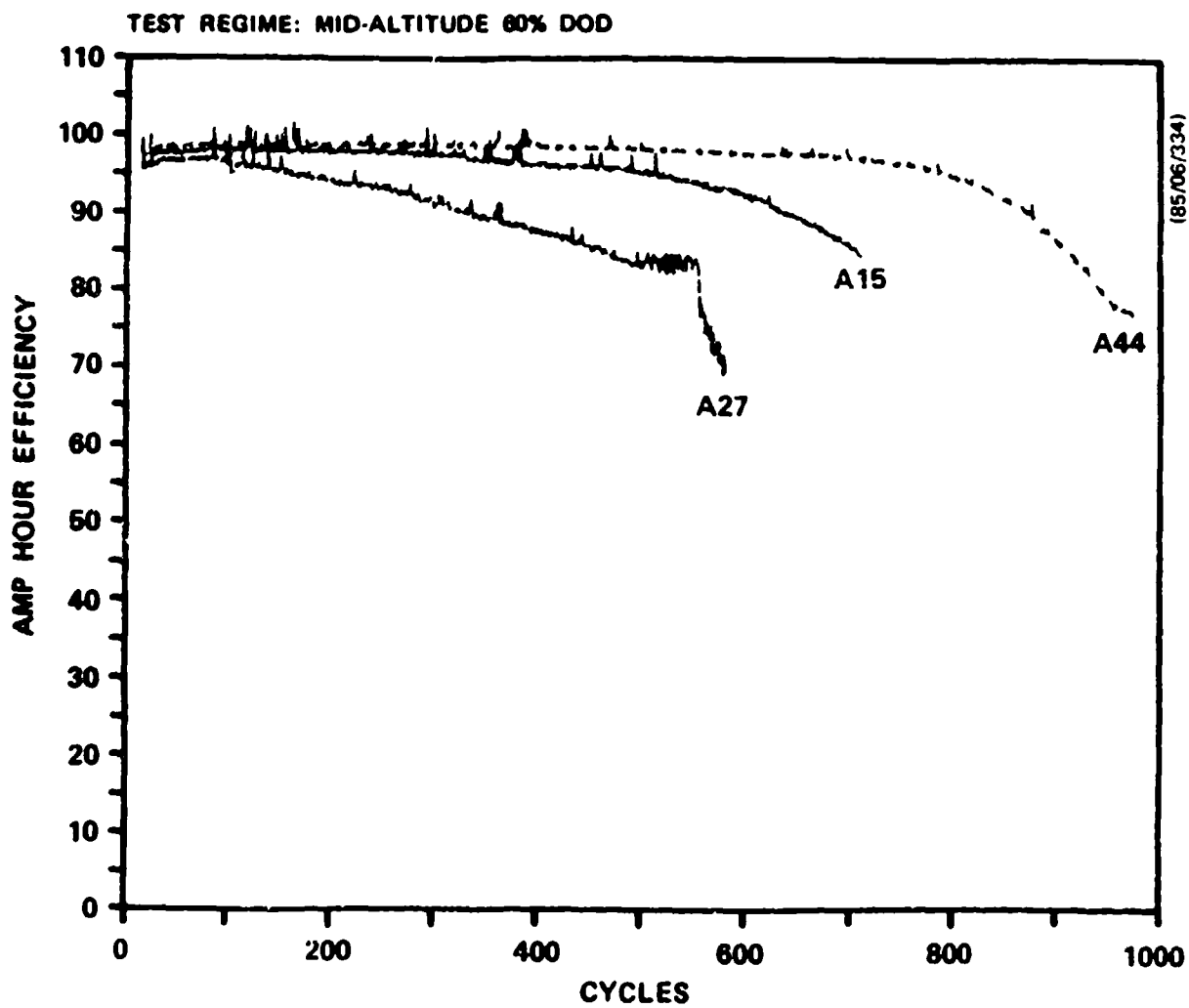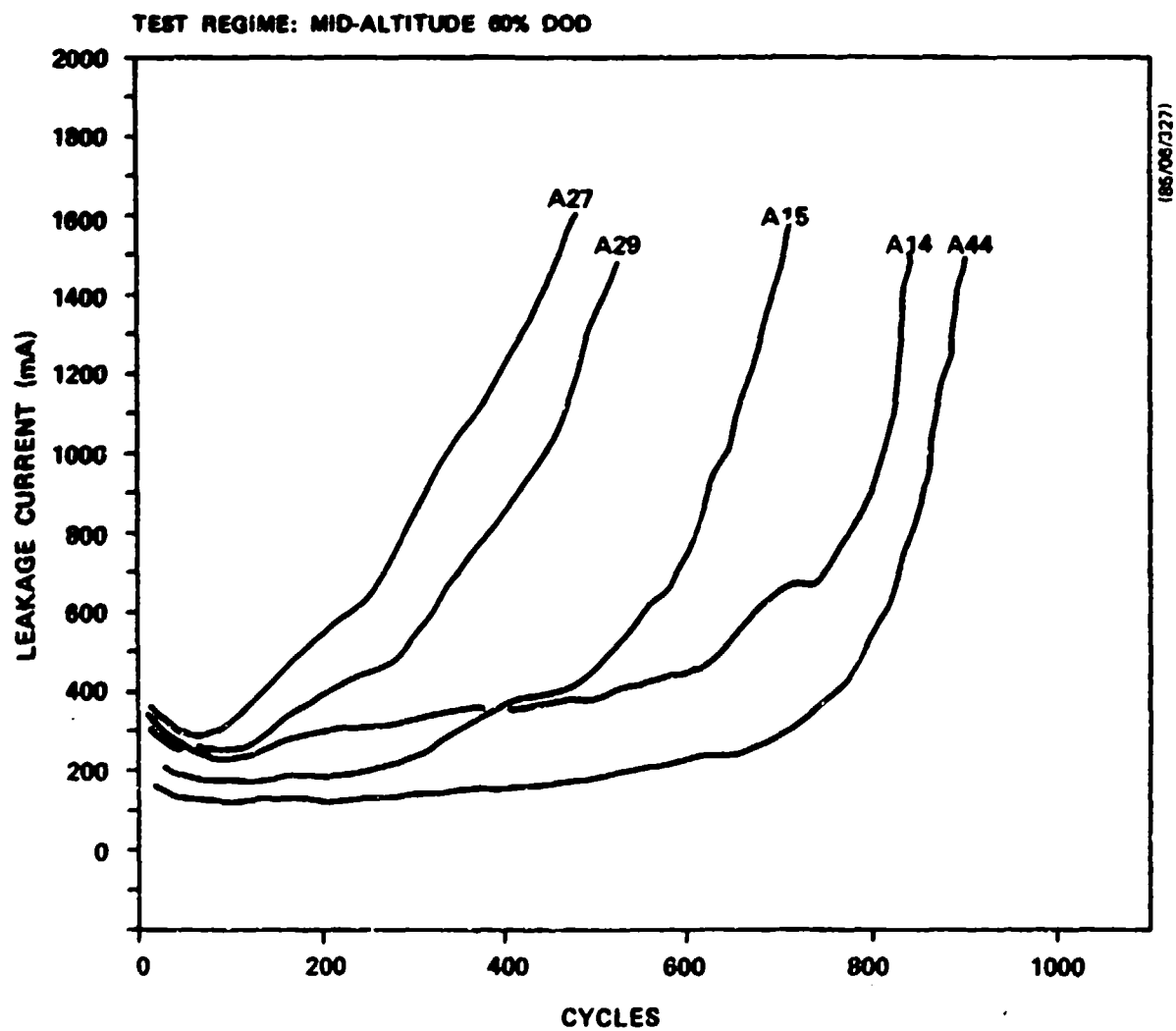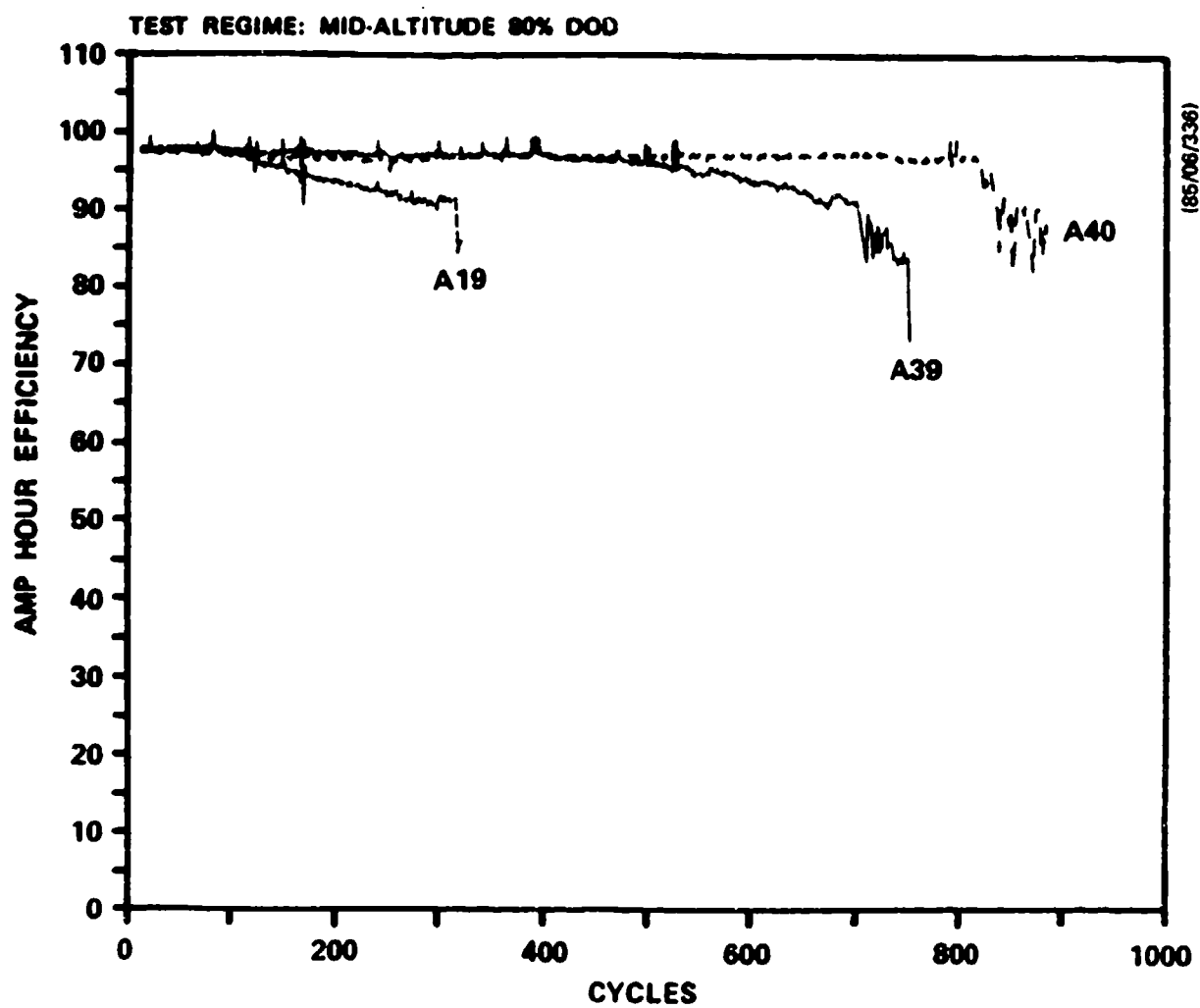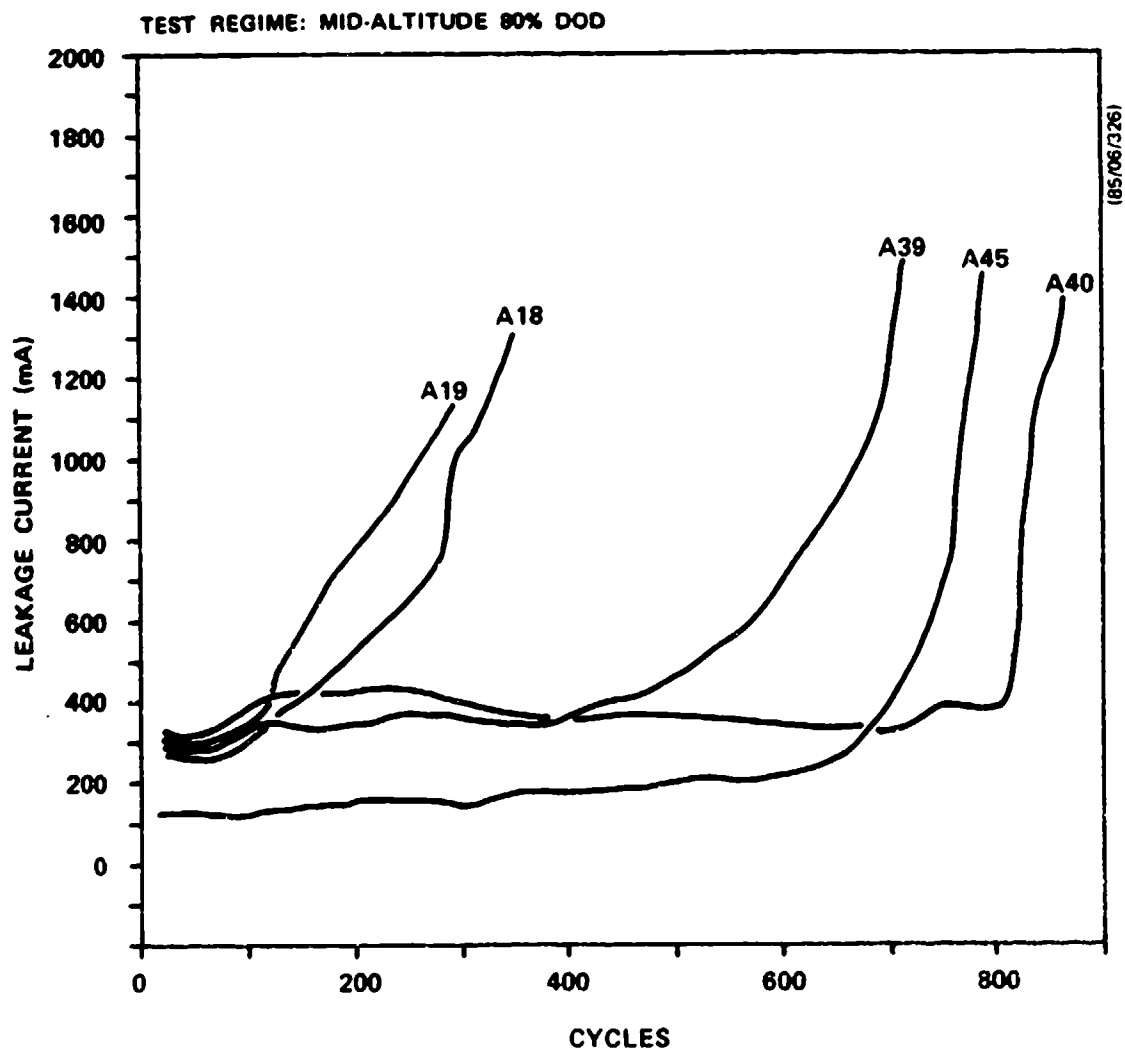Figure 24. Average Discharge Voltage with Cycling for 40% DOD Test on Mid-Altitude Regime

-56-

TEST REGIME: MID-ALTITUDE 60% DOD

(85/06/334)

Figure 25. Coulombic Efficiency with Cycling for 60% DOD Test on Mid-Altitude
Regime

Figure 26.   Leakage Current with Cycling for 60% DOD Test on Mid-Altitude
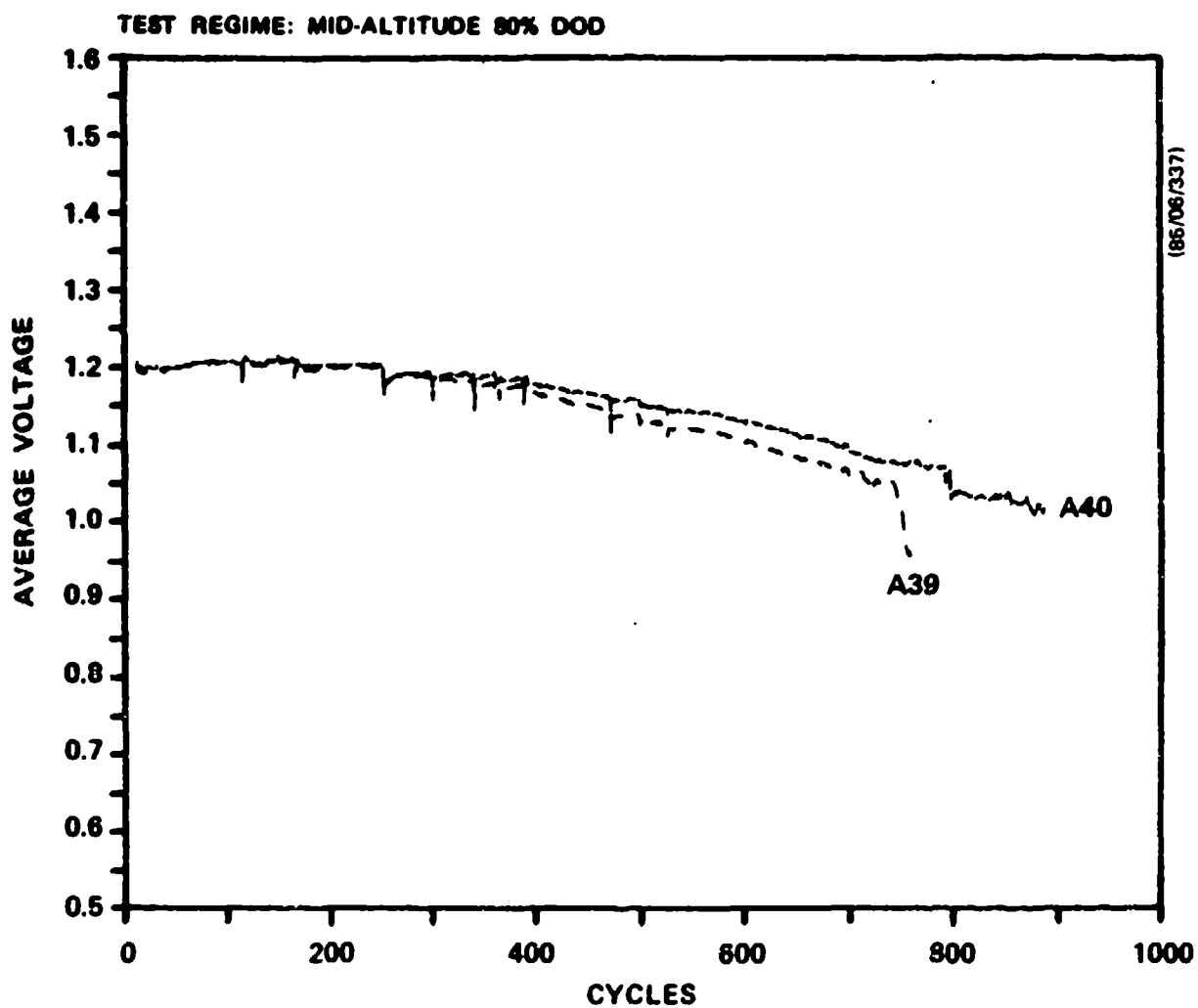   Regime
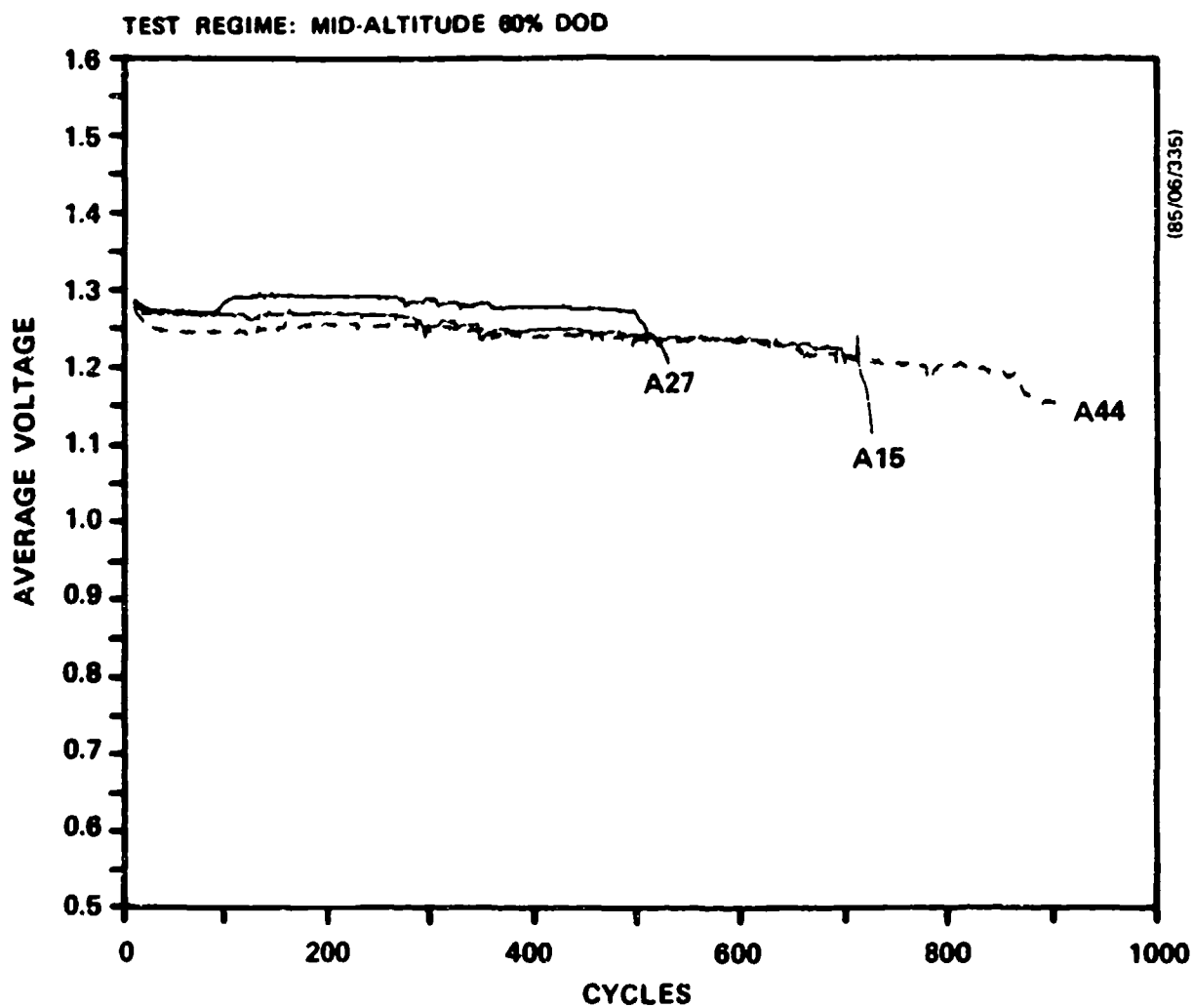
Figure 27. Average Discharge Voltage with Cycling for 60% DOD Test on Mid-Altitude Regime

Figure 28. Coulombic Efficiency With Cycling for 80% DOD Test on Mid-Altitude
Regime

-60-

Figure 29. Leakage Current with Cycling for 80% DOD Test on Mid-Altitude
            Regime

Figure 30.   Average Discharge Voltage with Cycling for 80% DOD Test on
             Mid-Altitude Regime

A high leakage current is attributed to extensive internal shorting within a cell. A leakage current of 1000 mA was selected as the failure point for determining cell life and not the original failure criteria defined in the contract statement of work. The reason for disregarding the failure criteria in the statement of work was that it defined cell failure as the point at which a cell is unable to deliver the load current for the specified time interval at a voltage $\geq$ 75% of the rated voltage under load; a condition that could always be met provided a cell was capable of being charged. The inability to charge a cell within the maximum specified time was the primary reason for failure and this is directly related to the cell leakage current, hence the 1000 mA failure criteria.

The average discharge voltage stayed relatively constant with cycling for cells on the 40% and 60% DOD regimes but did exhibit a steady decline on the 80% DOD regime. As would be expected, the average discharge voltage decreased as the depth of discharge increased (ie 1.34 volts at 40% DOD to 1.19 volts at 80% DOD).

The voltage profiles for cells at the three depths of discharge at the beginning and end of life are shown in Figures 31 to 33. The discharge voltage profiles change with cycling on the 60 and 80% DOD regimes but remain stable on the 40% DOD regime, in fact there was a small improvement in cell voltage for some of the cells. The voltage profiles after 200 cycles are compared in Figure 34 for cells on the three depth of discharge regimes. As one might expect the voltage profile is dependent upon the depth of discharge to which the cell is taken, with the shallowest depth of discharge having the highest voltage profile.

The life of the cells tested under the mid-altitude test regime are tabulated in Table 13. There is considerable overlap in the cycle life of the cells at the various depths of discharge. On averaging the cycle life data for each depth of discharge it is found that the mean life decreases with increasing depth of discharge. However, the effect of depth of discharge on
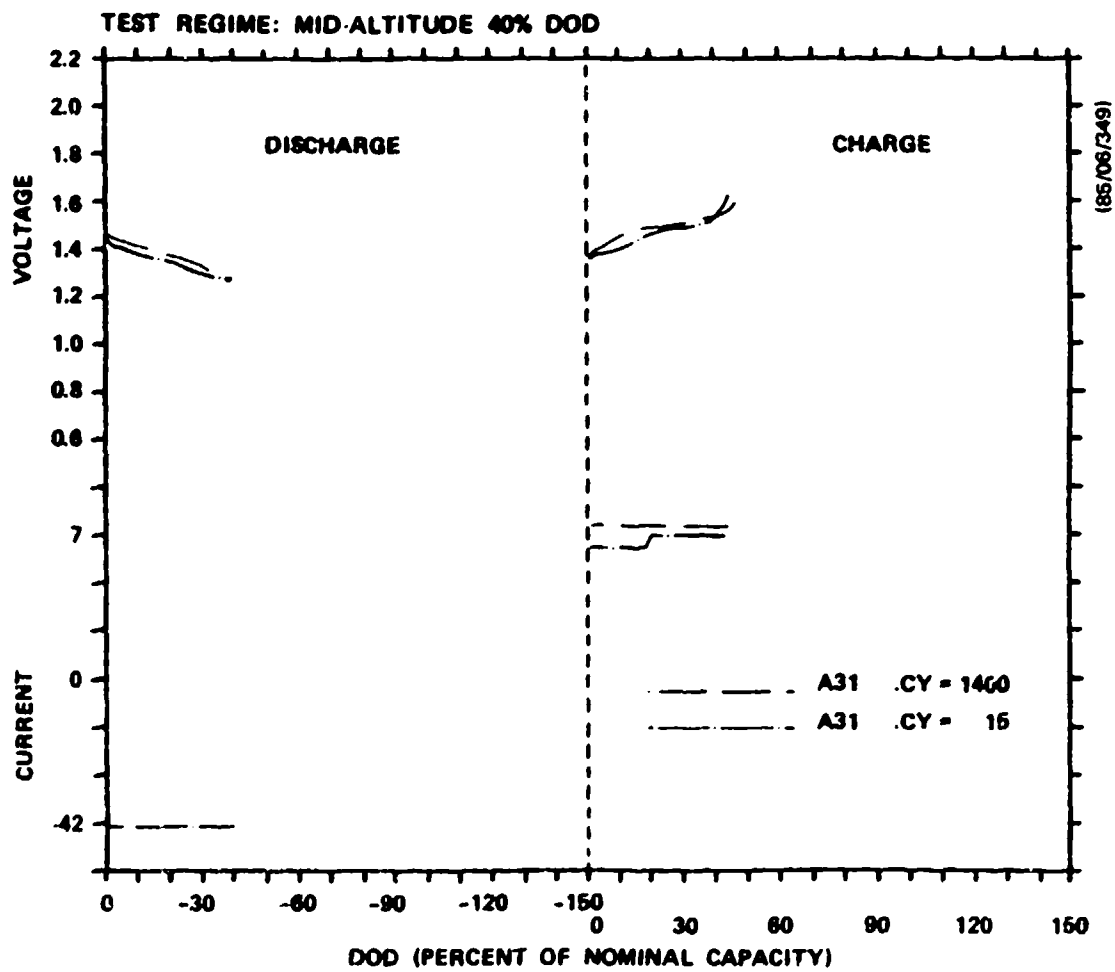
-63-

Figure 31. Cell Voltage Profiles with Cycling for 40% DOD Test on
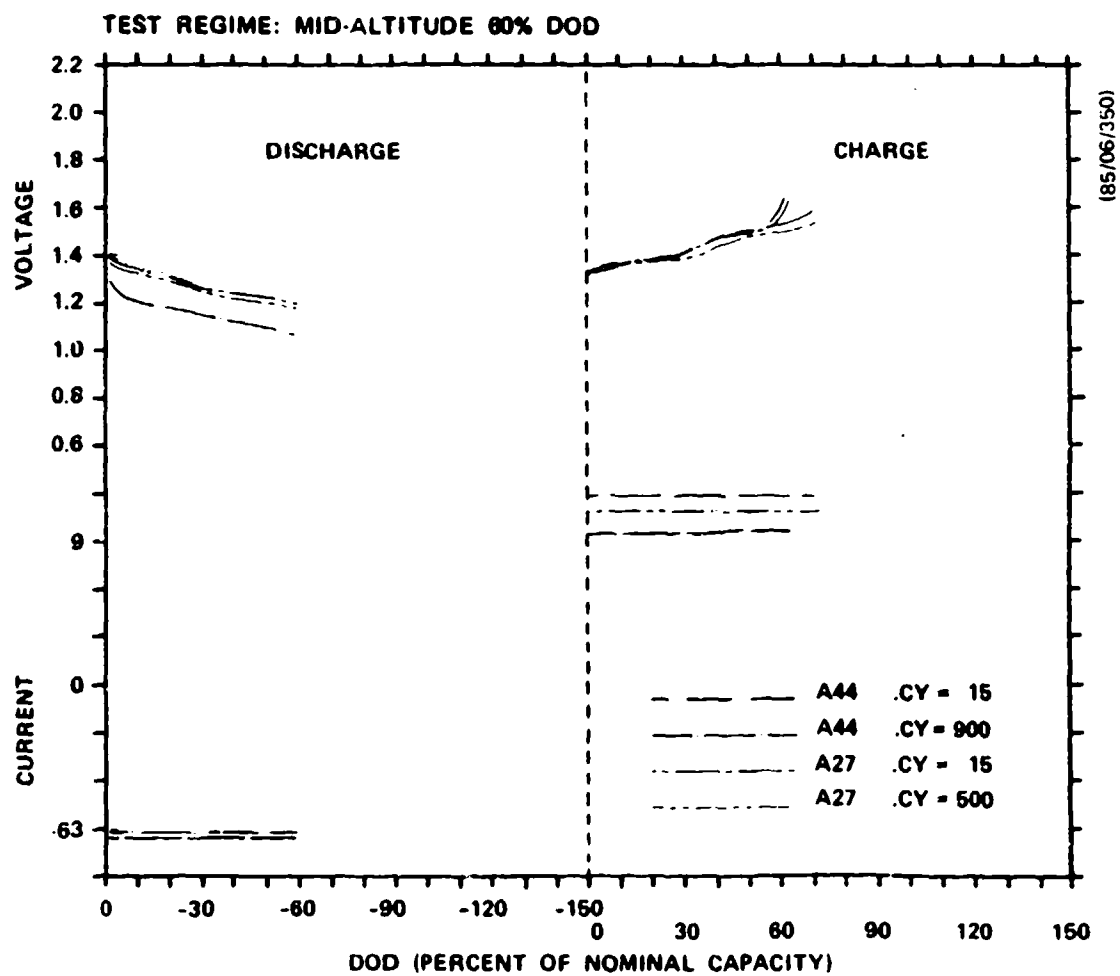Mid-Altitude Regime

Figure 32. Cell Voltage Profiles with Cycling for 60% DOD Test on
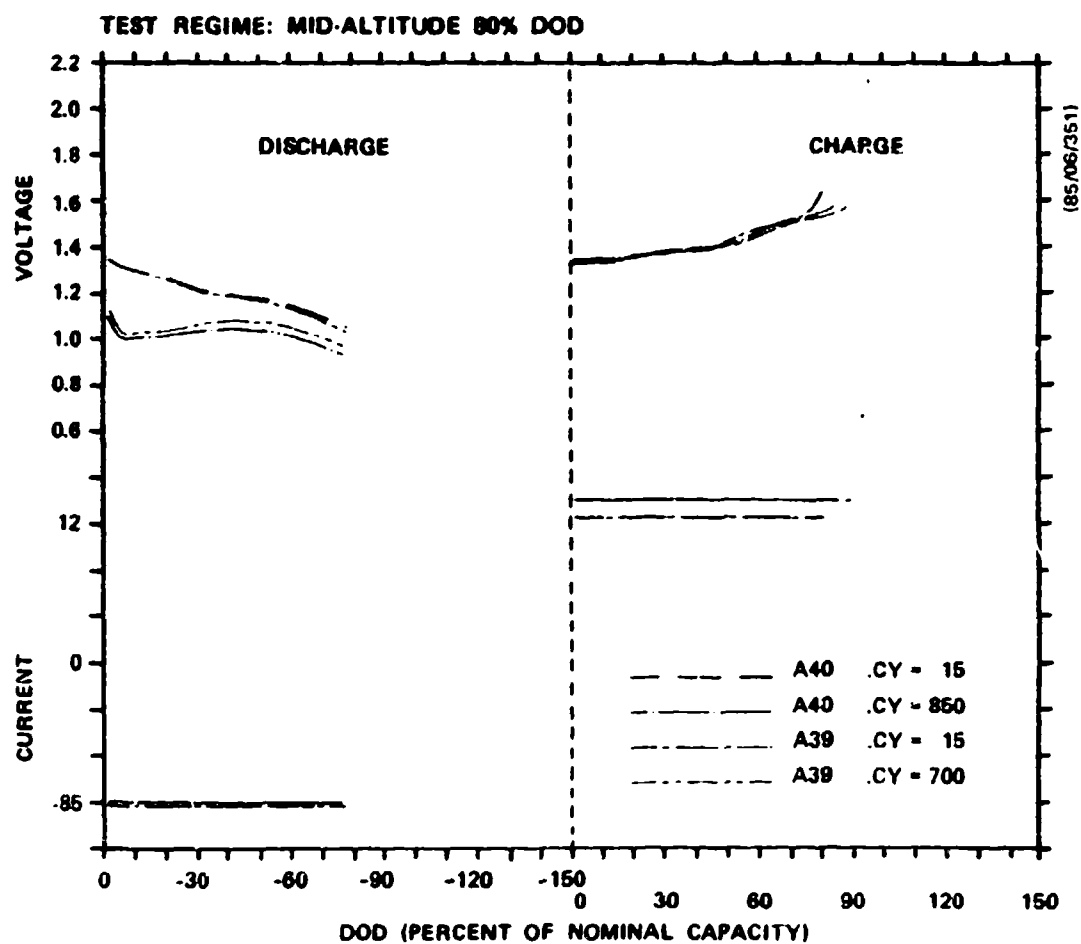Mid-Altitude Regime

Figure 33. Cell Voltage Profiles with Cycling for 80% DOD Test on
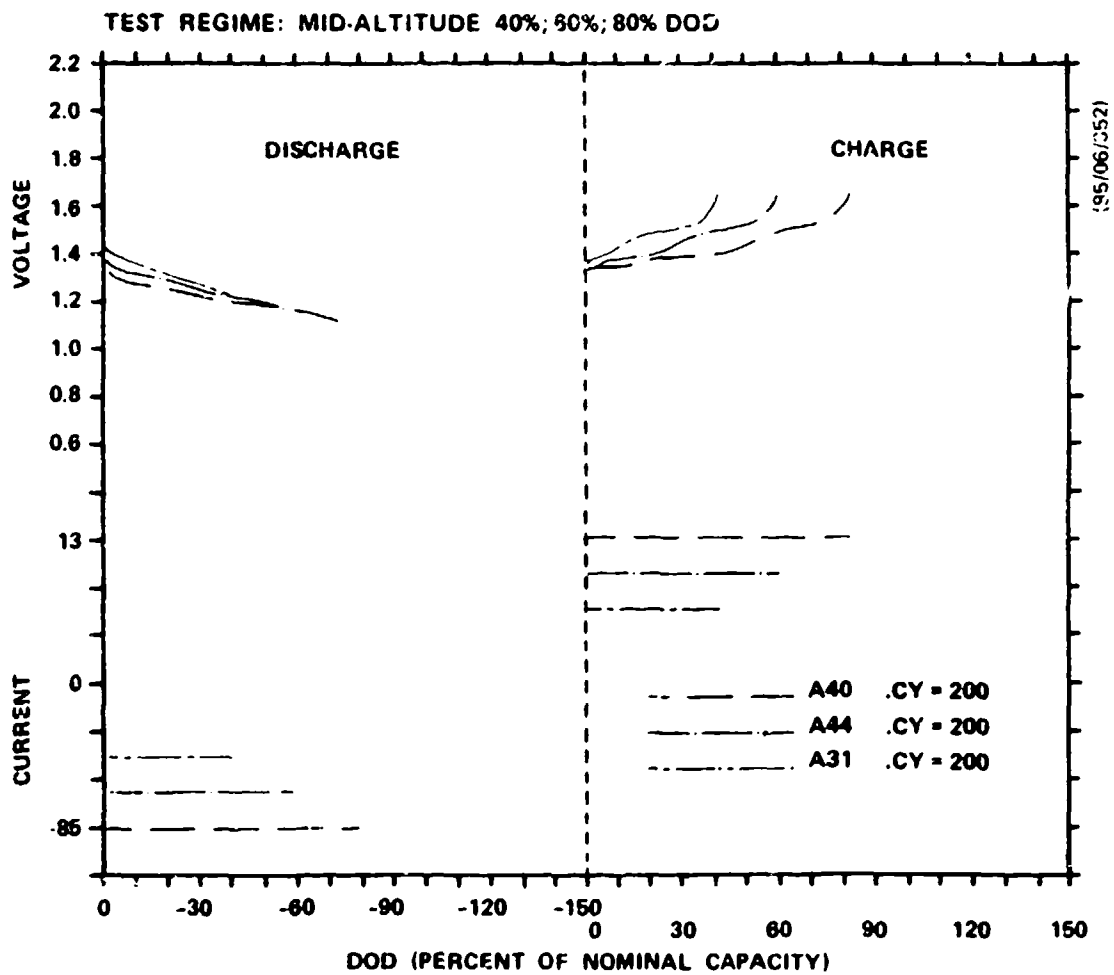Mid-Altitude Regime

Figure 34. Comparison of Cell Voltage Profiles on Cycle 200 for 40, 60
and 80% DOD Tests on Mid-Altitude Regime

Table 13. Summary of Cycle Life and Calendar Life for Level I Cells

Discharge Regime	Depth of Discharge	Cell Number	Number of Cycles	Number of Days at Temp.	Cycle Life (No of Cycles) Mean Life	Std Dev	Calendar Life (Days) Mean Life	Std Dev
Mid-Altitude	40%	A12	385	131				
		A13	367	130				
		A28	1267	349	866	487	252	120
		A31	1422	387				
		A43	889	263				
	60%	A14	816	235				
		A15	642	194				
		A27	355	111	626	222	194	59
		A29	453	135				
		A44	865	245				
	80%	A18	319	100				
		A19	261	83				
		A39	653	187	566	260	164	68
		A40	828	232				
		A65	768	217				
	Freeze-Thaw 70%	A16	323	139				
		A17	344	151				
		A30	369	163	370	39	168	26
		A33	388	182				
		A37	425	205				
	High Rate Charac +60%	A20	570	183				
		A48	622	189	640	81	196	18
		A49	728	217				
Geosynchronous	60%	A5	91	104				
		A6	95	110				
		A22	116	129	163	94	178	95
		A23	204	222				
		A38	309	326				
	80%	A7	85	98				
		A8	94	107				
		A10	154	172	175	100	193	105
		A24	218	237				
		A42	326	351				
	Sinusoidal 17-80%	A9	416	161				
		A11	543	201				
		A25	466	172	517	89	192	28
		A26	510	192				
		A36	652	233				

life for these cells is a second order effect as will be discussed later.

ii) High Rate Characterization

The purpose of this test was to determine the effect of cycling on the performance of a cell at various rates of discharge between C/3 and 3C. The cells were continuously cycled to 60% DOD on the mid-altitude regime and periodically (ie ~ every 150 cycles) subjected to 100% DOD tests at the various discharge rates. Typical performance of this group cells in terms of coulombic efficiency, leakage current and average discharge voltage with cycling are shown in Figures 35-37. The coulombic efficiency and leakage current with cycling of these cells is very similar to the other groups of cells tested on the mid-altitude regime to 60% DOD. The average discharge voltage of a cell exhibits a sharp decline during the high rate characterization tests. The lowest average discharge voltage occurs for a 3C rate discharge to 100% DOD whereas the plateaus are the average discharge voltage for a 0.75 hour discharge to 60% DOD. The average discharge voltage at the 3C discharge rate is seen to decline with cycling, this is due to a decrease in internal cell resistance with operation. Typical discharge voltage profiles for a cell operated at different rates between C/3 and 3C is shown in Figure 38. Both the cell voltage and the utilization of active material (based on the positive electrode) decrease with increasing rate. Figure 39 shows how the cell operating temperature increases with the discharge rate when no forced cooling is provided. At the 3C discharge rate the cell temperature increases from 455°C to approximately 500°C in 20 minutes, whereas at the C/3 discharge rate the temperature increase is in the order of 2-3°C over 3 hours. When the cell is switched to the charge mode however, the temperature quickly declines to the normal operating temperature of 455°C as the endothermic charge reaction cools the cell.

The average life of 640 cycles and 196 days for this group of cells was approximately the same as for the other group of cells on the 60% DOD mid-altitude regime that were not subjected to the periodic high rate characterization tests. A typical characterization plot of specific energy
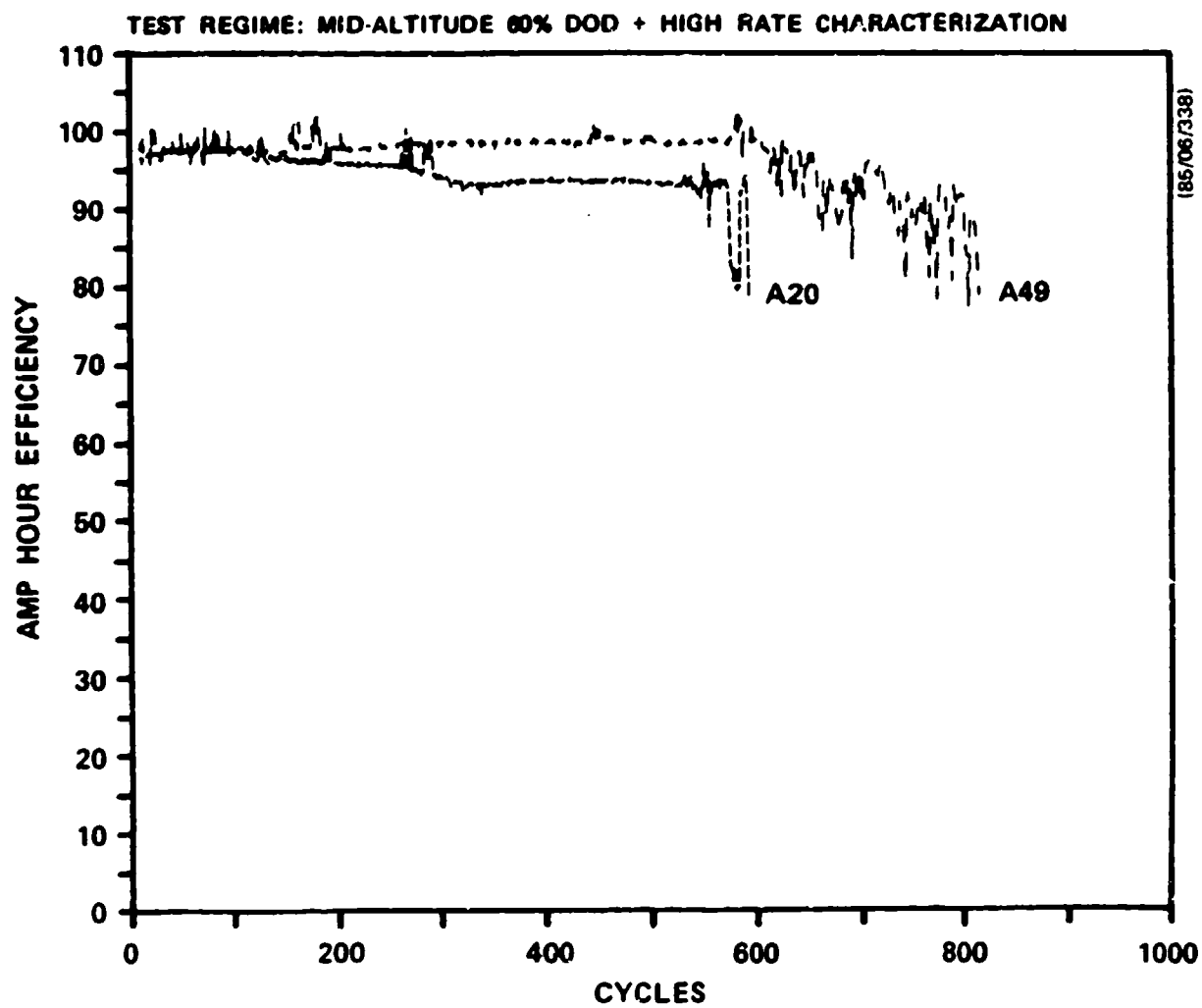
Figure 35. Coulombic Efficiency with Cycling for 60% DOD and High Rate Characterization test on Mid-Altitude Regime
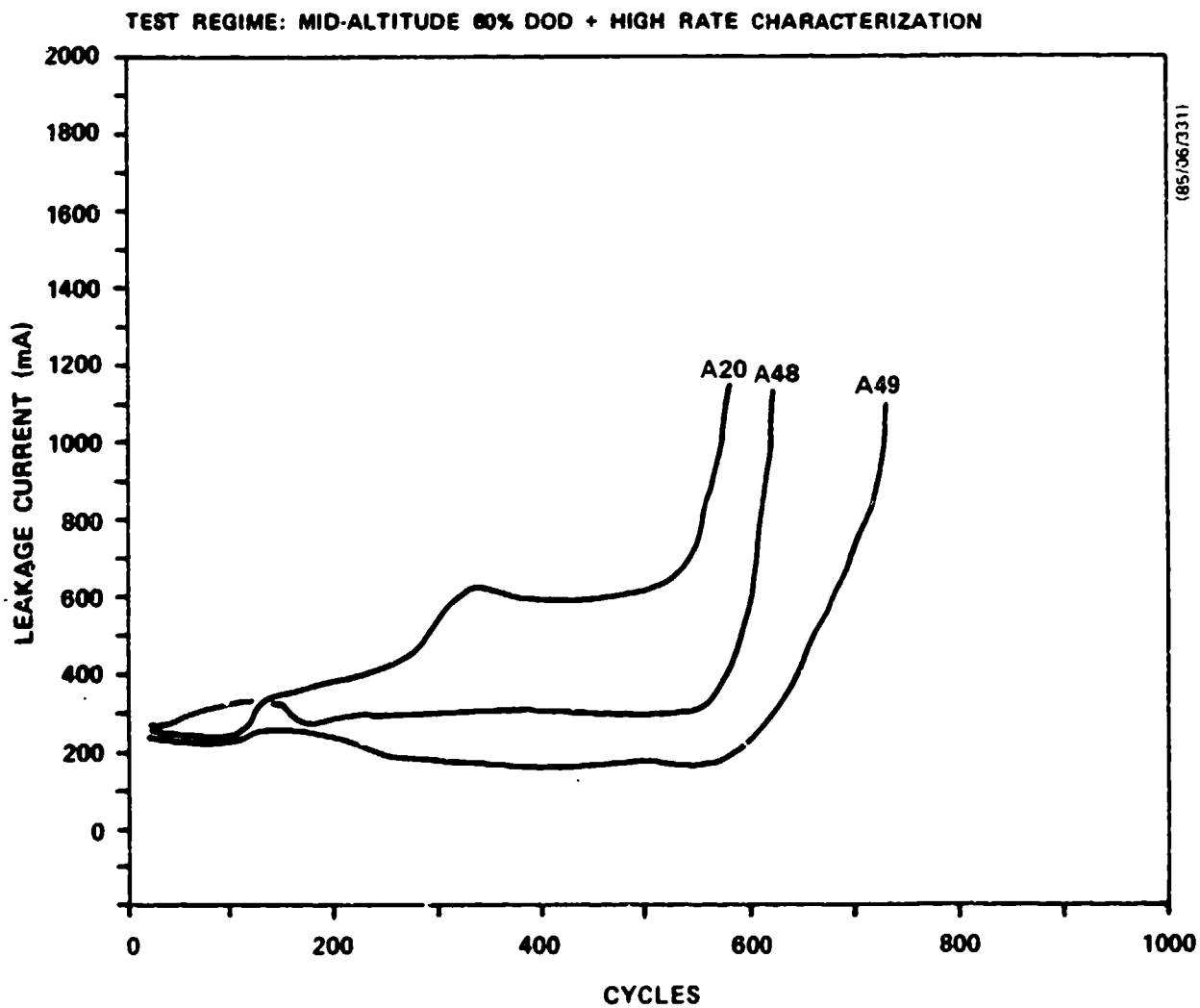
Figure 36. Leakage Current with Cycling for 60% DOD and High Rate
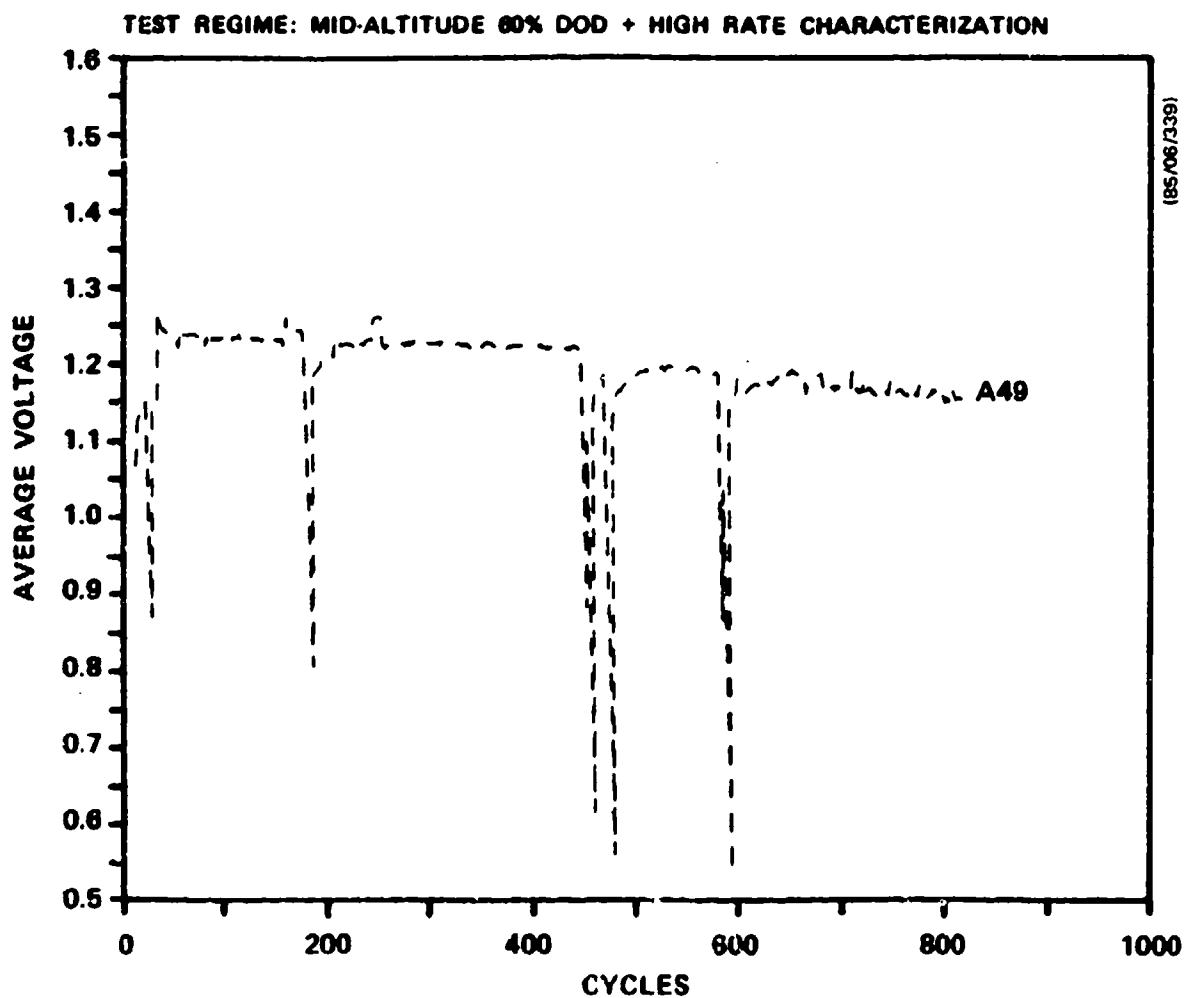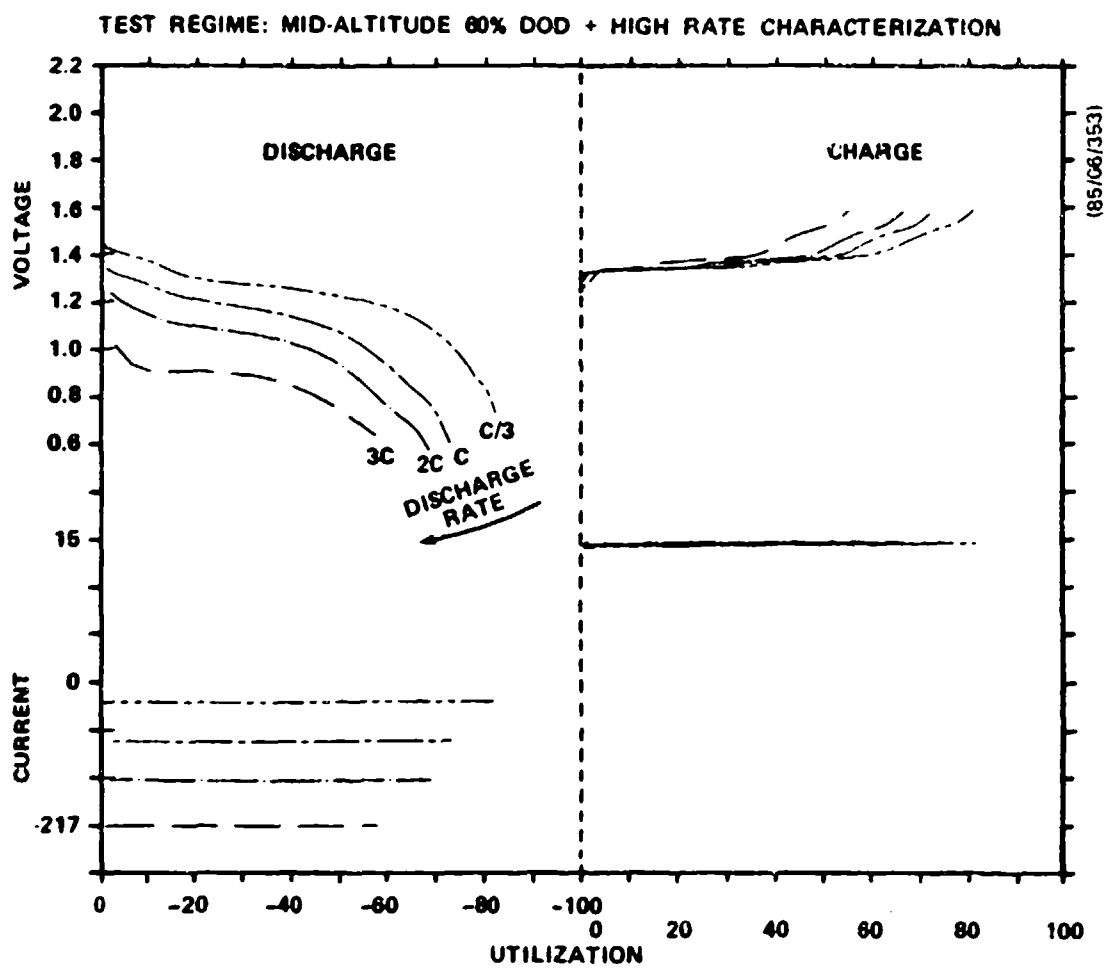Characterization Test on Mid-Altitude Regime

TEST REGIME: MID-ALTITUDE 60% DOD + HIGH RATE CHARACTERIZATION

(85/06/339)

Figure 37. Average Discharge Voltage with Cycling for 60% DOD and High Rate
Characterization Test on Mid-Altitude Regime

TEST REGIME: MID-ALTITUDE 60% DOD + HIGH RATE CHARACTERIZATION

Figure 38. Cell Voltage Profiles at Various Discharge Rates

-73-
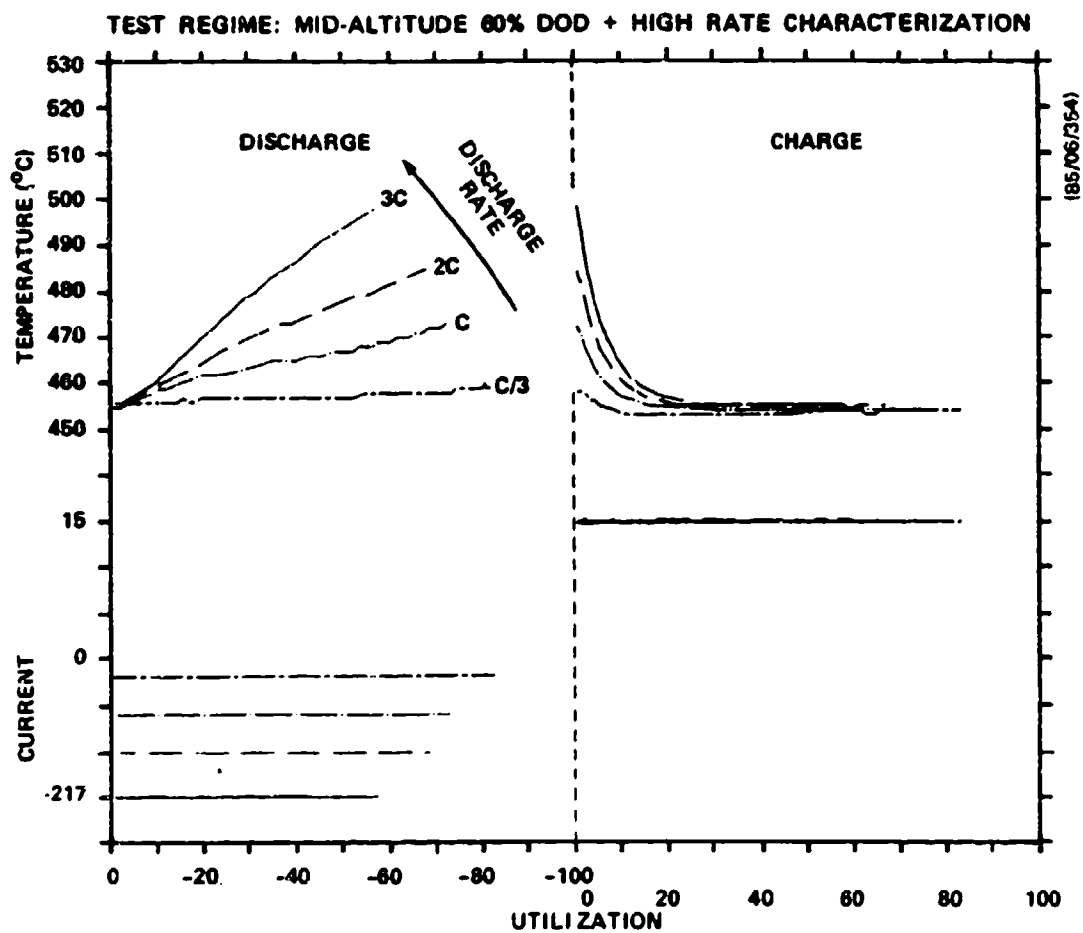
Figure 39. Cell Temperature Profiles at Various Discharge Rates

against sustained power is shown in Figure 40. The specific energy decreases with increasing discharge rate whereas the sustained power increases. The effect of cycling on the specific energy and sustained power is shown in Figure 41 for cell A48. The specific energy declines less rapidly at the lower rates of discharge with cycling. Data from all cells in this group has been plotted in Figure 42 to show an average decline in specific energy with cycling for three different rates of discharge (ie C/3, C and 3C). The rate of decline in specific energy with cycling is fairly constant for discharge rates in the range C/3 to C, but increases somewhat at the 3C discharge rate.

iii) Freeze-Thaw

The purpose of this test was to demonstrate the ability of cells to withstand repeated thermal shock without exhibiting a significant loss in performance or catastrophic failure. The test plan specified that the freeze-thaw routine was to be repeated a minimum of 30 times during cycling of the cells on the mid-altitude regime to 70% DOD.

The performance data for this group of cells in terms of coulombic efficiency, leakage current and average discharge voltage (see Figures 43-45) was very similar, throughout the life of the cells, to that exhibited by the other groups of cells on the mid-altitude test regime. The average discharge voltage for the 70% DOD test was 1.24 volts which is between the average discharge voltages of 1.27 and 1.19 volts for the 60% and 80% DOD tests respectively. The sharp decline in the average discharge voltage of cell A17 (see Figure 45) after ~ 90 cycles was due to badly oxidized and loose connections to the terminals of the cell, which when identified and replaced resulted in a return to the proper voltage value. This problem occurred several times during the test program, but was most prevalent when performing the freeze-thaw tests, most likely because of the differences in thermal expansivity of the materials employed in the connectors.

The cells completed between 26 and 35 freeze-thaw routines before failure, which clearly demonstrates the ability of the Li-alloy/FeS to
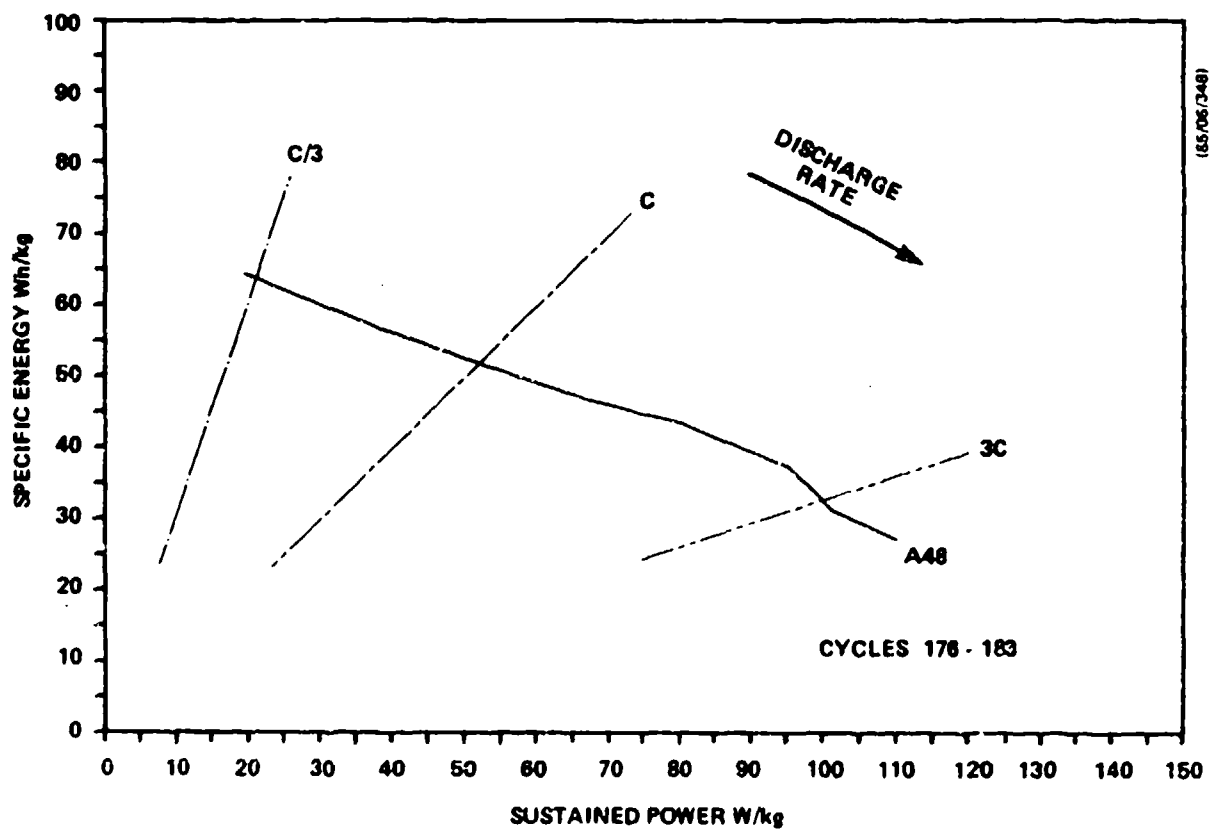
-75-

Figure 40. Cell Performance at Various Discharge Rates

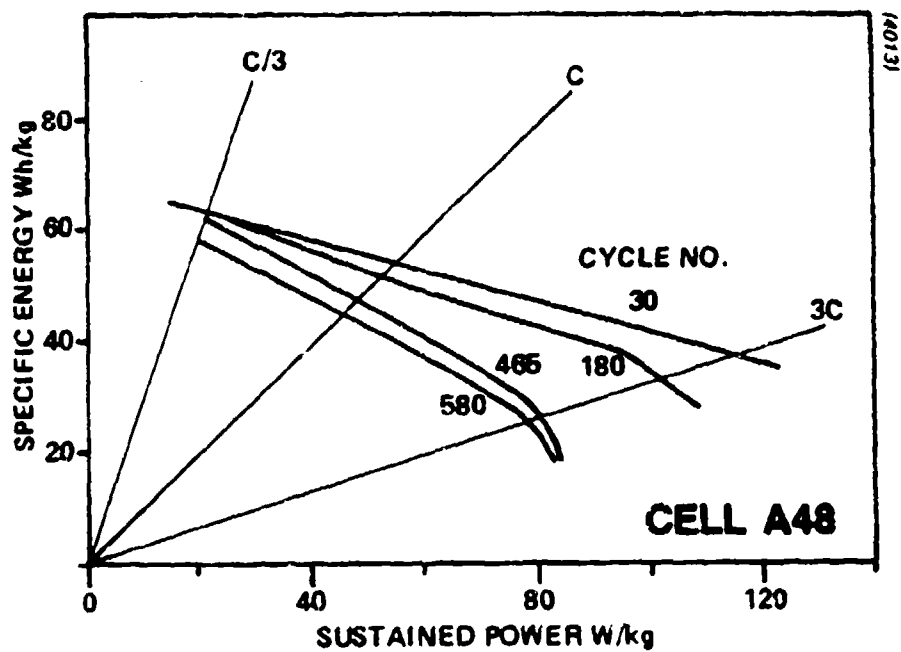TEST REGIME: MID-ALTITUDE 80% DOD + HIGH RATE CHARACTERIZATION

Figure 41.   Effect of Cycling on Specific Energy of Cell A48 at Various
             Discharge Rates

-77-

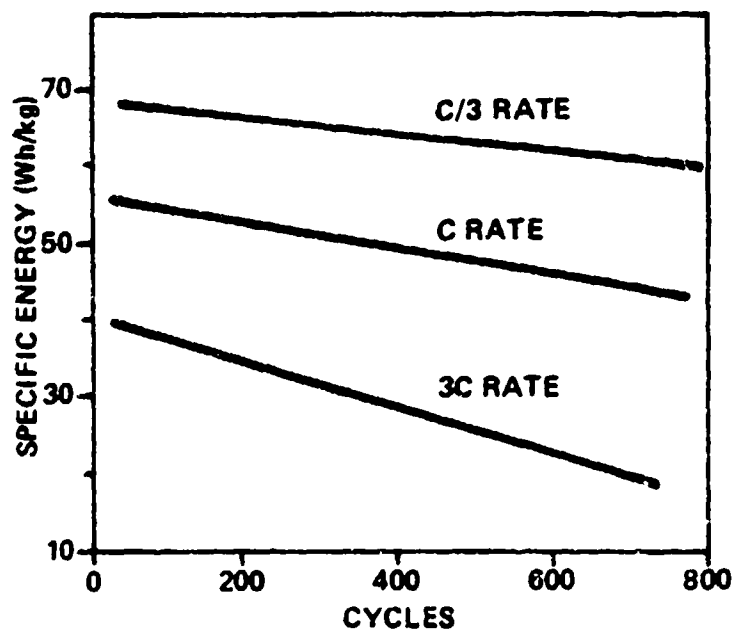**TEST REGIME: MID-ALTITUDE 60% DOD + HIGH RATE CHARACTERIZATION**

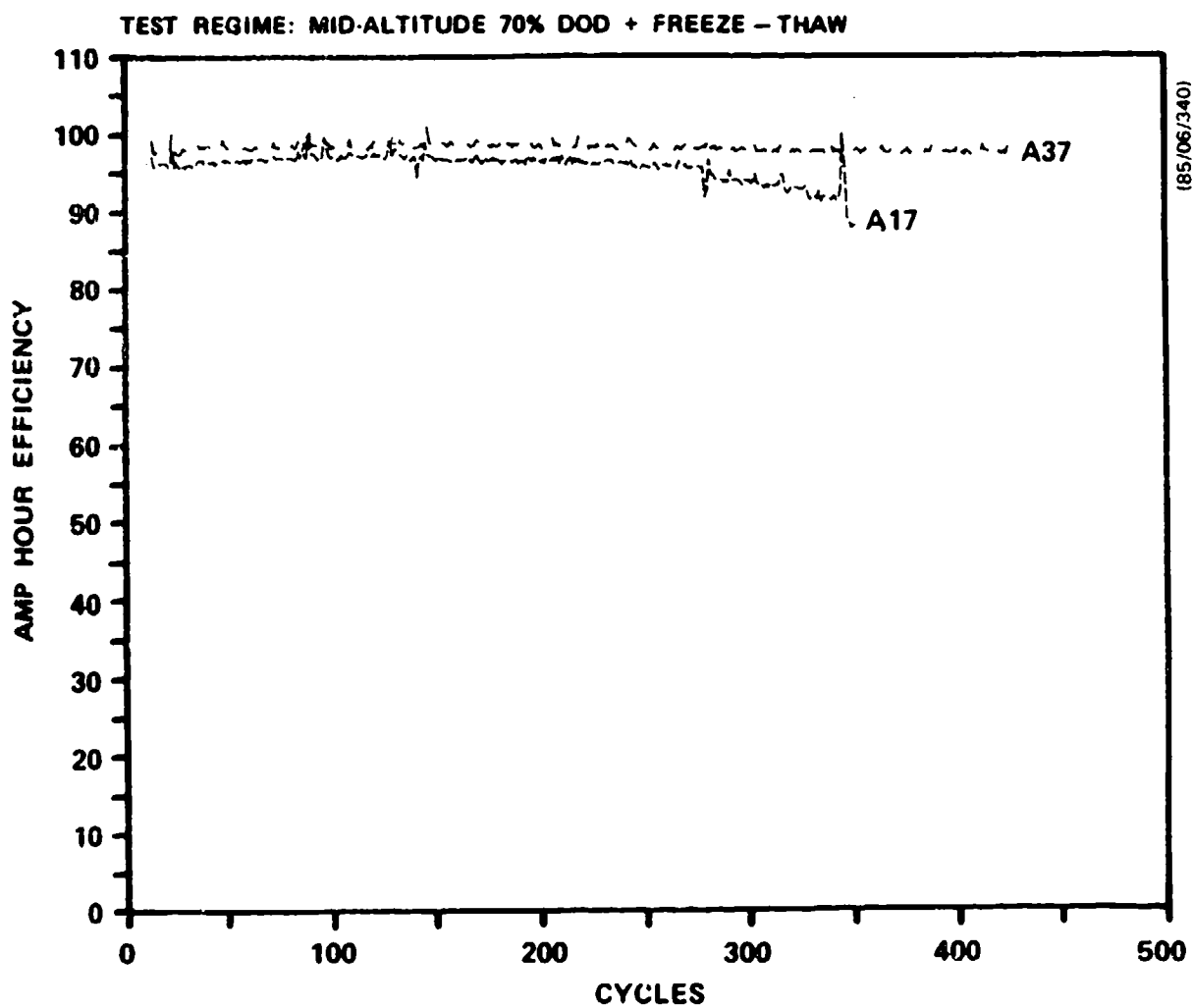Figure 42. Effect of Cycling on Specific Energy at Various Discharge Rates

Figure 43. Coulombic Efficiency with Cycling for 70% DOD and Freeze-Thaw Test on Mid-Altitude Regime
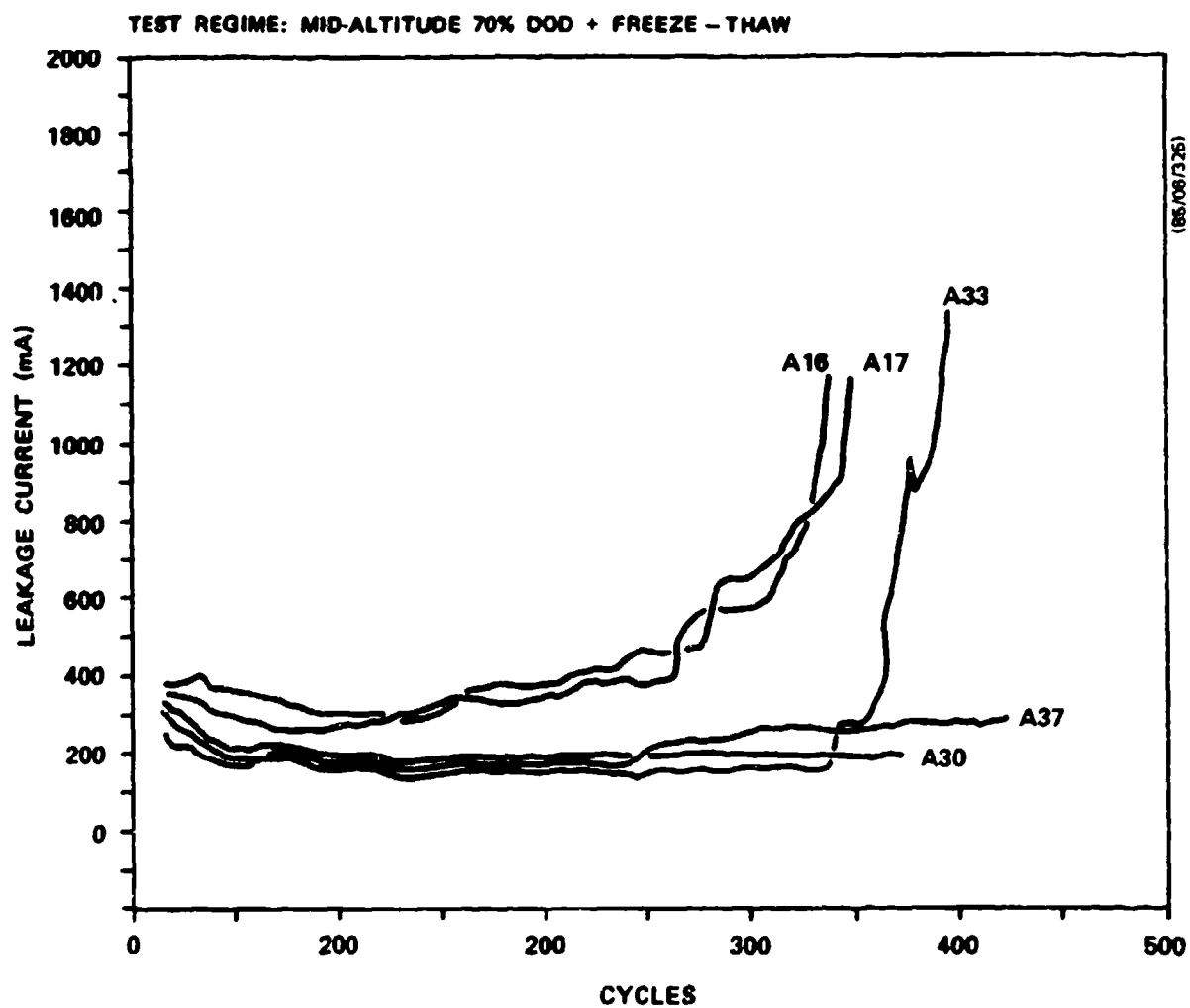
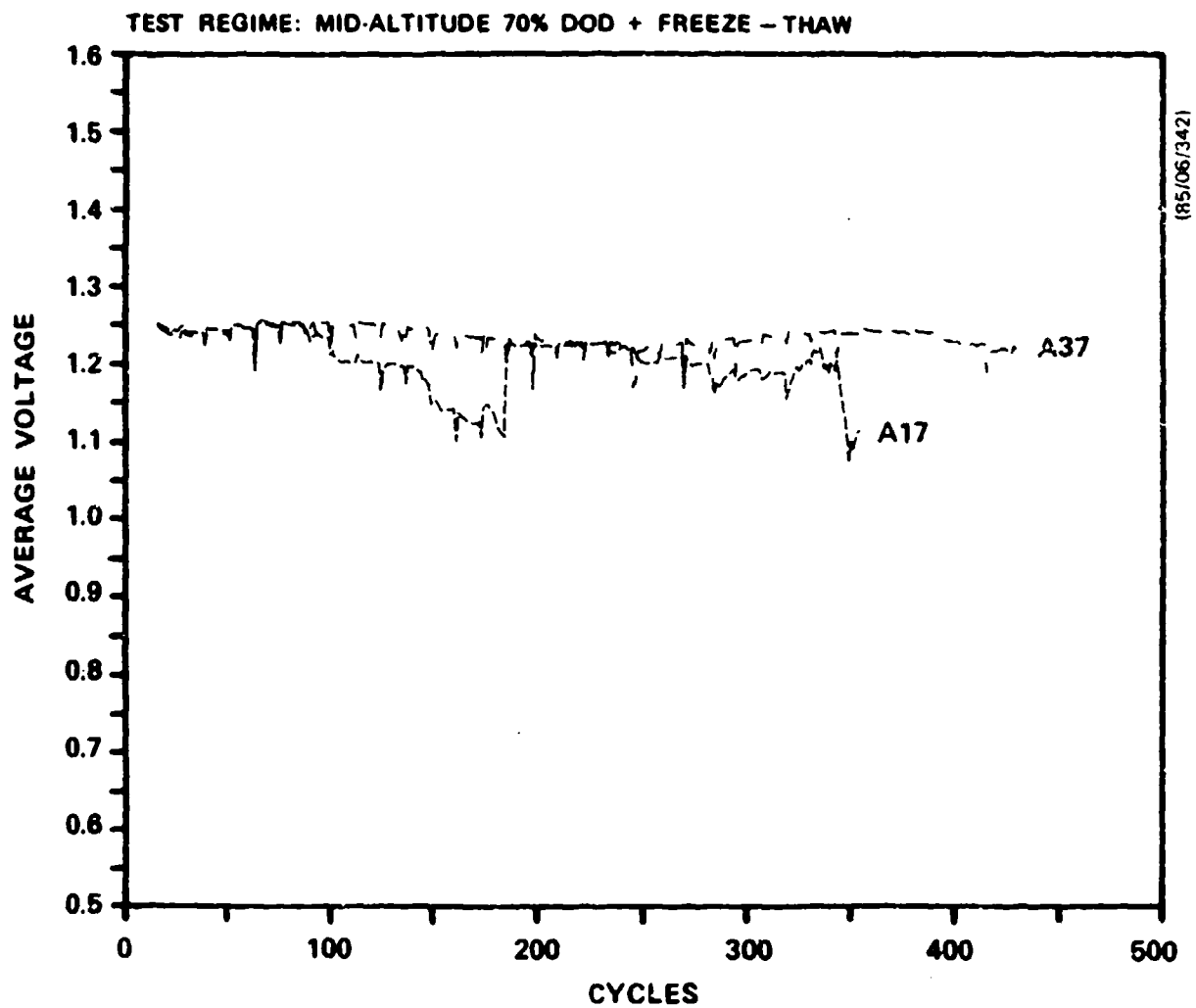Figure 44.   Leakage Current with Cycling for 70% DOD and Freeze-Thaw Test on Mid-Altitude Regime

Figure 45. Average Discharge Voltage with Cycling for 70% DOD and Freeze-Thaw
Test on Mid-Altitude Regime

withstand thermal cycling. The cause of failure for all cells in this group was a material failure in the positive cell terminal at the top of the feedthrough seal. This resulted in the terminals breaking-off due to a combination of the thermal cycling and severe corrosion of the copper core in the terminal. This problem can be readily corrected by replacing the copper-cored terminal by a solid nickel terminal.

Since the Li-alloy/FeS cells are able to withstand a considerable number of freeze-thaw cycles, several different modes of operation are feasible for the battery in the satellite application. For instance, one could launch the battery in the frozen state and bring it to operating temperature once the satellite is in orbit. Also, while in orbit the battery could be cooled down to prolong its life in those periods when it is not required, such as the long periods between the eclipse seasons in geosynchronous orbit.

Geosynchronous Tests

1) Depth of Discharge

The geosynchronous depth of discharge tests were performed in a similar manner to the mid-altitude tests except for the different charge and discharge times of ~ 22 hours and 1.2 hours respectively. Again the cell performance was monitored with cycling for coulombic efficiency, leakage current and average discharge voltage which is presented in Figures 46 to 51 for the two depths of discharge, 60 and 80%. The most striking observation on comparing the geosynchronous with the mid-altitude data is that the cells on the geosynchronous tests had much lower cycle lives than the mid-altitude cells, even though the geosynchronous regime is less arduous. In addition, the average cell cycle life on the 60% and 80% geosynchronous tests was approximately the same (see Table 13). This again indicates that depth of discharge was not the major parameter affecting life. The shape of the leakage current curves with cycling are very similar for both the mid-altitude and geosynchronous tests which suggests that the cell failure mechanism is the
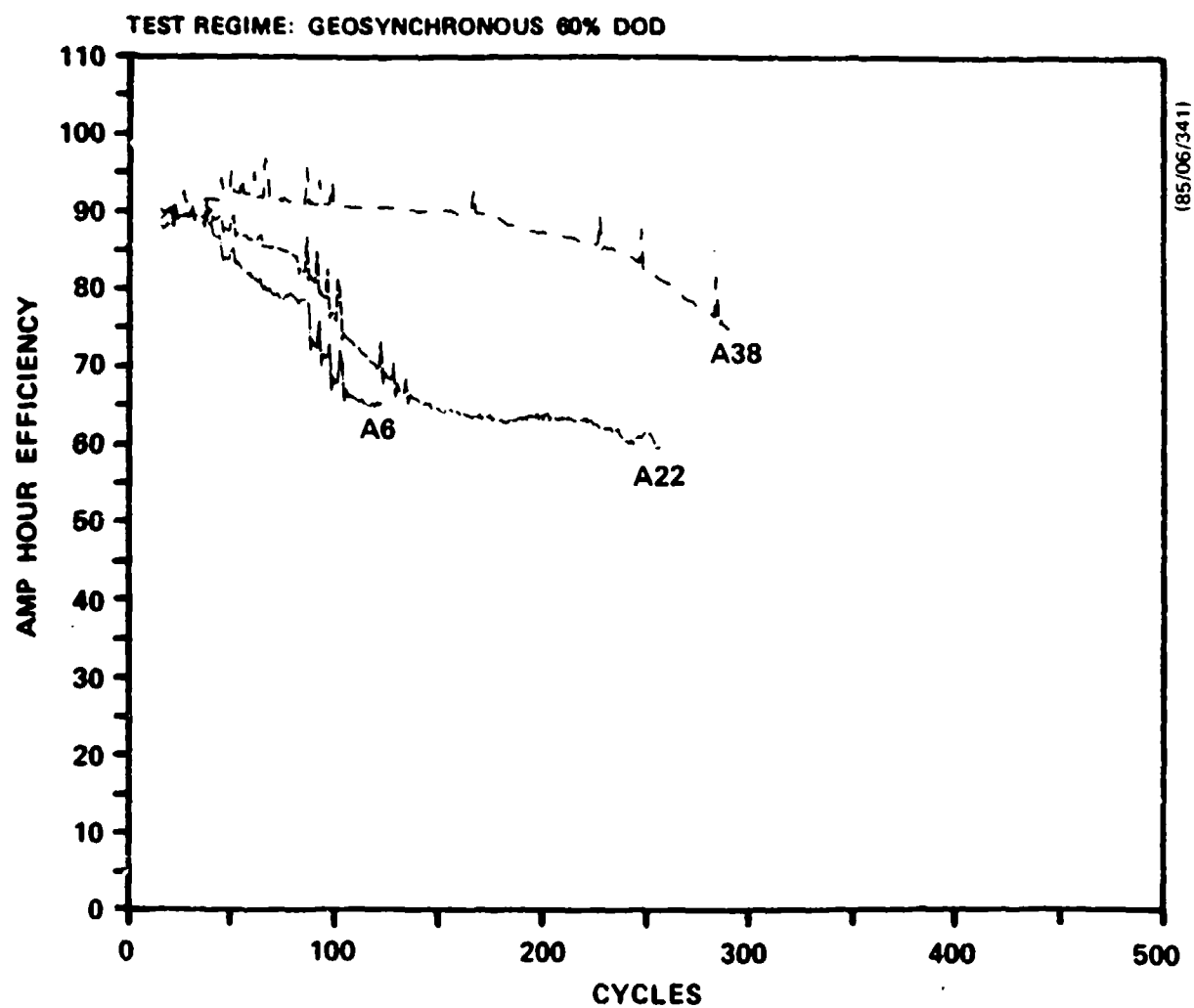
-82-

Figure 46. Coulombic Efficiency with Cycling for 60% DOD Test on Geosynchronous Regime
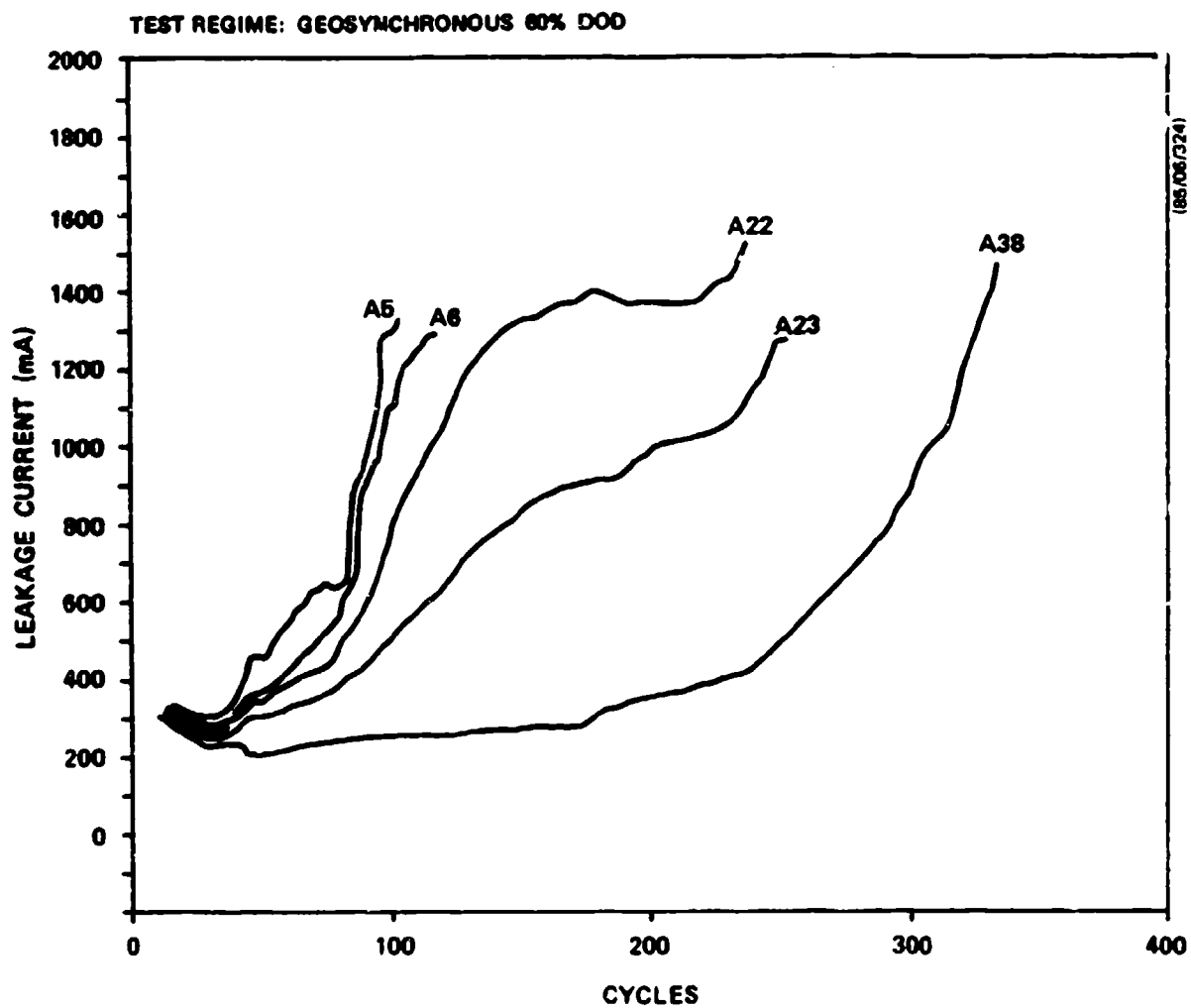
Figure 47.   Leakage Current with Cycling for 60% DOD Test on Geosynchronous
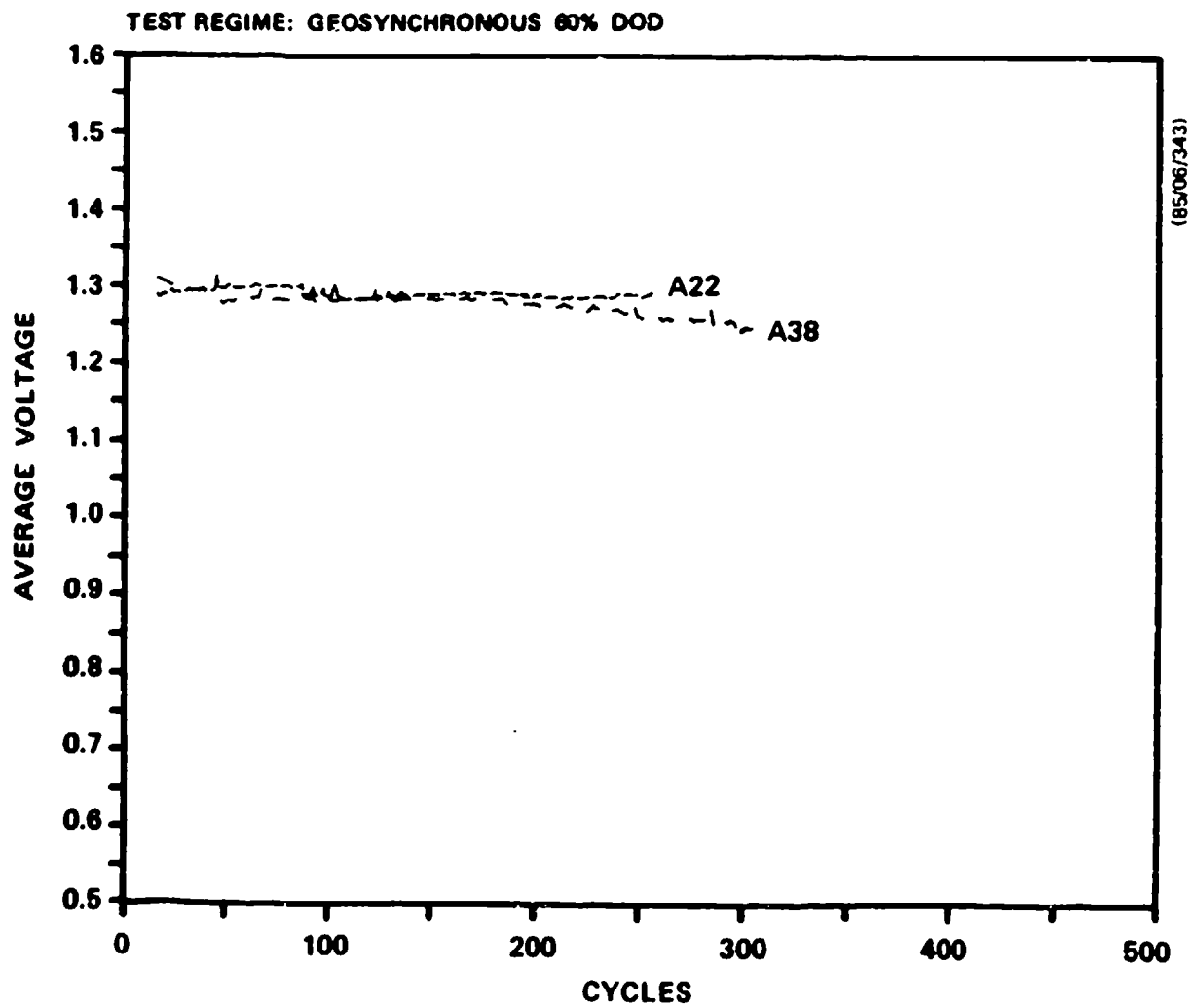Regime

Figure 48. Average Discharge Voltage with Cycling for 60% DOD Test on
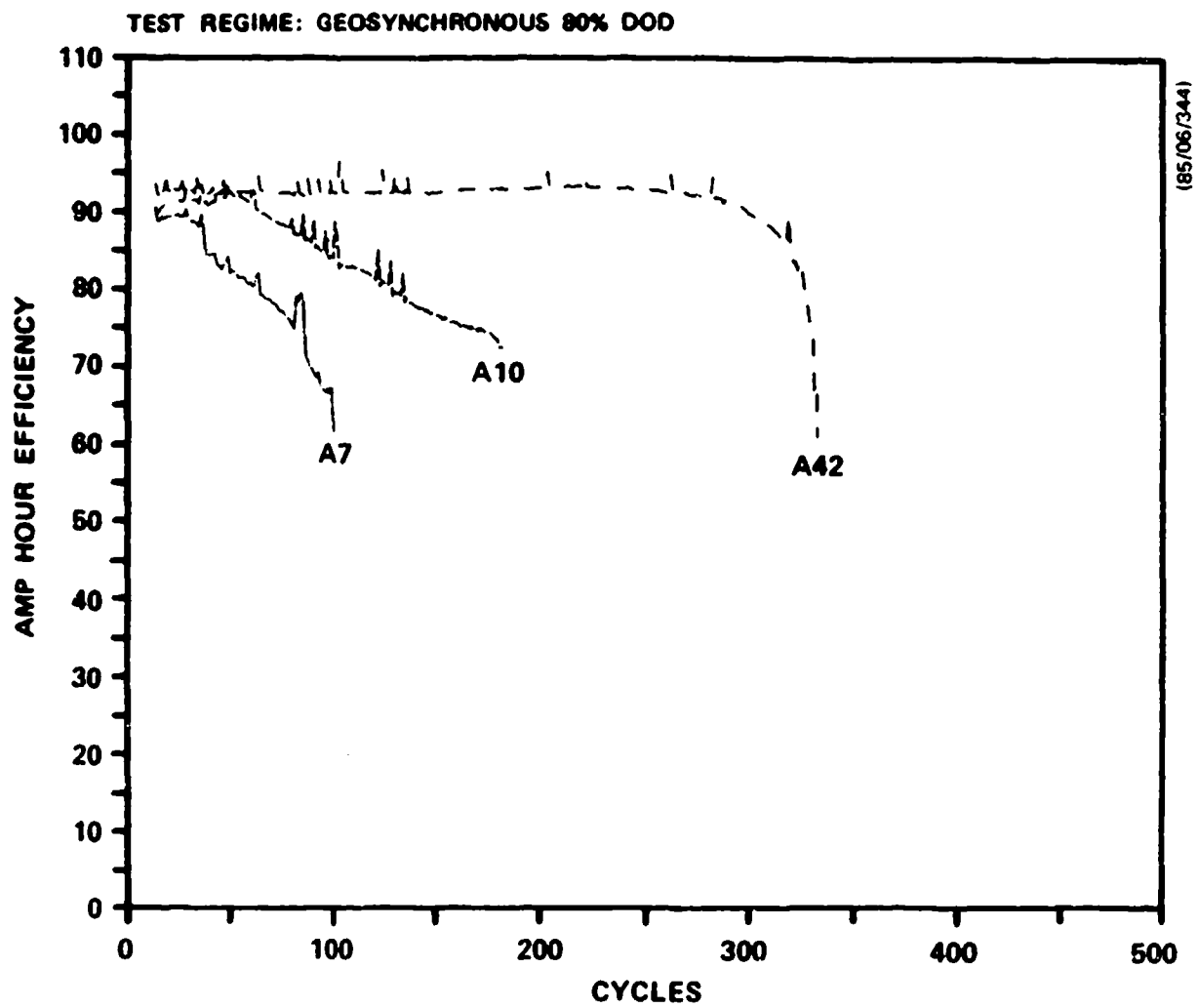Geosynchronous Regime

Figure 49. Coulombic Efficiency with Cycling for 80% DOD Test on Geosynchronous Regime
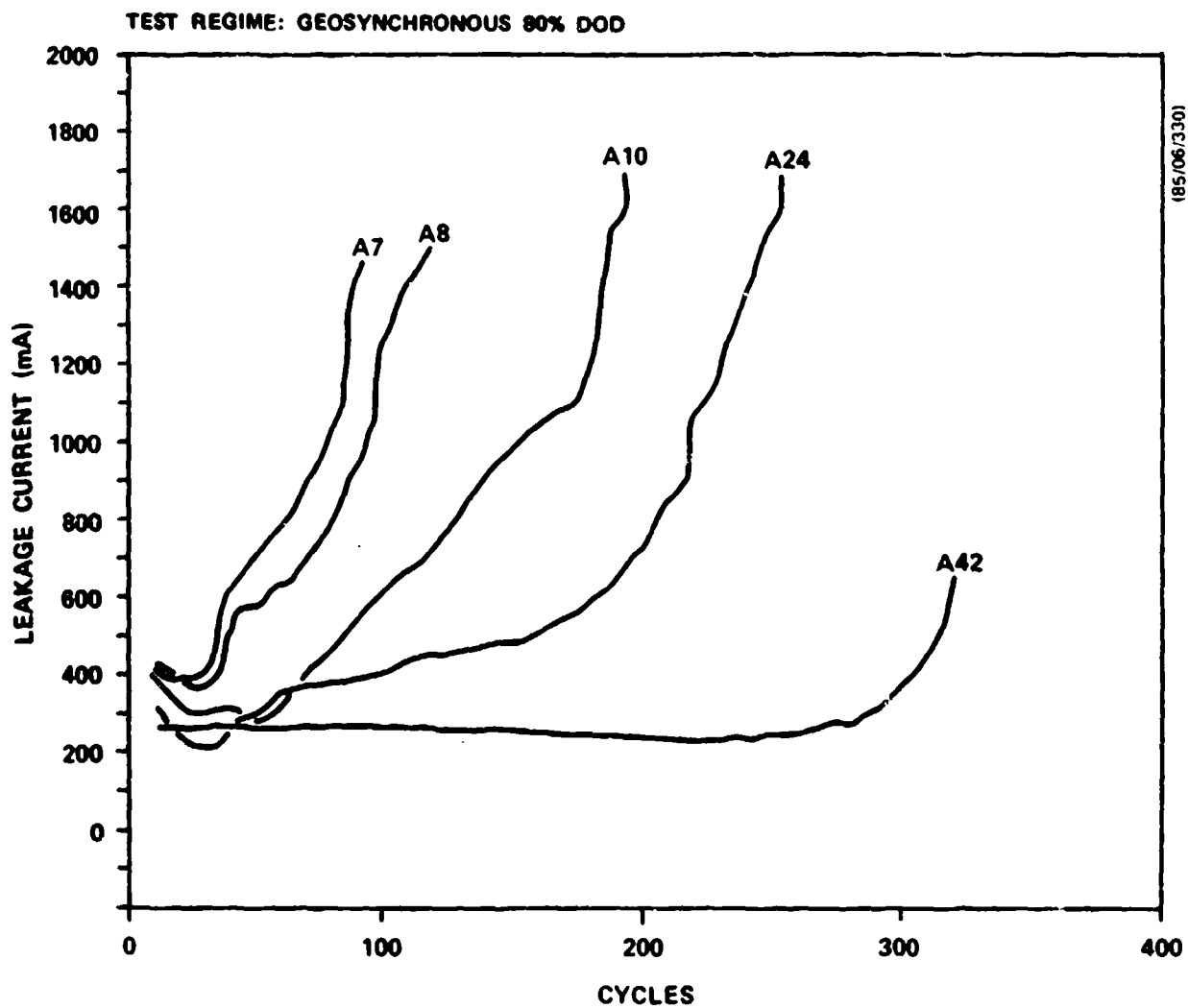
Figure 50. Leakage Current with Cycling for 80% DOD Test on Geosynchronous Regime
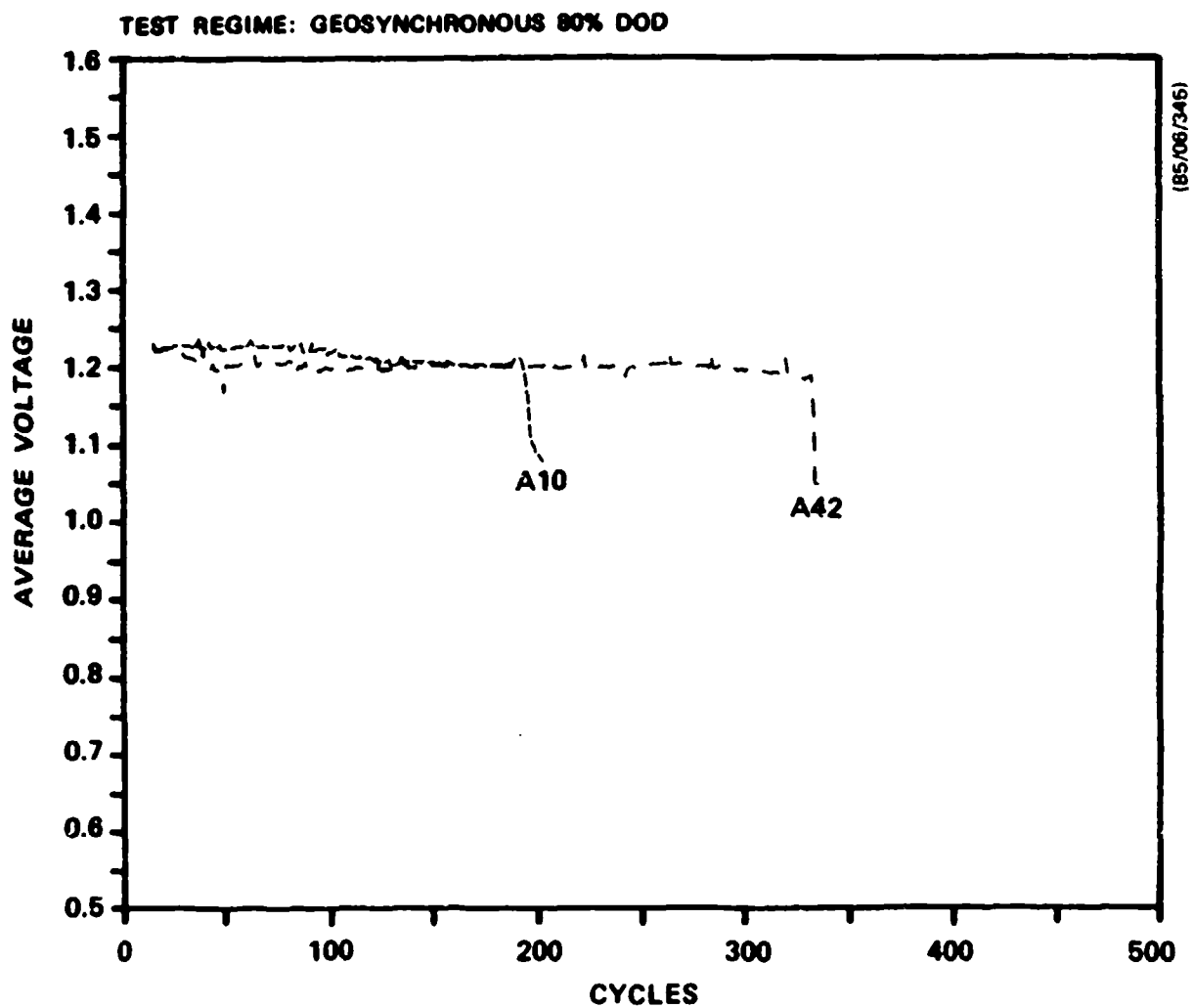
Figure 51. Average Discharge Voltage with Cycling for 80% DOD Test on Geosynchronous Regime

same, even though the cycle lives of the geosynchronous cells are much shorter than those of the mid-altitude cells. If however, the time (in days) the cells were at operating temperature of ~ 455°C is compared for both the geosynchronous and mid-altitude cells (Table 13), it is found that there is reasonably close correlation, with all groups of cells having a mean life in the range 164-252 days. When the geosynchronous and mid-altitude data is compared for the 60 and 80% DOD tests, there is even closer correlation in the mean life of 164-193 days. This tends to indicate that all cells failed by a common chemical or electrochemical corrosion phenomenon which is time dependent. Evidence of such a phenomenon could probably be revealed by metallographically examining the failed cells. This was not done due to early termination of the contract.

The average discharge voltage of a cell is dependent on depth of discharge, the rate discharge and the length of time the cell was operated. The greater, higher or longer of each of these parameters respectively resulted in a decline in the average discharge voltage, (Figure 52).

ii) Sinusoidal Test

In order to accumulate cycle life data at a faster rate, a decision was made to reduce the charge time on this test from 22 hours to 8 hours, hence at least 2 cycles/day were possible instead of 1 cycle/day. The discharge times were varied in a sinusoidal manner over 45 days to simulate the geosynchronous eclipse period.

The performance of the cells on the sinusoidal regine are plotted in Figure 53-55, which show the coulombic efficiency, leakage current and average discharge voltage, all three parameters vary sinusoidally with the number of cycles. The coulombic efficiency declines more rapidly at the shallowest depth of discharge (17% DOD) than at the highest depth of discharge (80% DOD) as the leakage current increases with cycling. However, the overall trend in both the coulombic efficiency and leakage current with cycling is the same as for the other geosynchronous and mid-altitude tests. The average discharge

-89-
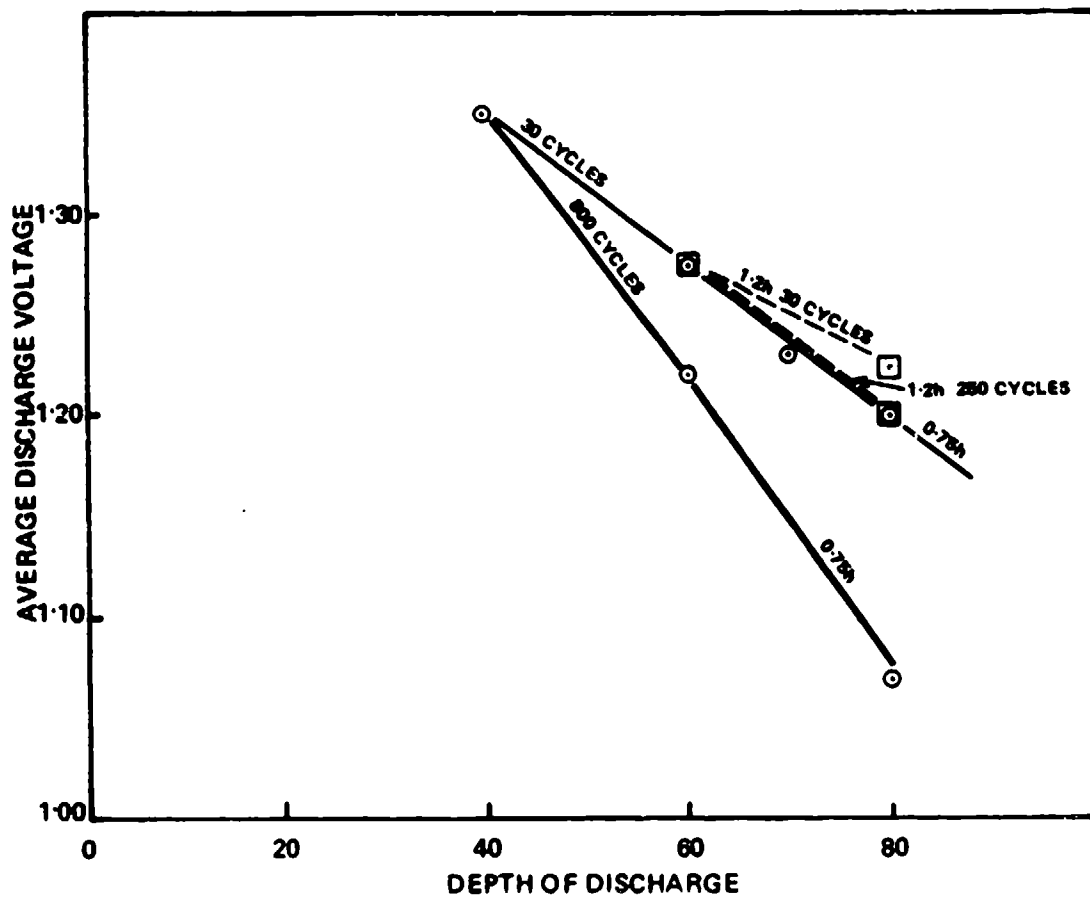
Figure 52. Effect of Depth of Discharge, Discharge Rate and Cycling on
Average Discharge Voltage

TEST REGIME: GEOSYNCHRONOUS SINUSOIDAL
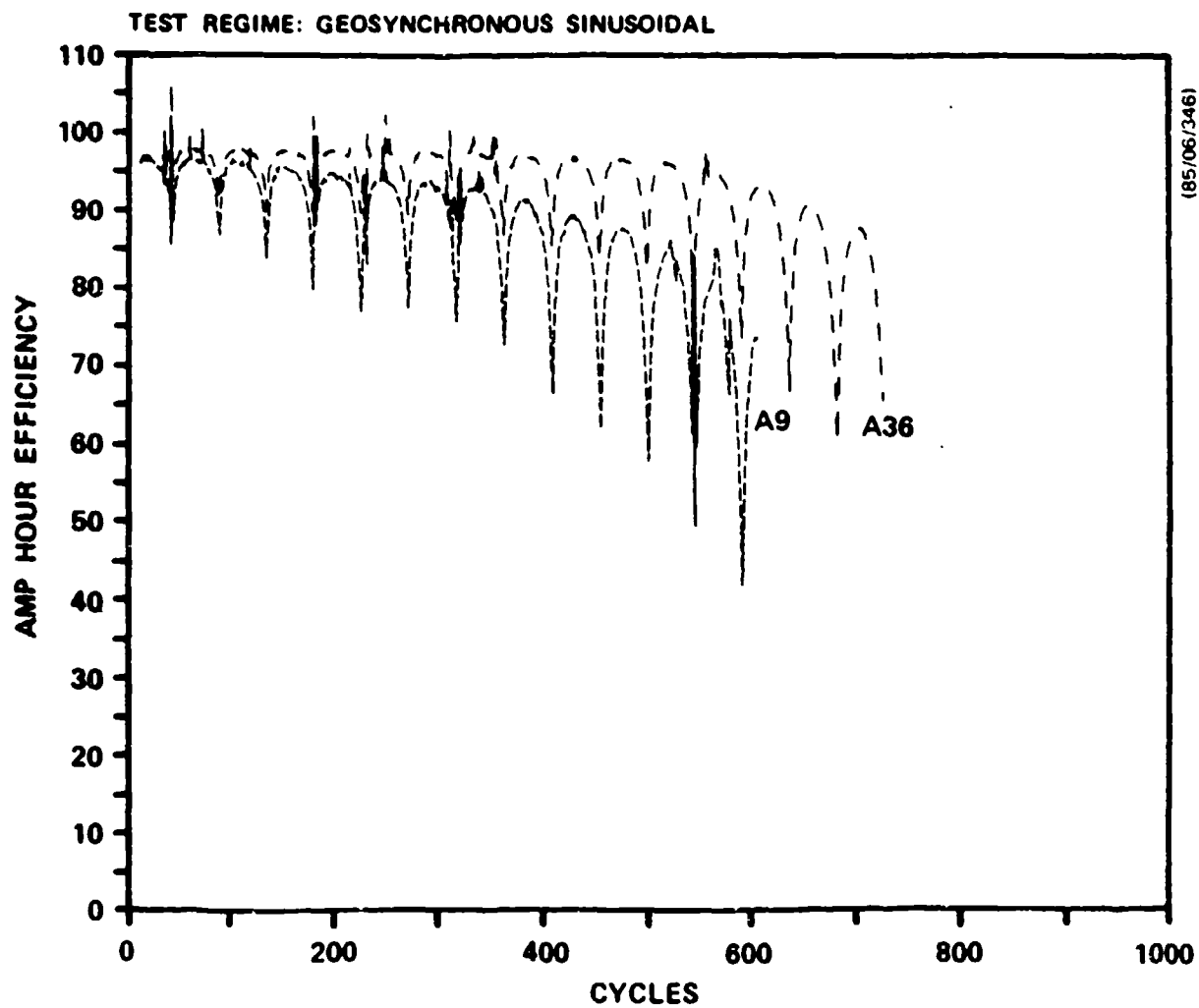
(85/06/346)

Figure 53.   Coulombic Efficiency with Cycling for Sinusoidal Test on
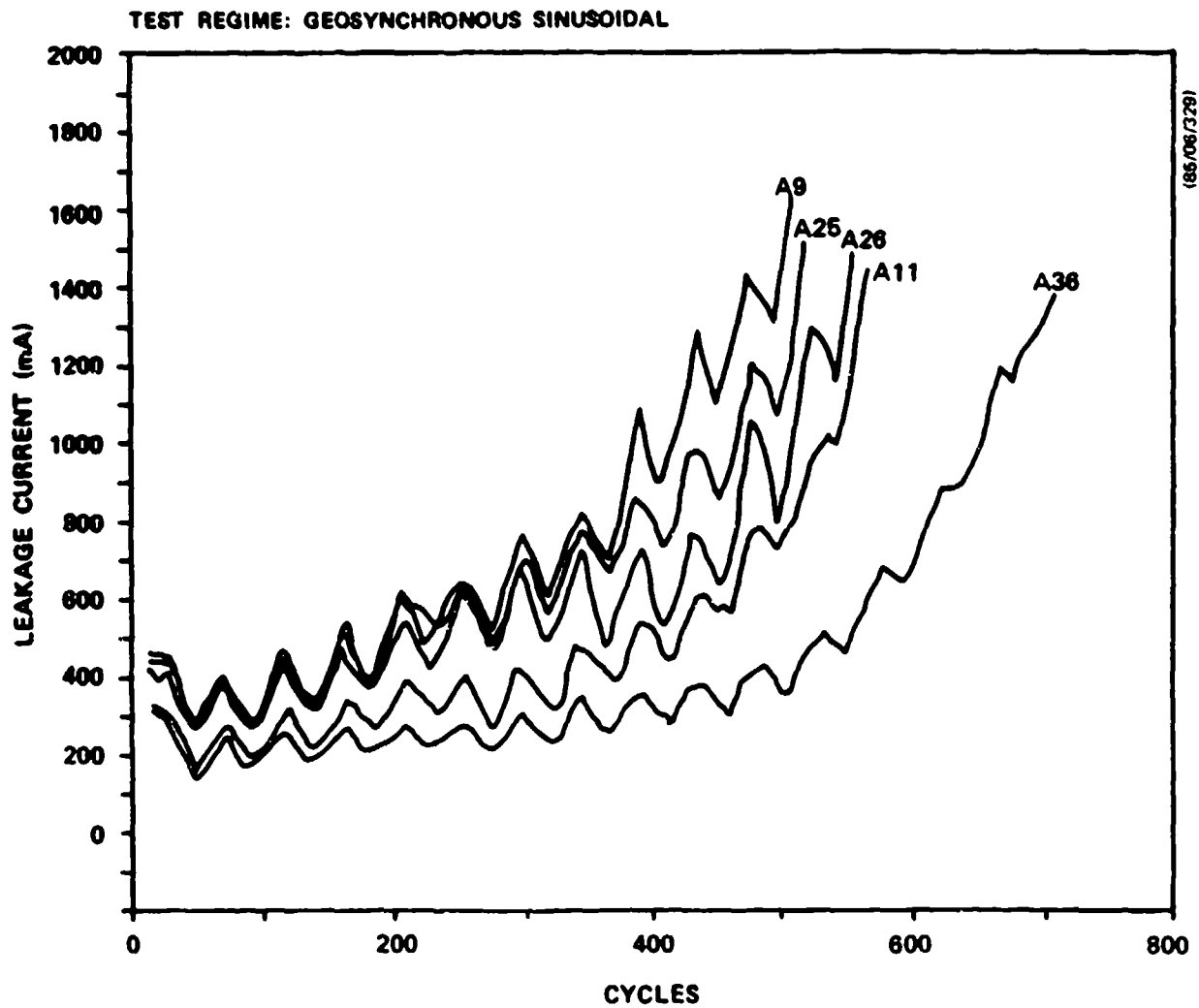Geosynchronous Regime

-91-

Figure 54. Leakage Current with Cycling for Sinusoidal Test on Geosynchronous Regime
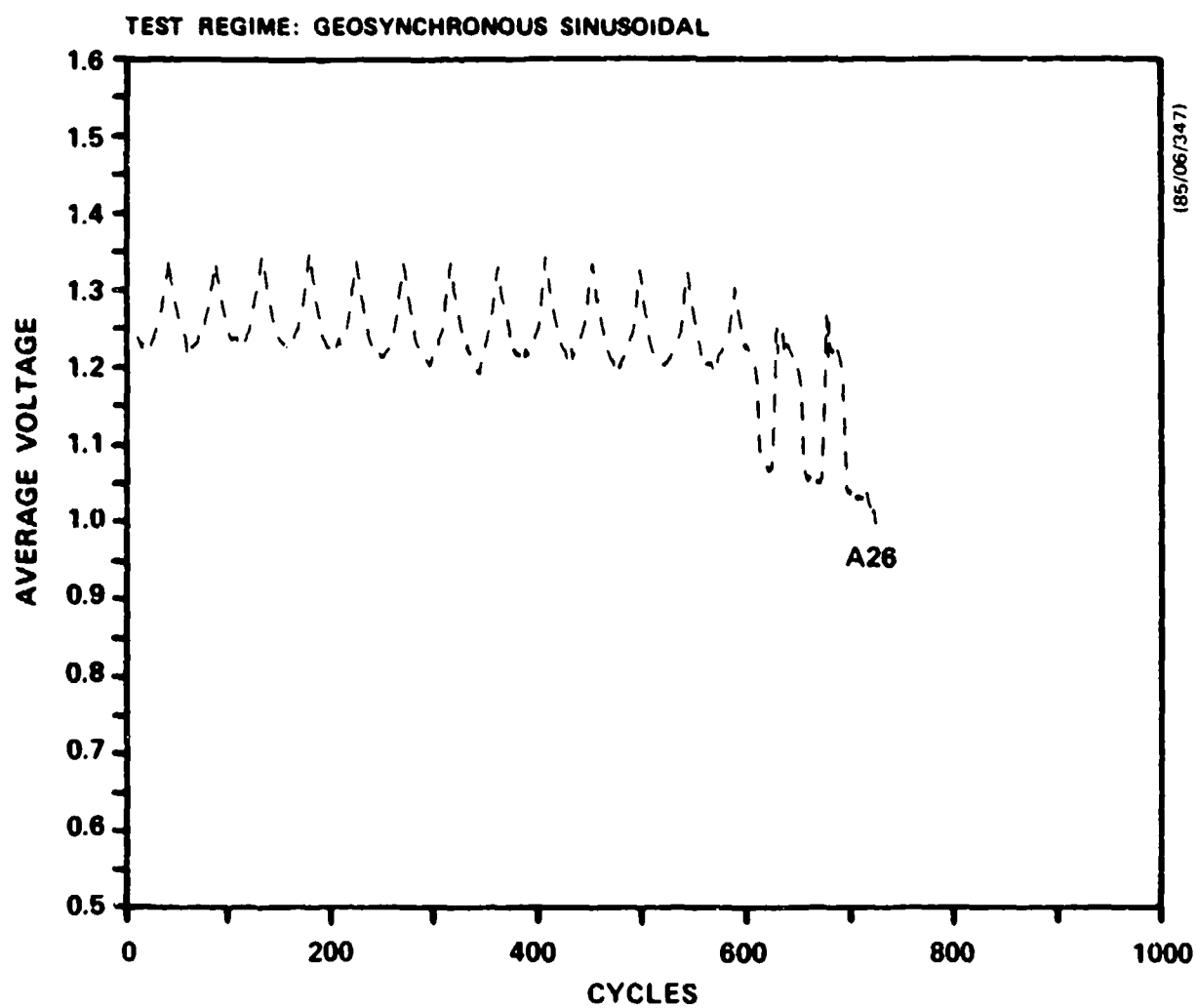
Figure 55. Average Discharge Voltage with Cycling for Sinusoidal Test on Geosynchronous Regime

voltage remained relatively stable throughout the life of the cells between the maximum and minimum voltages defined by a sinusoidal function until they failed, whereupon it declined rapidly. The number of cycles accumulated on the sinusoidal-test cells were on average approximately three times those accumulated on the other geosynchronous tests. However, the average number of days the cells were at operating temperature was approximately the same for all the geosynchronous test groups. This again supports the argument that the cell failure mechanism is mainly time related and only slightly dependent on the operating regime. The cycle life and days at operating temperature for all the cells tested under the mid-altitude and geosynchronous regimes are summarized in Figure 56 and 57.

Special Tests

The peak power of the Level I cells were determined at different depths of discharge by subjecting the cells to increasing (15 sec) current pulses. A typical peak power versus depth of discharge plot is shown in Figure 58. The peak power declines with depth of discharge particularly beyond 50% DOD when the resistance of the cell increases dramatically.

Since the performance of the Level I cells was far below the goals set for the first iteration design, no additional special tests (ie vibration) were carried out.
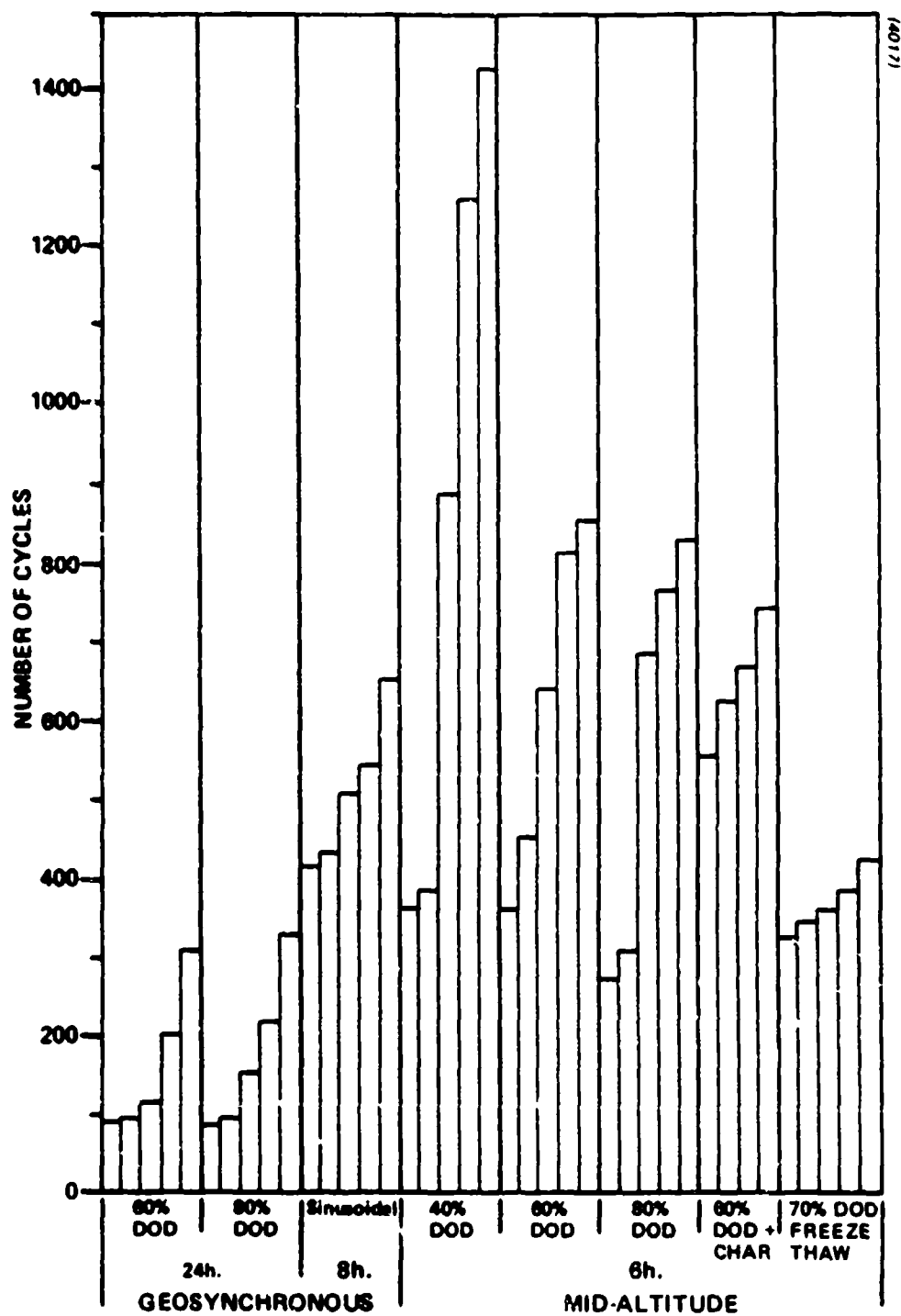
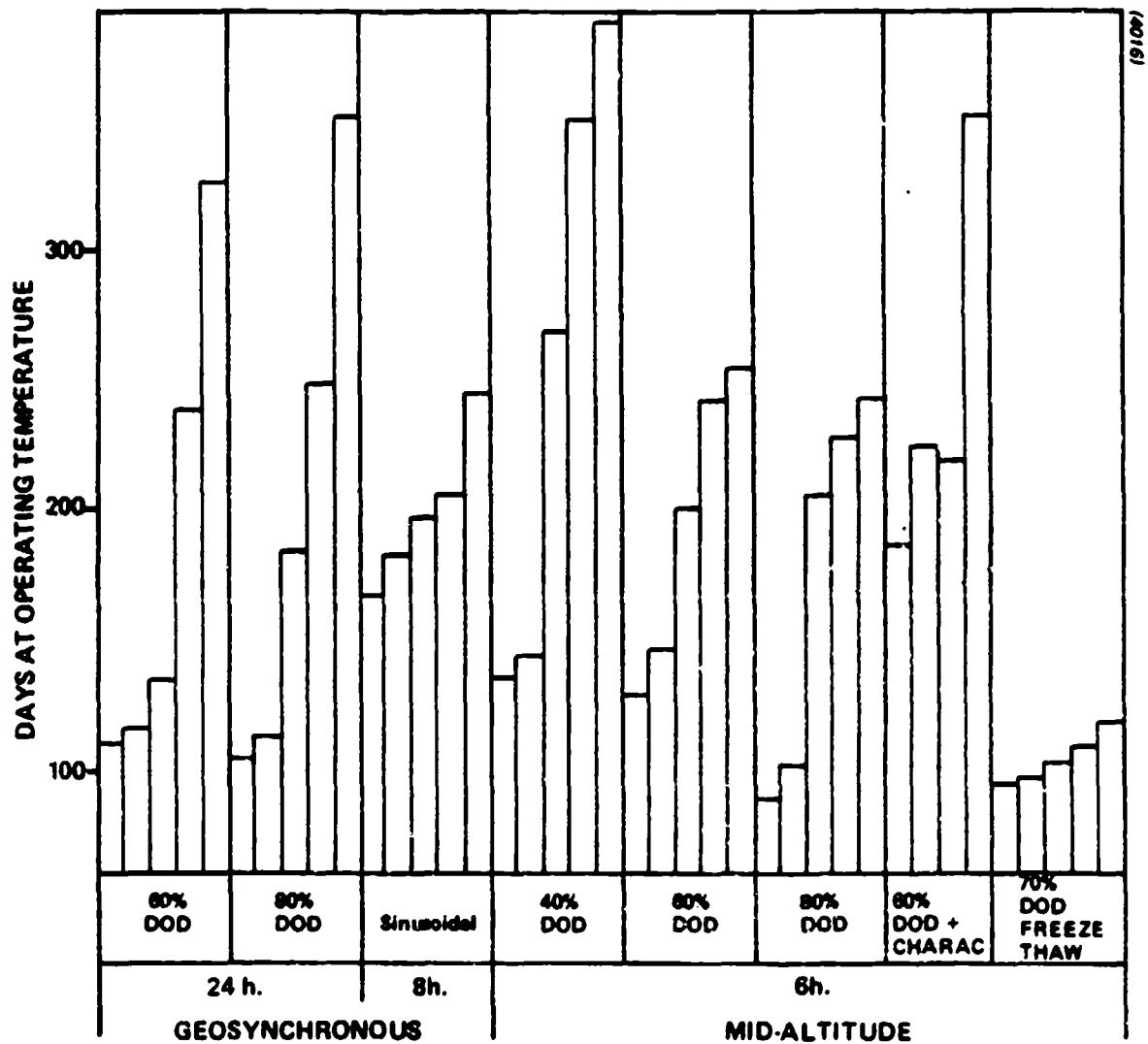Figure 56. Cycle Life Data for Level I Cells
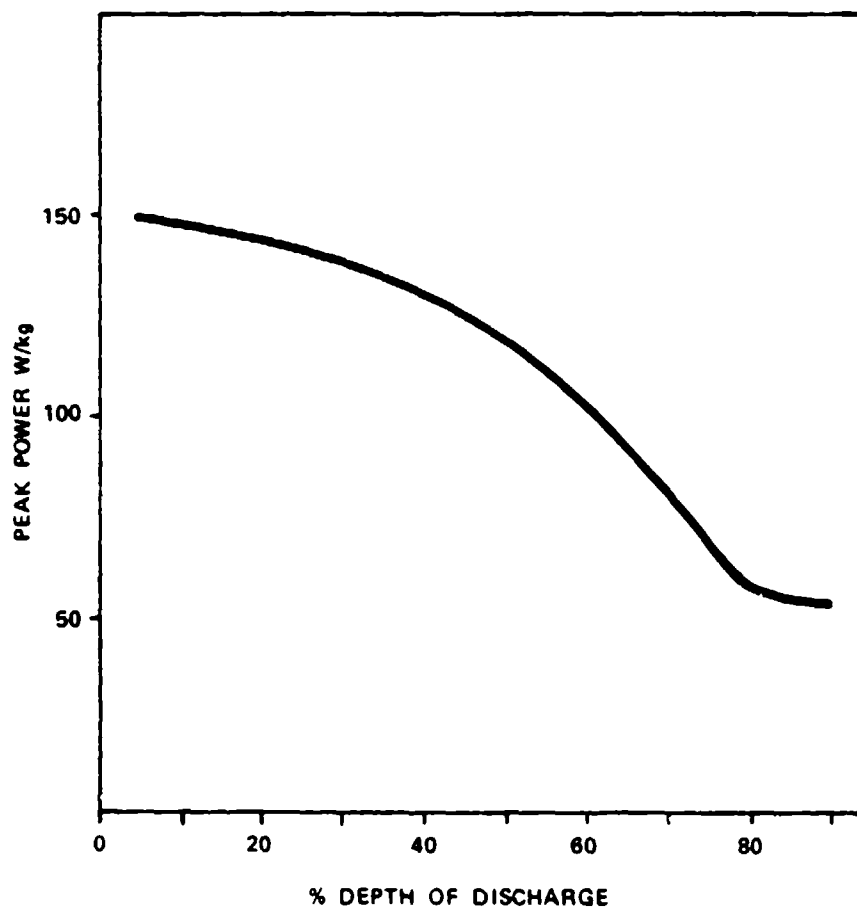
Figure 57. Calendar Life Data for Level I Cells

Figure 58.   Peak Power with Depth of Discharge for Level I Cell

-97-

LEVEL II CELL DEVELOPMENT

Since the energy density of the Level I cell was only ~ 55 Wh/kg at the
1 hour discharge rate, revolutionary design improvements were necessary for
the subsequent cell design iterations if the ultimate goal of 165 Wh/kg was
ever to be achieved.

For the Level II cell development effort, two different approaches were
pursued:
   o An iron disulfide monopolar cell design.
   o An iron monosulfide bipolar stack design.

Both of these approaches can be shown theoretically capable of delivering
specific energies in excess of 120Wh/kg, however a number of technical
problems have to be overcome with ~ch design before a practical system can
successfully attain the desired performance and life.

The following sections of this report discuss the development of these
two different approaches and their associated problems. The majority of the
experimental work in the development of the disulfide positive electrode and
the bipolar stack was performed in small 5Ah pellet cells.

Iron Disulfide-Monopolar Cell Development

Calculations show that specific energies in the range 115-140 Wh/kg are
potentially feasible from a practical iron disulfide-monopolar cell design
depending on whether only the upper or both upper and lower voltage plateaus
are utilized. In operation, however, the iron disulfide electrode has been
found to be rather unstable due to loss of sulfur. The sulfur appears to be
lost from the active material by thermal decomposition and its subsequent
reaction with other components within the cell. Thus, there is a fairly rapid
decline with operation of the upper pleateau capacity as the FeS_x
stoichiometry changes from x=2 to $1 < x < 2$. The primary objective of this

effort, therefore, has been to attempt to develop a cell environment in which the iron disulfide electrode can operate in a truly reversible manner.

Iron disulfide starts to thermally decompose at temperatures as low as ⁻ 350°C and the rate of decomposition increases with temperature. Therefore, if decomposition is to be prevented cells should be operated at temperatures below 350°c. This infers that the cell electrolyte should have a melting point much lower than that of the preferred electrolyte for the monosulfide cell (ie LiF-LiCl-LiBr, m.pt ⁻ 445°C). Several lower melting point electrolytes were identified, but those which were believed to offer the best promise are the all lithium halide type, containing lithium iodide in the range 50 - 60w/o since melting points as low as 340°C are possible. These all lithium cation electrolytes have the added advantage that they do not form relatively stable complex phases with the positive active material on discharge, (ie J-phase formation with electrolytes containing potassium) which can lead to local freezing particularly at high rates of discharge.

The higher activity of the iron disulfide active material also severely restricts the choice of material for the cell hardware such as the current collectors and particle retainer system. The metals and alloys (ie nickel and stainless steel) commonly used for these components are agressively corroded when in contact with iron disulfide at the cell operating temperature. Only the refractory metals, molybdenum and tungsten, have been shown to survive this harsh environment. Unfortunately, the use of these metals are not a simple solution to the problem since they can not be readily joined by conventional welding techniques. Specialized welding expertise was sought in an effort to overcome this problem since it was germane to the success of an iron disulfide cell. The fabrication of molybdenum hardware will be discussed later.

In order to obtain any meaningful data from our pellet cell studies on iron disulfide electrodes it was necessary to make a number of changes to the pellet cell design. These changes resulted in a positive electrode package

consisting of a molybdenum cup current collector to hold the active material pellet, to the surface of which was bonded a very thin layer of magnesia powder and a ceramic felt that functioned as a particle retainer system.

Electrolytes for Metal Disulfide Electrodes

The initial cells constructed with the modified positive package had an iron disulfide electrode containing the LiCl-LiF-LiBr ternary eutectic electrolyte. However, on cycling only 37% utilization was obtained from the upper plateau and transition regions (Figure 59) instead of the expected 50%. An analysis of the fused positive mix revealed that a substantial amount of the sulfur had been lost during processing prior to pressing the electrode plaque.

In order to minimize this problem cells were built in which the ternary electrolyte was replaced by the lower melting point LiCl-KCl eutectic electrolyte. These cells when operated at 380°C had greatly improved utilizations of 30% and 15% for the upper plateau and transition regions respectively (Figure 60), which are much nearer the theoretical values of 33.5% and 16.7% for these regions. However, the performance of these cells was very sensitive to current density and exhibited a marked drop in utilization as the current density was increased. This is believed to be a consequence of the formation of complex phases containing potassium and some local freezing in the cell.

In an effort to avoid the problems associated with potassium ions in the electrolyte, cells were built with a LiF-LiCl-LiI ternary eutectic electrolyte which has a melting point of ~ 340°C. This enabled the positive electrode mix to be fused at 380°C and the cell to be operated at ~ 370°C. The utilization of the upper plateau and transition regions was approximately the same as for the LiCl-KCl eutectic cell (Figure 61). These iodide electrolyte cells were also not as sensitive to increasing discharge rates as the potassium containing cells. The performance of the two types of cells are
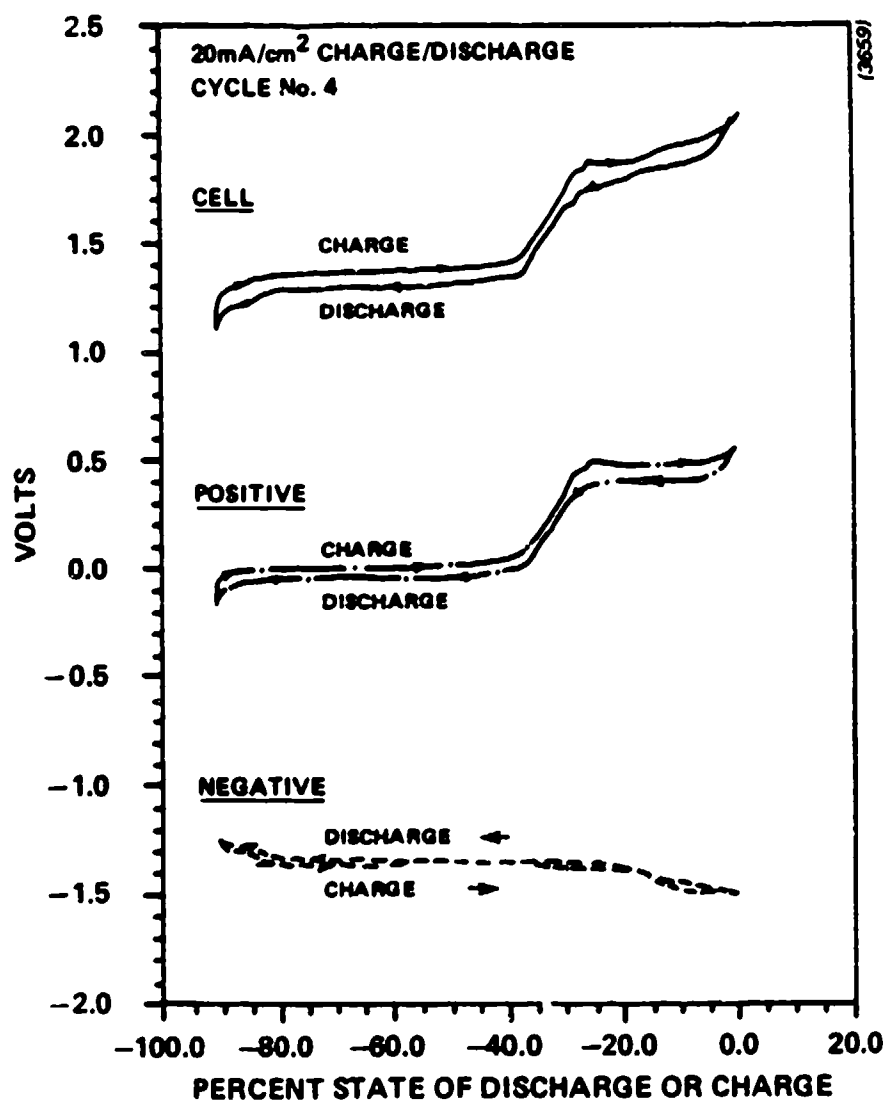
Figure 59. Performance of Iron Disulfide Cell Containing LiF-LiCl-LiBr
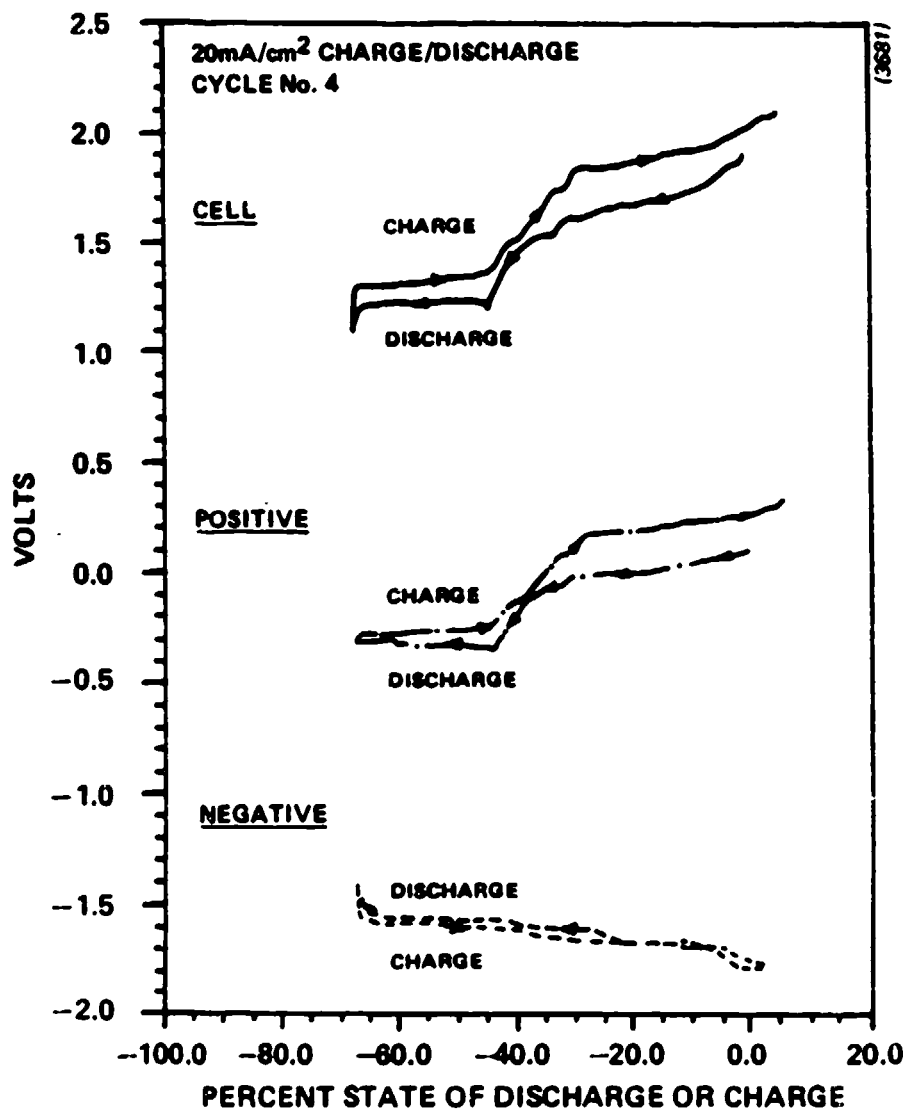Electrolyte and Operated at 455°C

Figure 60. Performance of Iron Disulfide Cell Containing LiCl-KCl Electrolyte and Operated at 380°C
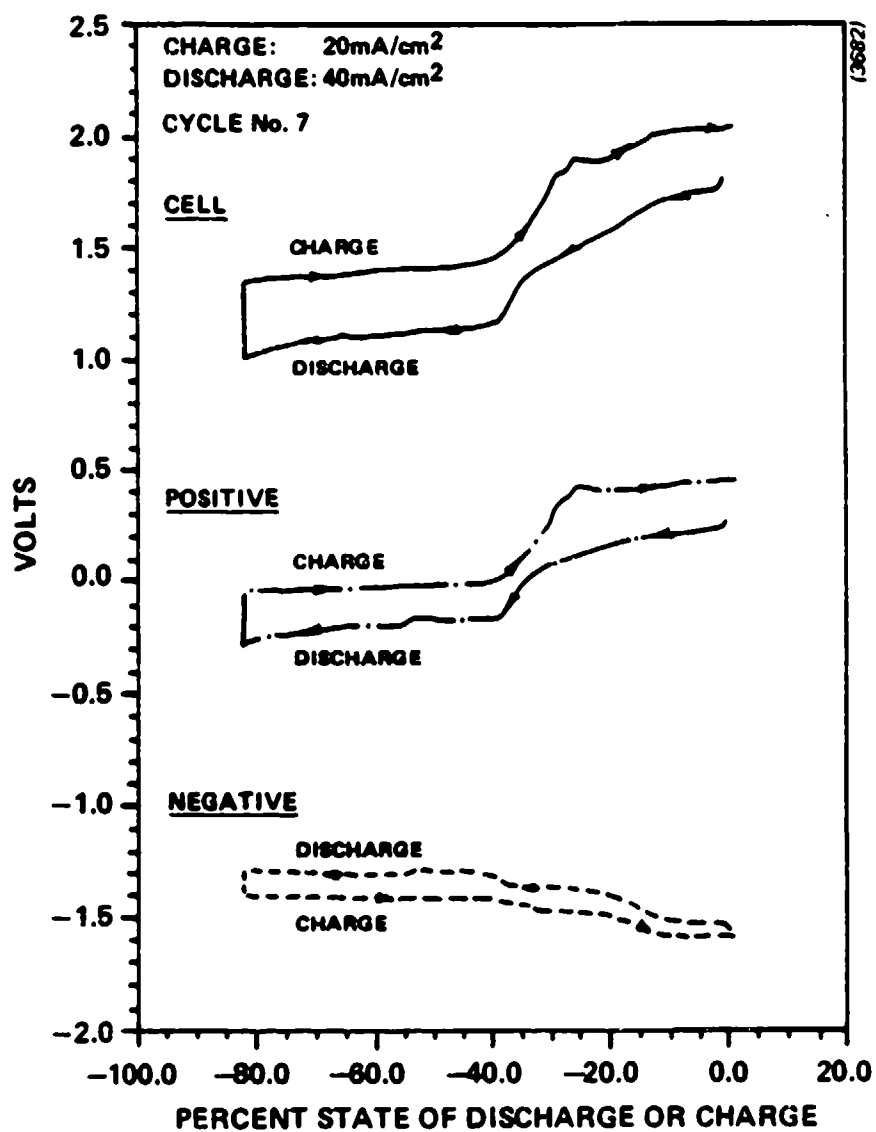
-102-

Figure 61. Performance of Iron Disulfide Cell Containing LiF-LiCl-LiI
Electrolyte and Operated at 370°C

-103-

compared in Figure 62 in which the potassium containing cell exhibits a decreasing lower plateau capacity as the current density is increased whereas there is minimal change in the cell containing only lithium. In operating these cells, the charge voltage cut-off was limited to 2.05 volts in order to minimize the loss of sulfur. However, this resulted in a slight reduction of the upper plateau capacity due to the incomplete conversion of the FeS to FeS_2.

The use of the ternary iodide electrolyte did not come without problems in that cells with this electrolyte had a significantly higher impedance due to the high specific resistance of the iodide salt. This high impedance resulted in a sharp decline in the performance of the cells at discharge rates > 1C rate. Hence, further work is required to identify a completely satisfactory electrolyte for operating iron disulfide electrodes at high discharge rates without them exhibiting significant capacity decline.

Separator/Particle Retention System

One of the major problems seen early in the development of an iron disulfide cell was the inability of the pressed magnesia powder separator to survive more than about 30 cycles before it was penetrated by positive active material. The reason for this poor life is that the iron disulfide electrode undergoes significantly greater volume changes during a charge/discharge cycle than a monosulfide electrode. Consequently these increased volume changes generate greater stresses in the separator system and thus shorten its life.

In our efforts to improve the stability of the separator system a number of different ceramic powder/fiber combinations were examined. The most promising combination identified prior to termination of the contract was a layer of boron nitride cloth heavily impregnated with magnesia powder sandwiched between two thin layers of compressed magnesia powder. Some other ceramic felts were examined also but they were found to be too fragile or not corrosion resistant enough to survive in the very agressive environment adjacent to the positive electrode.
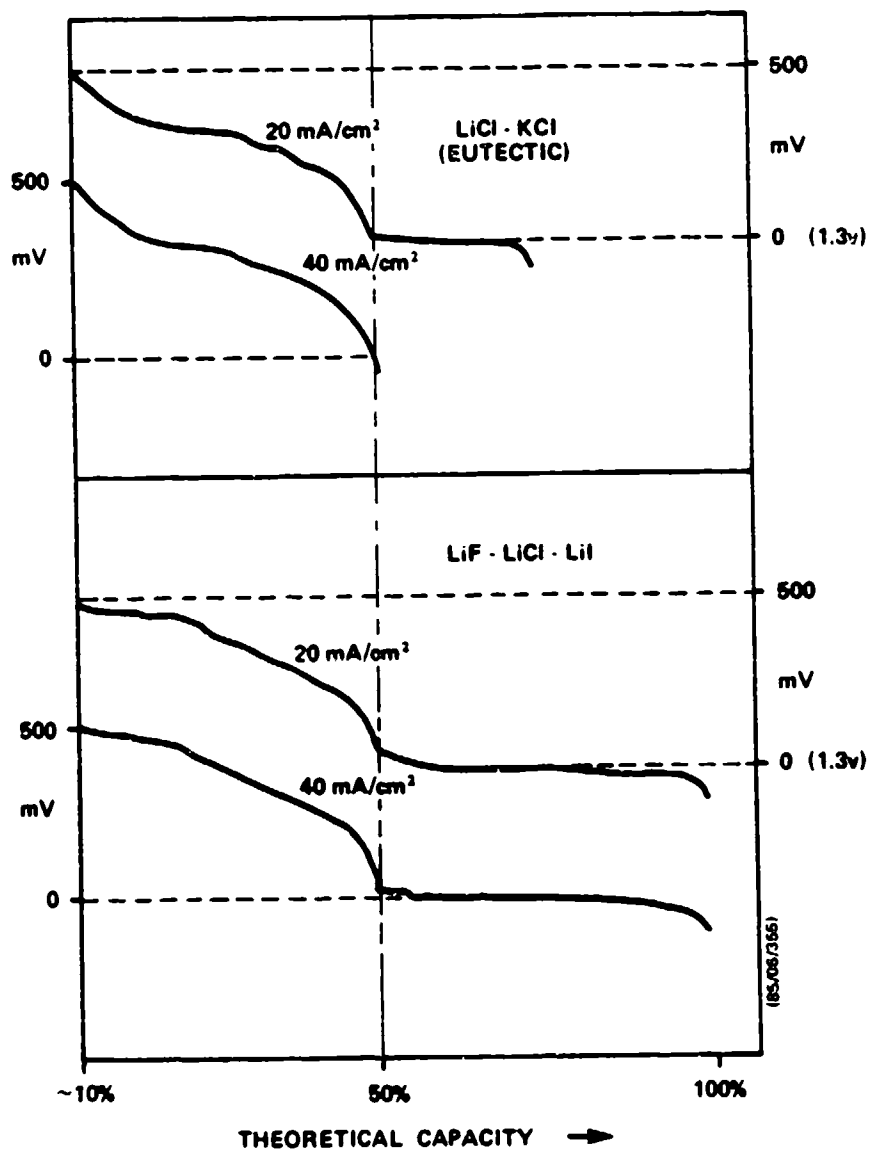
Figure 62. Performance Comparison of Iron Disulfide Cells Containing
Different Electrolytes at Two Current Densities

Although the magnesia/boron nitride combination showed promise further process optimizatiion is necessary before this separator system could be considered satisfactory for incorporation into large scale engineering cells.

Molybdenum Hardware

Concurrent with the work to develop a stable iron-disulfide electrode a sub-contract effort was carried out at Turbine Metals Technology (TMT) Inc. to fabricate molybdenum hardware for the positive iron disulfide electrode of a Level I size engineering cell.

The hardware components to be designed and fabricated from molybdenum were as follows:

o Collector plate and bus bar assembly.
o Particle retainer baskets.
o Terminal and distribution plate assembly.

In addition to manufacturing the components from high purity molybdenum, welding techniques were to be developed to join the individual components together into sub-assemblies and subsequently join these subassemblies together during final cell assembly. Once the welding techniques had been established it was planned that this welding expertise and equipment be transferred from TMT Inc. to Gould, since several of the molybdenum welds would be made during cell assembly which is carried out in a dry room because of the high reactivity of the lithium components used in the cell.

Molybdenum can be fusion welded by the TIG process but fit-up of the components, welding conditions and atmosphere surrounding the weld area are all extremely critical in achieving a satisfactory weld. In order to meet these exacting conditions it was necessary to build a number of sophisticated automatic welding machines to join the various components together. In addition it was necessary to house these welding machines in an argon-

atmosphere glove-box in order to prevent oxidation during the welding. Once the welding conditions were defined, it was planned that hardware for ten cells would be made to contain the iron disulfide electrode in an Li-alloy/FeS$_2$ of similar design to the Level I cell.

At the termination of the contract all the individual molybdenum components had been manufactured and the automatic welding machines had been built. However, no welding trials had been carried-out so the questions related to whether or not molybdenum cell hardware can be successfully joined by the TIG welding process remains unanswered.

In conclusion, although some progress was made towards the development of a Li-alloy/FeS$_2$ cell, there still remains a substantial amount of work to be done before a practical high-performance, long-life iron disulfide cell can be built. With recent improvements in the monosulfide cell, the difference in achievable performance between the two types of cell is diminishing. Therefore, it may be wiser to continue with the monosulfide positive electrode because of the less inherent problems it presents, particularly with regard to achieving long life.

Iron Monosulfide-Bipolar Stack Development

In our efforts to achieve the Level II performance goals, an iron monosulfide bipolar stack design was selected as a viable alternative to the monopolar disulfide cell for investigation since a bipolar design offers a number of potential advantages over a monopolar design. Also, if a bipolar design proves successful and a stable iron disulfide electrode can be developed, it is possible that the ultimate in performance will be attained by combining the two approaches. However, because of the challenging problems that each approach presents it was decided that at this early stage it would improve the probabilities of success if the two approaches were pursued separately, but concurrently, until each approach has demonstrated good performance and life.

Bipolar Design

A schematic drawing of the proposed bipolar design is shown in Figure 63. The bipolar electrode assembly comprises one negative and one positive active material plaque placed either side of a sheet current collector which is the bipolar membrane. Each bipolar assembly is electronically isolated from adjacent assemblies by a separator layer. The stack is completed by placing a negative plaque at one end of the stack and a positive plaque at the other. The current path through the stack is perpendicular to the electrode faces. The voltage is dependent upon the number of cells that are stacked in series. The major advantage of a bipolar design over a monopolar cell is the substantial reduction in hardware weight. In particular, the current collector system weight is greatly reduced since bus bars are not required and the current distribution plates can be reduced in size since they are required to carry much lower currents than an equivalent energy monopolar design. In addition, the current density distribution on the electrodes will be much more uniform since the current flow is perpendicular to the electrodes and path distances are relatively short. The greatly reduced hardware weight and low cell resistance should significantly improve the Li-alloy/FeS system performance, particularly at the higher rates of discharge. The projected performance of a bipolar stack is shown in Figure 64. The electrode and separator formulations used in this design are similar to those used in the Level I cell. The bipolar element weight was assumed to be 300g. and that of the terminal/end plate assemblies 600g. It can be seen that the specific energy of the bipolar stack is about the same as the Level I cell (ie 75 Wh/kg at C/3 discharge rate) when the stack contains only 4 cells. The specific energy rapidly increases as the number of cells in the stack is increased until the weight of the terminal/end plate assemblies becomes small compared to the stack weight at which point the specific energy reaches a maximum of ~ 125 Wh/kg.

In order to operate a bipolar stack successfully, however, two major hurdles have to be overcome. First, special care is required in the design
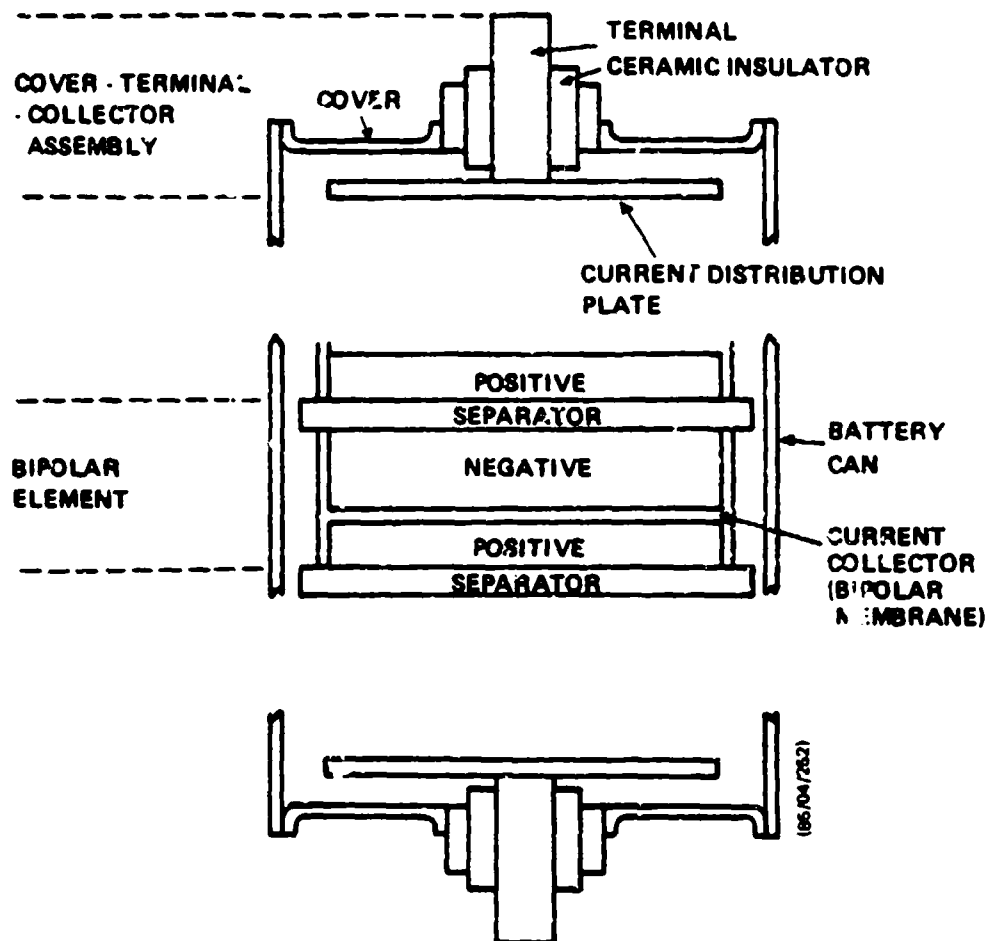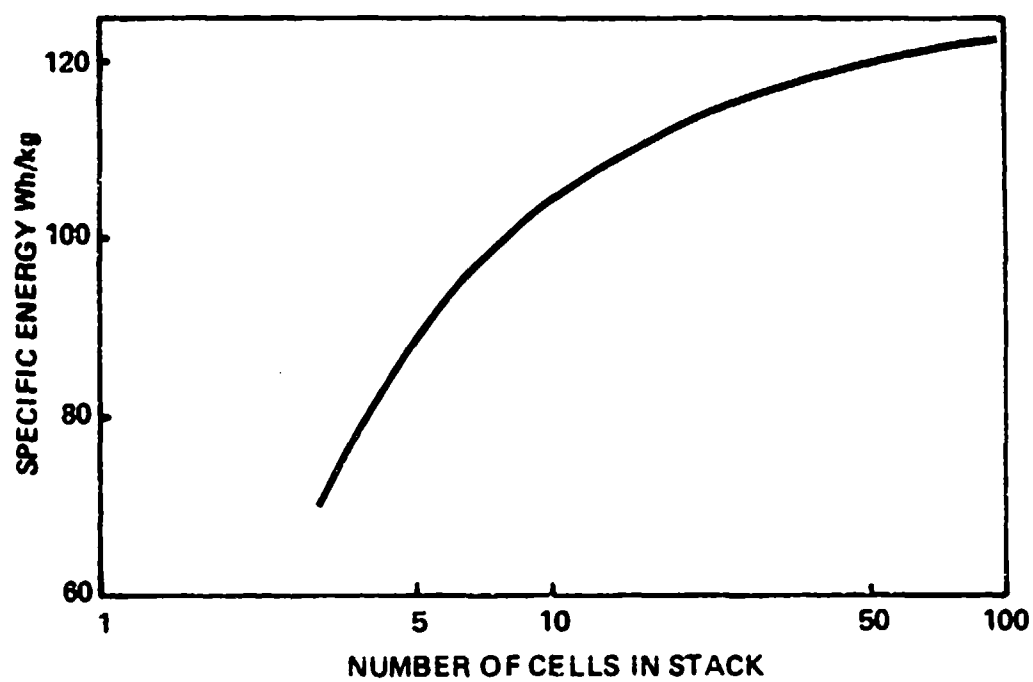
Figure 63. Schematic Drawing of Bipolar Stack Design

85/135

Figure 64. Projected Performance of Bipolar Stack Design

-110-

and construction of the stack to ensure there are no stray conductive paths (electronic and ionic) which allow shunt currents to discharge the stack. Generally these conductive paths are formed between adjacent cells or the metallic cell container as a result of electrolyte seepage from the electrodes and separator.

The other more difficult problem is to maintain an electrochemically balanced stack during operation so that all the cells are approximately at the same state of charge/discharge as cycling proceeds. This requires some form of equalization. One method of equalization would be to individually control the charging of each cell in the stack but this requires a sophisticated charger and current leads to every cell which detracts from the overall specific energy of the system. An alternative is to provide a mechanism for electrochemical equalization in the cell by overcharging or overdischarging. In order to overcharge the bipolar stack, a means must be provided for passing current through the fully charged cells without causing damage while the remaining cells in the stack are brought to top of charge. A shuttle reaction would be one such means, in which a chemical specie is oxidized at the positive electrode as the next sequential oxidation reaction after the iron is converted to FeS. The oxidized specie would then diffuse to the negative, where it would be reduced. This reduced specie would then migrate back to the positive where it could again be oxidized, thus completing the shuttle. Such a shuttle mechanism, involving oxygen is employed in sealed aqueous battery systems (eg Pb-acid and Ni-Cd).

Overdischarge equalization would rely on leakage currents as the means to pass current through fully discharged cells. Hence each cell in the stack could be driven to complete discharge at a current which would be limited to the lowest leakage current in the stack. Since this would require an extended period of time, it is envisaged that it would be performed as a periodic maintenance procedure.

Much of the preliminary experimental work in developing a practical

bipolar stack has been performed by testing small stacks of up to 4 cells using modified pellet cell components. Initially many of the stacks failed after a few cycles due to shorts associated with electrolyte bridging between the cells and the container. A two-cell stack, however, was successfully cycled for approximately a 100 times before testing was terminated due to declining capacity. The electrode and separator compositions used were the same as those in the Level I cell. The performance of the stack at various current densities is shown in Figure 65. The utilization declines with increasing current density and is approximately 10% lower at all current densities than for a monopolar construction with similar electrode and separator compositions. The stack resistance was somewhat higher than predicted, but this was probably due to inadequate pressure on the stack resulting in poor contact between the electrodes and the current collectors. In the current density range 40-200mA/cm^2, the utilization to 1.0V/cell can be expressed by the following equation:

Utilization, % = 82 - 0.167 x current density (mA/cm^2)

A four cell stack with 105 cm^2 size electrodes was also built and tested. Sense leads were attached to each bipolar electrode pair in order to monitor individual cell voltages and thus prevent cells being grossly overcharged. The performance of this 4-cell stack is shown in Figure 66. Over the first forty cycles the stack was fairly well balanced with the coulombic and watt-hr efficiencies remaining high and uniform. The utilization was somewhat lower than one would expect from previous individual cell data. However, the upper cut-off voltage on charge was limited to 1.55 volts instead of the usual 1.65 volts employed when operating monopolar cells. The cut-off voltage was lowered to prevent massive overcharge of an individual cell when the stack eventually became unbalanced. The lowering of this cut-off voltage influenced the available capacity from the cells due to the cells not being fully charged. The rapid decline in performance beyond 40 cycles was due to the stack becoming unbalanced. It was found-out after
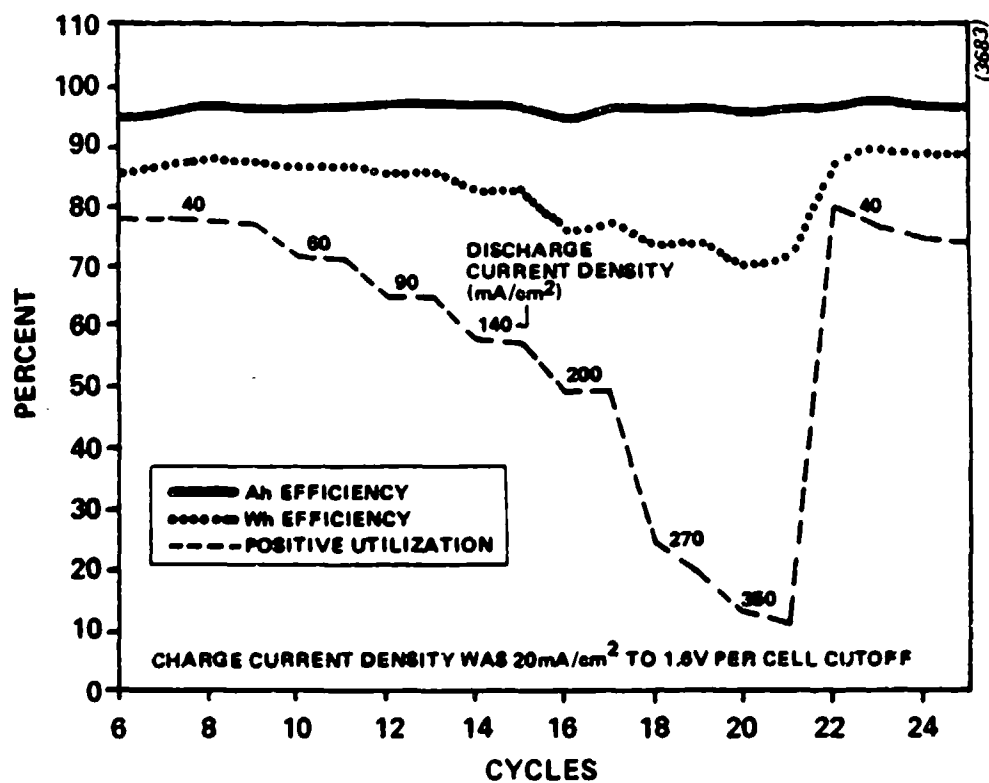
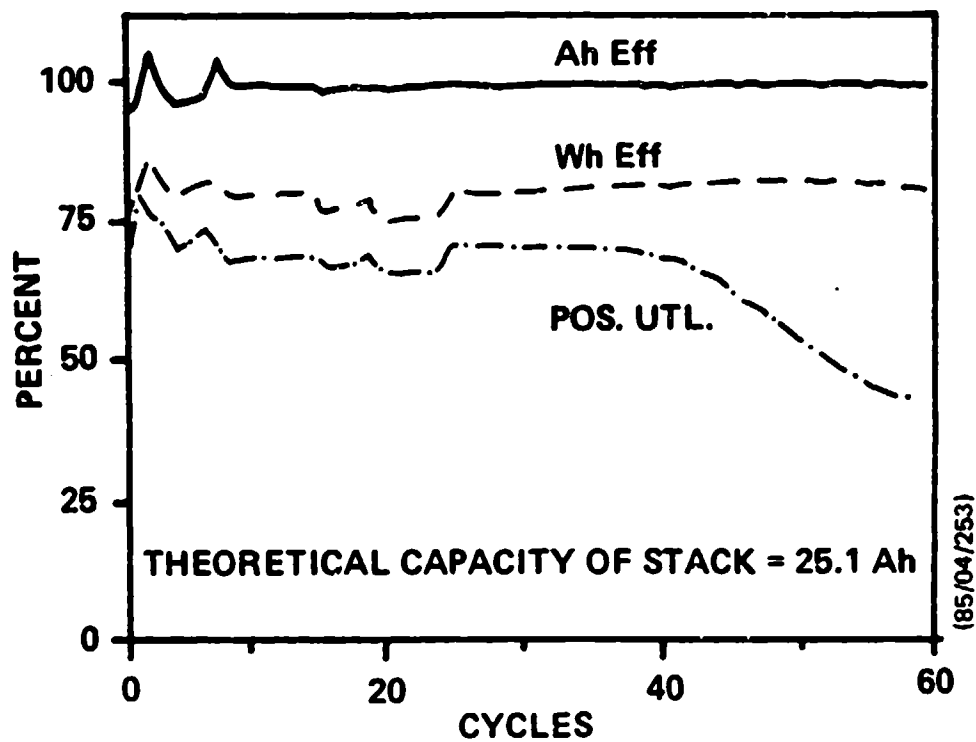Figure 65.   Performance of Two Cell Li-Alloy/FeS Bipolar Stack

Figure 66. Performance of Engineering 4-Cell Stack

testing that due to an error during the construction of this bipolar stack one of the cells in the stack was grossly mismatched in capacity to the others. It was this cell that caused the stack to become unbalanced.

The preliminary results from this work on a bipolar construction is encouraging and with further development both in hardware design and modifications to the electrode and separator formulation it should be possible to build a high performance long life bipolar battery that would come nearer to meeting the performance goals of the high energy density rechargeable battery program than is feasible with a monopolar design.

References

1. C. Kasper, Trans. Electrochem. Soc., $\underline{77}$, 335 (1940).

2. C. W. Tobias and R. Wijsman, J. Electrochem. Soc., $\underline{100}$, 10, 459 (1953).

APPENDIX

LEVEL I CELL DESIGN SUMMARY

Table A1   Electrode and Separator Formulations used in Level I Cell.

Chemical

Positive Electrode

Formulation M15

Material	W/O	V/O
Iron Sulfide (FeS)	74	52.1
Iron	5	2.2
Molybdenum	3	1.0
Electrolyte	18	20.9
Porosity	–	23.8

Negative Electrode

Formulation L28

Material	W/O	V/O
Lithium-Aluminum	52	45.5
Lithium-Silicon	13	16.7
Electrolyte	35	18.2
Porosity	–	19.6

Electrolyte

Ternary Lithium Halide Salt

	W/O	Mole %
Lithium Fluoride	9.56	22
Lithium Bromide	68.41	47
Lithium Chloride	22.03	31

Melting point ~ 445°C

Separator

Formulation – E9

	W/O	V/O$_{(S)}$	V/O$_{(L)}$
Maglite D	35	22.5	22.5
Electrolyte	65	52.0	69.5
Porosity		25.5	8:0

-117-

Table A2   Physical and electrochemical Parameters for Level I Cell.

Physical

Electrode size		in.	cm.
	Height (H)	3.32	8.43
	Width (W)	4.90	12.45

Aspect ratio $H/W = 0.68$

Electrode area $= 105$ cm^2

Number of electrodes   7   (3 Positive : 4 Negative)

Electrode thickness		in	cm.
	Positive	0.050	0.127
	Negative	0.105	0.267
Separator thickness		0.055	0.140

Cell
    Weight ~ 1.8kg
    Volume ~0.6ℓ

Electrochemical

- Theoretical capacity   119 Ah
  (based on positive electrode)
- Negative to positive capacity ratio   1.35

	Discharge Rate	
Parameter	1.5h (0.67C)	20 min. (3C)
Utilization %	85.6	65
Cell capacity Ah	101.8	77.2
Average voltage V	1.201	1.013
Specific energy Wh/kg	67.9	43.1
Sustained power W/kg	45.3	129.2
Current density mA/cm^2	102	368

Table A3   Materials of Construction for Level I Cell Hardware

Component	Material
Cell case	Stainless Steel
Electrode baskets	Stainless Steel
Current collectors	
Bus bars	Nickel
Distribution plates	
Outer feedthrough	
Inner feedthrough	Copper
Positive feedthrough seal	Beryllia
	Boron Nitride

TECHNICAL PUBLICATIONS DURING CONTRACT

1. B. A. Askew and G. Barlow, "The Development of a Secondary Lithium-Metal Sulfide Cell for Satellite Applications," Proc. of 30th Power Sources Symposium, p. 54, 1982.

2. D. M. Allen, R. A. Putt and G. Barlow, "Lithium-Metal Sulfide Cell Development for Satellite Batteries," Proc. of 18th IECEC, Vol. 4., p. 1460, 1983.

3. S. S. Misra, "Investigations on the Li-Al-Si Alloy/Iron Disulfide Molten Salt Battery System," Proc. of Fall ECS Meeting, Washington, D.C., Extended Abstract No. 84, p. 134, 1983.

4. S. S. Misra, "Electrochemical Investigations of the Lithium-Alloy/Iron Sulfide Molten Salt Battery System with MgO Powder Separator," Proc. of Fall ECS Meeting, Washington D.C., Extended Abstract No. 85, p. 136, 1983.